Doctoral Thesis

Study of Top Quark FCNC Couplings at Future Colliders

Subhasish Behera

A thesis
submitted for the degree of
Doctor of Philosophy

Supervisor:
Prof. Poulose Poulose

Department of Physics
Indian Institute of Technology Guwahati
Guwahati - 781 039, India

August 2019

भारतीय प्रौद्योगिकी संस्थान गुवाहाटी
Indian Institute of Technology Guwahati

Study of Top Quark FCNC Couplings at Future Colliders

Subhasish Behera

A thesis
submitted for the degree of
Doctor of Philosophy

Supervisor:
Prof. Poulose Poulose

Department of Physics
Indian Institute of Technology Guwahati
Guwahati - 781 039, India

August 2019

भारतीय प्रौद्योगिकी संस्थान गुवाहाटी
Indian Institute of Technology Guwahati

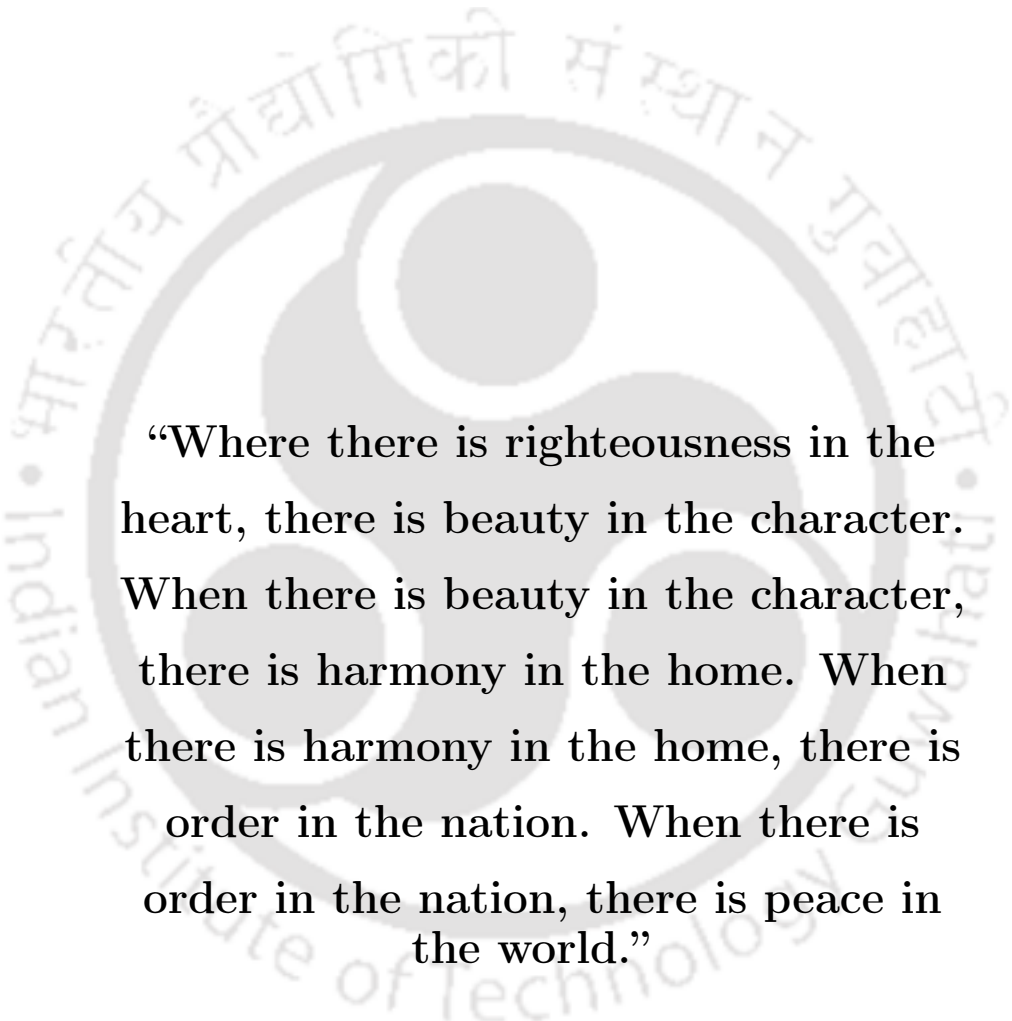

"Where there is righteousness in the heart, there is beauty in the character. When there is beauty in the character, there is harmony in the home. When there is harmony in the home, there is order in the nation. When there is order in the nation, there is peace in the world."

- A. P. J. Abdul Kalam

भारतीय प्रौद्योगिकी संस्थान गुवाहाटी
Indian Institute of Technology Guwahati

Prof. Poulose Poulose
Department of Physics
Indian Institute of Technology Guwahati
Guwahati - 781039, INDIA
Email: poulose@iitg.ac.in

CERTIFICATE

This is to certify that the work contained in the thesis entitled ***"Study of Top Quark FCNC Couplings at Future Colliders"*** by **Mr. Subhasish Behera**, a Ph.D student of the Department of Physics, Indian Institute of Technology Guwahati was carried out under my supervision and has not been submitted elsewhere for award of any degree.

The thesis, in my opinion, has reached the standard fulfilling the requirement for the award of degree of **Doctor of Philosophy** in accordance with the regulations of Indian Institute of Technology Guwahati.

Date:

Prof. Poulose Poulose
(Professor)

भारतीय प्रौद्योगिकी संस्थान गुवाहाटी
Indian Institute of Technology Guwahati

This thesis is dedicated to
my parents and family members,
who taught me
the merits of discipline
and the rewards of education,
and
equally dedicated to
my lovely wife
whose love and support
gives me strength to persue.

भारतीय प्रौद्योगिकी संस्थान गुवाहाटी
Indian Institute of Technology Guwahati

Declaration of Authorship

I, **Subhasish Behera**, declare that this thesis titled, "**Study of Top Quark FCNC Couplings at Future Colliders**" and the work presented in it are my own. I confirm that:

- This work was done wholly or mainly while in candidature for a research degree at Indian Institute of Technology Guwahati.
- Where I have consulted the published work of others, this is always clearly attributed.
- Where I have quoted from the work of others, the source is always given. With the exception of such quotations, this thesis is entirely my own work.
- I have acknowledged all main sources of help.
- Where the thesis is based on work done by myself jointly with others, I have made clear exactly what was done by others and what I have contributed myself.

Date: _____ **Subhasish Behera**

भारतीय प्रौद्योगिकी संस्थान गुवाहाटी
Indian Institute of Technology Guwahati

Acknowledgments

I am highly indebted to my supervisor Prof. Poulose Poulose for giving me an opportunity to carry out the work under his guidance. His way of looking into physics problems, formulating questions and trying to understand the basic of any topic in physics motivated me a lot. His friendly behavior which made me comfortable with him for the entire period. I got a talented supervisor when I join but left with one of the good friend of mine. I am fortunate enough to get a supervisor like him.

I would also like to thank my Doctoral committee members Prof. Bipul Bhuyan (Chairman), Dr. Arunansu Sil, Dr. Subhaditya Bhattacharya, for giving me numerous comments and valuable suggestions during my PhD tenure. I want to thank my collaborators Dr. Satendra Kumar, Dr. Mukesh Kumar, Dr. Rashidul Islam, Mr. Rafiqul Rahaman(IISER Kolkata), Prof. Daniel Jeans(KEK, Japan) for helping me with the understanding of physics problems. It was quite wonderful experience and learning while collaborating with them. I am especially grateful to Prof. Daniel Jeans for imparting knowledge of International Large Detector model, providing access to events samples for ILC process study. I also thankful for my selection to the KEK Student Program 2018 and allow me to work with him. I am thankful to Prof. Girish Sampath Setlur, Prof. Tarak Nath Dey, Prof. Padma Kumar Padmanavan, Prof. Sourav Basu, Prof. A. Perumal for their excellent lectures during the course work days. I am thankful to present HoD Prof. Subhradip Ghosh and former HoD Prof. Saurabh Basu for all the help and support during my entire PhD career. I also thank all the members of our HEP Journal Club at IITG. I have learnt many things from the discussions in the journal club meetings. I extend my gratitude to all the faculty members and staff of the Department of Physics, who supported me in several ways during this period. I am grateful to Mr. Basab Purkayastha and Mr. Hemanta Medhi for their timely help to resolve the technical issues.

I am thankful to my 2013 batch mates, Dr Bibhuti Bhushan Dash, Mr Ghanashyam Meher, Mr S. S. Gautam Buddha for their moral support throughout. I would like to thank my research group friends, Biswaranjan, Shibananda, Deepanjali, Sreemanti, Suresh. I especially thankful to Shibananda for physics discussion during my Ph.D. I thank all my seniors, especially Sourav and Kallol for helping me in solving issues with computer softwares.

I must also mention that I had very good friends in my M.Sc. Dr. Prakash Mahakul, Mr. Anshuman Behera, Mr. Madhav Anand who stands for me in every situation in my life. I want to thank all my teachers from School days up to PhD for their inspiration, motivation and dearness shown to me throughout my career. I would specially thankful to my lecturer from Sambalpur University Sambalpur, Odisha for teaching me the value of Physics.

I am thankful to my supervisor's wife Ms. Stavelin who had always inspired to finish PhD soon and their sweet kids Hasvid and Onella for all the funny moments.

At the end, I would like to thank my family members: Bapa and Maa, Hirakud Bapa and Maa, Late my Dada-i, Late Mamudada, Mamui, My Wife (Tapaswini Mohanty), Bada Nani-Jiju, Dada, Sana Nani-Jiju, Bada Mausi-Mausa, Sana Mausi-Mausa, Om, Aryan, KUNU, ADWIK and MOON, for their immense love and care towards me. I would be remain grateful to my Bapa-Maa for their sacrifice in making us educated. I would like to thank Mr Nikesh Behera(Babu) for his help in finalizing the quotes mentioned in each chapters of the thesis. I would like to thank all my relatives residing at my village from whom I learnt the behavior, moral and ethic of life.

I would like acknowledge to MHRD, Government of India for the research fellowship.

Last but not the least I thank to Almighty for his help during these tough and hard fought days.

Date: **Subhasish Behera**

Acronyms

SM	:	Standard Model
NP	:	New Physics
FCNC	:	Flavour Changing Neutral Current
BSM	:	Beyond Standard Model
LHC	:	Large Hadron Collider
HL-LHC	:	High Luminosity Large Hadron Collider
ILC	:	International Linear Collider
LHeC	:	Large Hadron Electron Collider
HE-HL LHC	:	High Energy-High Luminosity Large Hadron Collider
FCChe	:	Future Circular Collider for Hadron Electron
ILD	:	International Large Detector
ATLAS	:	A Toroidal LHC Apparatus
CMS	:	Compact Muon Solenoid
2HDM	:	Two Higgs Doublet Model
DM	:	Dark Matter
GeV	:	Giga electron Volt
TeV	:	Tera electron Volt
QFT	:	Quantum Field Theory
QCD	:	Quantum ChromoDynamics
QED	:	Quantum ElectroDynamics
EW	:	Electroweak
EFT	:	Effective Field Theory

VEV	:	Vacuum Expectation Value
EWSB	:	Electroweak Symmetry Breaking
GUT	:	Grand Unified Theory
SUSY	:	Supersymmetry
MSSM	:	Minimal Supersymmetric Standard Model
ExD	:	Extra Dimensions
EGMs	:	Extended Gauge Models
DOFs	:	Degress of Freedoms
MET	:	Missing Transverse Energy
BR	:	Branching Ratio
h.c.	:	Hermitian Conjugate
UFO	:	Universal FeynRule Output

Abstract

Top quark is the only quark available within the Standard Model (SM) of particle physics, which decays before forming bound state with other quarks, including its anti-particle. This property of the top quark makes it unique as it provides a way to study the properties of a *bare quark*. The SM predicts branching ratio, BR($t \to Wb$)$\sim$100%. On the other hand, the *Flavor Changing Neutral Current* (FCNC) interactions are forbidden within the SM, with possible contributions arising at higher order corrections only.

In this thesis work we study three different processes of single top quark productions at proposed colliders such as the *Large Hadron Electron Collider* (LHeC), the *International Linear Collider* (ILC) and the *Future Circular Collider for Hadron and Electron* (FCC-he). The choice of the processes under study is advantageous at such colliders due to the fact that, (1) the process is forbidden in the SM, thus reduces the background considerably, (2) the associated production of electron or light quark (produced along with the top quark) provides a handle in disentangling the *Lorentz structure* of the new physics (NP) couplings. We choose SM Effective Field Theory (SMEFT) as the theoretical framework. We consider both vector and tensor structure of their couplings with left- or right-chirality separately. Assuming simultaneous presence of relevant FCNC couplings, we obtain the reach of each of the couplings at 95% C.L., through the processes considered in each of the colliders. Suitable observables related to the top quark polarization and angular distributions of the final state particles are appropriately exploited to disentangle the effects of different couplings. We have also demonstrated the utility of electron beam polarization in obtaining better reach, and further as a tool to discriminate different couplings wherever possible. Our study predicts the limits on the couplings with their simultaneous presence.

The details of the study is given in Chapters 3 to 5 of the thesis.

भारतीय प्रौद्योगिकी संस्थान गुवाहाटी
Indian Institute of Technology Guwahati

Contents

1 Introduction **1**

1.1 Brief Introduction to TOP quark 4

1.1.1 TOP Quark Productions Theory and Experiments 6

1.1.1.1 Access to Top Quark Polarization 8

1.2 FCNC in Top Quark Sector 10

1.2.1 FCNC limits from Experiments 13

1.2.2 Effective Field Theoretical approach to FCNC Top Physics . 14

1.3 Future Colliders and their Advantages 15

1.4 Outline Of Chapters 17

2 Software and Analysis Strategy **21**

2.1 A Brief Summary of The Tools Used 21

2.2 Analysis Strategy 23

2.2.1 Top quark Polarization observables 24

2.2.1.1 Numerical Calculation of P_x, P_y and P_z 28

3 Top quark FCNC interaction via tqZ couplings at LHeC **29**

3.1 Introduction 29

3.2 Formalism 31
3.2.1 The Process 31
3.2.2 Polarization of the top quark 32
3.2.3 Angular asymmetry of the recoiled electron 34
3.3 Simulation and Analysis 34
3.3.1 Asymmetries 37
3.3.2 Multi-parameter Analysis 39
3.3.2.1 χ^2 Analysis 41
3.3.2.2 Likelihood mapping of the parameter space 42
3.4 Discussion and conclusion 45

4 Investigating FCNC anomalous top quark coupling through $e^-e^+ \to tj$ at the ILC 47

4.1 Introduction 47
4.2 Event Generation, Detector Simulation and Reconstruction 50
4.3 Events Selection and Numerical Analysis 53
4.3.1 Preselection of events: 53
4.3.2 Case 1: Beam polarization of $(-80\%, +30\%)$ 53
4.3.2.1 Event Selection: Muonic final state 54
4.3.2.2 Event Selection: Electronic final state 58
4.3.2.3 Further analysis: making use of asymmetries 61
4.3.3 Case 2: Beam polarization of $(+80\%, -30\%)$ 66
4.4 Discussion: Reach of the couplings 74
4.4.1 Asymmetries as discriminator 76
4.5 Possibilities at Higher Energy ILC 77

4.6 Summary and Discussion 79

5 Tracing the anomalous tqg and $tq\gamma$ flavor changing interactions at the FCC-he **81**

5.1 Introduction 81

5.2 Signal and Background 83

5.3 Event Generation and Analysis 86

5.3.1 Combined analysis: taking μ^+ and e^+ together 95

5.4 Top polarization Asymmetries 96

5.4.1 Disentangling different types of couplings 98

5.5 Summary and Conclusion 100

6 Summary and Conclusion **103**

A Reconstruction of Neutrino and Top quark Momenta for Semi-leptonic decay of top quark **107**

B EFT Lagrangian implementation as UFO model file **111**

C Analytical expression of Invariant Amplitude and Cross Section for $pe^- \to e^- t, (t \to b\ell^+\nu_\ell)$ **117**

C.1 Production Cross Section 119

C.1.1 Analytical calculation of the production density matrix . . . 121

C.2 Decay width 123

भारतीय प्रौद्योगिकी संस्थान गुवाहाटी
Indian Institute of Technology Guwahati

List of Figures

1.1 Loop Contributions to Higgs Mass. 3

1.2 Feynman diagrams for the three top quark production modes via $q\bar{q}$ or gq initial state. Fig (a) and (b) show the t-channel diagrams, (c) shows the s-channel process, and (d) shows the Wt associated production channel. 7

1.3 Fig (a) and (b) shows the two possibilities of W^+-helicity which conserves angular momentum in case of top quark decay. 9

1.4 One loop FCNC process for $t \to q(u,c)\gamma$ within SM. 11

1.5 FCNC process for top quark in Two Higgs Doublet model. H and A are the new scalar and pseudo-scalar of the 2HDM. 11

1.6 Feynman diagram for FCNC process for top quark in SUSY models. The $\tilde{g}$ is the fermionic partner of the gluon and $\tilde{t}$ is the scalar partner of the top quark. 12

1.7 Non-standard FCNC vertices in top quark sector. 15

3.1 Signal processes: The Ztq anomalous vertex at production channel of top and decay of top via SM coupling vertex only. The final state charge lepton is ℓ^+ in our study to make proper distinction between charged lepton (e^-) coming out of the e^-Ze^--primary vertex and decay of the top it self. 31

3.2 Polar angle distributions of the scattered e^- in the final state for (a) unpolarized, (b) -80% polarization and (c) $+80\%$ polarization of electron beam. Note that X and κ denote the vector and tensor couplings respectively. 37

3.3 Single parameter reach with an integrated luminosity of 2 ab^{-1}. . . 42

3.4 Two parameter reach with an integrated luminosity of 2 ab^{-1}. . . . 42

3.5 MCMC two parameter contour at 95% (deep blue), 99% (light blue) C.L. integrated luminosity of 2 ab^{-1} is used. The tensor couplings are considered at $\Lambda = m_t$. 44

4.1 Signal process: The Feynman diagram corresponding to single top production at ILC enabled by the anomalous $tq\gamma(Z)$, with the leptonic decay of top quark. 50

4.2 Cross section of signal process : $e^-e^+ \to tj$, $(t \to W^+b,\ W^+ \to \mu^+\nu_\mu\ (e^+\nu_e))$ at different $\sqrt{s}$ values. The superfix in the legends represents the handedness of the couplings. The solid(dashed) lines represents the LR(RL) samples. The graph of $\kappa^{L(R)}_{\gamma qt}$ for LR and RL samples overlap each other. 51

4.3 Distributions after the events are identified with one light-jet, one $b-$jet and one μ of either charge. The beam polarizations combination of $(-80\%, +30\%)$ is assumed. Signal corresponds to the coupling $\kappa^L_{\gamma qt}$, and the backgrounds are (a) $e^-e^+ \to WW \to l\nu_l 2j$ (b) $e^-e^+ \to ZZ \to 2l2j + 2\nu_l 2j$ (c) $e^-e^+ \to Z \to 2j + 2b$ (d) $e^-e^+ \to ffh$ 56

4.4 Distributions after the events are identified with as containing one light-jet, one $b-$jet and one *electron* of either charge. The beam polarizations of $(-80\%, +30\%)$ are assumed. Signal corresponds to the coupling $\kappa^L_{\gamma qt}$, and the backgrounds are (a) $e^-e^+ \to WW \to l\nu_l 2j$ (b) $e^-e^+ \to W^\pm e^\mp \nu \to 2je\nu$ (c) $e^-e^+ \to Ze^-e^+ \to 2je^-e^+$ (d) $e^-e^+ \to Z \to 2j + 2b$ (e) $e^-e^+ \to ffh$ 59

4.5 Normalized angular distributions of the final state particles (reconstructed) in the case of *top quark, muonic* decay, for different type of couplings, taken one at a time. Beam polarizations of $(-80\%, +30\%)$ is assumed. . 61

4.6 Normalised angular distributions of the final state particles (reconstructed) in the case of *anti-top quark, muonic* decay, for different type of couplings, taken one at a time. Beam polarizations of $(-80\%, +30\%)$ is assumed. . 62

4.7 Normalised angular distributions of the final state particles (reconstructed) in the case of *top quark, electronic* decay, for different type of couplings, taken one at a time. Beam polarizations of $(-80\%, +30\%)$ is assumed. . 62

4.8 Normalised angular distributions of the final state particles (reconstructed) in the case of *anti-top quark, electronic* decay, for different type of couplings, taken one at a time. Beam polarizations of $(-80\%, +30\%)$ is assumed. 63

4.9 Distributions after the events are identified with as containing one light-jet, one $b-$jet and one μ of either charge. The beam polarization combinations of $(+80\%, -30\%)$ are assumed. Signal corresponds to the coupling $\kappa^L_{\gamma qt}$, and the backgrounds are (a) $e^-e^+ \to WW \to l\nu_l 2j$ (b) $e^-e^+ \to ZZ \to 2l2j + 2\nu_l 2j$ (c) $e^-e^+ \to Z \to 2j + 2b$ (d) $e^-e^+ \to ffh$. 67

4.10 Distributions after the events are identified with one light-jet, one $b-$jet and one *electron* of either charge. The beam polarizations of $(+80\%, -30\%)$ are assumed. Signal corresponds to the coupling $\kappa^L_{\gamma qt}$, and the backgrounds are (a) $e^-e^+ \to WW \to l\nu_l 2j$ (b) $e^-e^+ \to W^\pm e^\mp \nu \to 2je\nu$ (c) $e^-e^+ \to Ze^-e^+ \to 2je^-e^+$ (d) $e^-e^+ \to Z \to 2j + 2b$ (e) $e^-e^+ \to ffh$. . 69

4.11 Normalised angular distributions of the final state particles (reconstructed) in the case of *top quark, muonic* decay, for different type of couplings, taken one at a time. Beam polarizations of $(+80\%, -30\%)$ is assumed. . 71

4.12 Normalised angular distributions of the final state particles (reconstructed) in the case of *anti-top quark, muonic* decay, for different type of couplings, taken one at a time. Beam polarizations of $(+80\%, -30\%)$ is assumed. . 71

4.13 Normalised angular distributions of the final state particles (reconstructed) in the case of *top quark, electronic* decay, for different type of couplings, taken one at a time. Beam polarizations of $(+80\%, -30\%)$ is assumed. . 72

4.14 Normalised angular distributions of the final state particles (reconstructed) in the case of *anti-top quark, electronic* decay, for different type of couplings, taken one at a time. Beam polarizations of $(+80\%, -30\%)$ is assumed. 72

5.1 Signal processes $pe^- \to e^- tj$. There are 2 gluon initiated processes with either u or c quark in the final state and 2 quark (u or c quark) initiated process with gluon in the final state along with top quark and e^- having 16 diagrams each. 82

5.2 Unpolarized sample: Distributions of observables for signal and background. The solid (dotted) line graphs represents the signals (background) events. The legends for signal samples are indicated by the couplings parameters. 87

5.3 (-80%) sample: Distributions of observables for signal and background. The solid (dotted) line graphs represents the signals (background) events. The legends for signal samples are indicated by the couplings parameters. 88

5.4 (-80%) sample: Distributions of observables for signal and background. The solid (dotted) line graphs represents the signals (background) events. The legends for signal samples are indicated by the couplings parameters. 89

5.5 The graph shows the significance against the required number of signal events corresponding to the respective background events at unpolarized, -80% and $+80\%$ cases of electron beam polarizations. The solid lines are for samples with one μ^+ and dotted for combined samples of μ^+ and e^+ together. 94

5.6 Figure showing the θ_{e^-} distributions at the lab frame, for unpolarized, -80% and $+80\%$ polarized initial beam samples. Fig (a), (b) and (c) in the 1st row for *top quark* events and Fig (d), (e) and (f) in the 2nd row for *anti-top quark* events are plotted. 97

C.1 Flavour Changing Neutral Current (FCNC) process in $e^- p$ collider. The dashed line separates the top quark production and decay amplitude. . . 118

List of Tables

1.1 FCNC limits on $\mathcal{B}(t \to q(u,c)Z)$ in various BSMs. 12

1.2 The second and third column represents value of the BR of top quark for LHC(Run I, II). Projected limits on the BR for anomalous flavor changing top couplings at HL-HE LHC are presented in the third and fourth column. All limits are for the 95% C.L. 13

3.1 The partonic cross section of the signal process for different anomalous $tqZ, (q = u, c)$ couplings at beam energies, $E_{e^-} = 60$ GeV and $E_p = 7$ TeV for electron polarization 0%, -80% and $+80\%$. The value of the couplings are set to unity here. 35

3.2 The signal cross sections for different anomalous $Ztq, (q = u, c)$ couplings, g_{Ztq}, at beam energies, $E_{e^-} = 60$ GeV and $E_p = 7$ TeV for polarized electron beam of -80%. The cross section can be obtained from the above table as $\sigma = |g_{Ztq}|^2[\sigma(pe^- \to e^- t, t \to W^+ b, W^+ \to \ell^+ \nu_\ell)]$. In the case of tensor couplings, the scale $\Lambda = m_t$. 36

3.3 The SM background cross sections at beam energies, $E_{e^-} = 60$ GeV and $E_p = 7$ TeV for electron polarization -80%. 36

3.4 Asymmetries for one fixed value of coupling at a time. It shows the distinction among X^L_{zqt}, X^R_{zqt}, κ^L_{zqt} and κ^R_{zqt} by just looking at the sign of A_z (Top quark rest frame observable) and A_e^{FB} (Lab frame observable) as discussed in the equations for asymmetries. 38

3.5 The list of simultaneous limits on FCNC parameters obtained from MCMC analysis including the cross-section and all other asymmetries for e^-p collider at $E_{e(p)} = 60$ (7000) GeV with integrated luminosity of 2 ab^{-1}. 43

3.6 Limiting values of the couplings that can be reached (refer Table 3.5), and the branching fractions of the corresponding top quark decays. 44

4.1 The partonic cross section of the signal process : $e^-e^+ \to tq$, $(t \to Wb,\ W \to \mu\nu_\mu\ (e\nu_e))$ for different anomalous $tq\gamma(Z)$ couplings at $\sqrt{s}$=250 GeV. The values of the couplings are set to unity in all cases. 51

4.2 Signal with *muonic* final state (coupling values set equal to unity) and background events at different stages of selection. The beam polarizations of $(-80\%, +30\%)$ are assumed. 57

4.3 Signal with *electronic* final state (coupling values set equal to unity) and background events at different stages of selection. The beam polarizations of $(-80\%, +30\%)$ are assumed. 60

4.4 **After Detector:** top quark case. The mean value of the asymmetries at $\sqrt{s}$=250 GeV with beam polarizations of $(-80\%, +30\%)$. All coupling values are set to unity. 64

4.5 **After Detector:** anti-top quark case. The mean value of the asymmetries at $\sqrt{s}$=250 GeV with beam polarizations of $(-80\%, +30\%)$. All coupling values are set to unity. 65

4.6 Signal with *muonic* final state (coupling values set equal to unity) and background events at different stages of selection. The beam polarizations of $(+80\%, -30\%)$ are assumed. 68

4.7 Signal with *electronic* final state (coupling values set equal to unity) and background events at different stages of selection. The beam polarizations of $(+80\%, -30\%)$ are assumed. 70

4.8 **After Detector:** top quark case. Table showing the mean value of the asymmetric observables at $\sqrt{s}$=250 GeV with beam polarizations of $(+80\%, -30\%)$. All coupling values are set to unity. 73

4.9 **After Detector:** anti-top quark case. Table showing the mean value of the asymmetric observables at $\sqrt{s}$=250 GeV with beam polarizations of $(+80\%, 30\%)$. All coupling values are set to unity. 74

4.10 The upper limits on the couplings for 95% C.L. signal significance are quoted for two different beam polarizations considered in this study. The cases of top quark decay to final states with μ and e are presented separately. An assumed integrated luminosity of 0.45×2 ab^{-1} is used. 76

4.11 The response of the asymmetries to different type of couplings in case of top quark production, corresponding to the two different beam polarizations considered in this study, clearly indicating the power of the process in partial discrimination of the nature of the coupling. 77

4.12 The response of the asymmetries to different type of couplings in case of anti-top quark production, corresponding to the two different beam polarizations considered in this study, clearly indicating the power of the process in partial discrimination of the nature of the coupling. 77

4.13 The partonic cross section of the signal process $e^-e^+ \to tq$, $(t \to Wb,\ W \to \mu\nu_\mu\ (e\nu_e))$ for different anomalous $tq\gamma(Z)$ couplings and major background processes at $\sqrt{s}$ = 350 and 500 GeV. Both ℓ^+ and ℓ^- arising from t and $\bar{t}$ are included. The value of the anomalous couplings are set to unity in all signal events. 78

5.1 **No Cut:** The partonic cross section of the signal process : $pe^- \to e^-tj, (t \to Wb, W \to l\nu_l)$ for different FCNC couplings. The value of the NP couplings are set to unity. 84

5.2 **No Cut:** The partonic cross section of the signal process : $pe^- \to e^-tj, (t \to Wb, W \to l\nu_l)$ for different FCNC couplings. The value of the NP couplings are set to unity. 85

5.3 **No Cut:** The partonic cross section of the background process at different beam polarization at (50TeV, 60GeV) beam energy for proton and electron. 85

5.4 The table shows the value of the cross section (σ (fb)) with unpolarized electron beam after application of each cut. In the case of signal, coupling values are taken as unity. 91

5.5 The table shows the value of the cross section (σ (fb)) with -80% electron beam polarization after application of each cut. In the case of signal, coupling values are taken as unity. 91

5.6 The table shows the value of the cross section (σ (fb)) with $+80\%$ electron beam polarization after application of each cut. In the case of signal, coupling values are taken as unity. 92

5.7 The table shows the signal significance with an assumed value of the coupling, $\frac{\kappa^2}{\Lambda^2} = \frac{2\times10^{-4}}{m_t^2}$ with the final state containing one μ^+. . . 93

5.8 The table shows the reach on the couplings with different beam polarizations at 2 ab^{-1} integrated luminosity. The limits are calculated for samples with one μ^+ in the final state. 94

5.9 The table shows the signal significance with an assumed value of the coupling, $\frac{\kappa^2}{\Lambda^2} = \frac{2\times10^{-4}}{m_t^2}$ with the final state containing one lepton (e^+, μ^+). 95

5.10 The table shows the reach on the couplings with different beam polarizations at 2 ab^{-1} integrated luminosity. The limits are calculated for combined samples with μ^+ and e^+ together. 96

5.11 For the *top quark* case, the table gives the mean value of the asymmetric observables of three possible polarization for initial electron beam. All coupling value are set to unity. 98

5.12 for the *anti-top quark* case, the table gives the mean value of the asymmetric observables of three possible polarization for initial electron beam. All coupling value are set to unity. 98

5.13 Qualitative properties of the top polarization asymmetries and the forward-backward asymmetry of the scattered electron, allowing one to distinguish the effects. 99

5.14 Demonstrating the power of beam polarization to disentangle the effects of different types of couplings. The arrows $\Uparrow$ and $\Downarrow$, respectively, indicate increase or decrease in the cross section when the electron beam polarization is switched from $P_e = -0.8$ to $P_e = +0.8$. The horizontal arrow ($\Leftrightarrow$) says this case is practically insensitive to the change of beam polarization. 100

भारतीय प्रौद्योगिकी संस्थान गुवाहाटी
Indian Institute of Technology Guwahati

– An equation for me has no meaning, unless it expresses a thought of God.

Srinivasa Ramanujan

1 Introduction

In Particle Physics, we deal with elementary constituents of matter. By elementary we mean the particles that have no substructure and can be treated as point-like objects. The dynamics of elementary particles are described by the Standard Model (SM) of particle physics. It is based on the mathematical framework of Gauge Field Theory. The particle content of the SM can be divided into Fermions and Bosons. The fermion sector consists of three generations/flavors of leptons (light mass, weakly and electromagnetically interacting particles) and quarks (strongly and weakly and electromagnetically interacting particles). The bosons with spin-1 are considered as force carriers governed by the principle of "gauge symmetry". The force carrier which mediate electromagnetic interactions, photon (γ) and that of the strong interactions, gluon (g) are massless and charge neutral whereas mediator of weak interactions known as the weak gauge bosons, $W^{\pm}$ (charged) and $Z-$bosons (charge neutral) are massive. In addition, the SM consists of a spin-0 (scalar) neutral boson called the Higgs boson (H), responsible for providing mass to every SM particle (fermions/bosons) by virtue of its interactions with them. Particles having large interactions with the Higgs field are more massive. Among the particle content of the SM the heaviest of the fundamental particle is the *Top Quark*. The top quark is one of the important members within the SM, due to various reasons including the fact that even slight change in its mass affects the vacuum stability of the Higgs field. Its various properties, including the mass and interactions with other particles are not precisely measured in the experiments so far.

Among many success of the SM, I believe the biggest success is the prediction of the Higgs Boson. The particle has been experimentally discovered in 2012 [1, 2] after it has been theorized for over 50 years. However, the real potential of the SM comes with the so called precision measurements. For instance the measured mass of the Z-boson agrees with the theoretical predictions of the SM. The anomalous gyro-magnetic moment of electron and muon are also the part of the success story for SM. Although there are still discrepancies of the latter with the experimental data, the former gives the best agreement between theory and experiment. This results in our most precise value of the EM coupling constant or the *fine structure constant* as $\alpha^{-1} = 137.035999084$ with precision better than one part in a *billion*.

To every theory there are certain drawbacks as it may happen that a certain theory is valid up to a certain scale in energy. The SM too suffers with the difficulties at higher energy scale, for instance beyond 1 TeV. Therefore it can't be considered as a model valid all the way up to the Planck's scale. Rather we may consider it as an effective description of particle dynamics at 100-1000 GeV energies.

In the following I briefly discuss some of the difficulties of SM:

1. Neutrino Mass -: It is experimentally established that the neutrino can oscillate from one flavor to another. This implied that neutrinos have mass and mixing exist between flavor and mass eigenstate. However not having a right handed neutrino, SM can not accommodate massive neutrinos. This feature can be included into the SM without much difficulties. But we have no agreement yet on the mechanism of providing masses to neutrinos.

2. Dark Matter or Dark Energy -: The existence of Dark Matter and Dark Energy in the universe is confirmed from various experiments such as study of Galaxy Clusters, Galactic Rotation Curves, The Cosmic Microwave Background, The Bullet Cluster and Large-Scale Structure Formation. The Dark matter constitutes 27% of total energy, while dark energy constitute 68% of total energy content of the Universe. The SM is not able to explain this large section of the particle(s) and the energy of the universe.

3. Baryon Asymmetry -: The observed imbalance in baryonic matter and anti-baryonic matter in the observed universe termed as the Baryonic Asymmetry problem or matter-antimatter asymmetry problem. Neither the SM, nor the theory

of general relativity provides an explanation for why this should be so, and it is a natural assumption that the universe be neutral with all conserved charges.

4. Hierarchy Problem -: The observed Higgs mass is roughly 125 GeV. In Eq. (1.1) the first term of expression for m_h^2 is a tree level relation. The second term of the equation is due to the inclusion of higher order quantum corrections as shown in Fig. 1.1. The dominant loop diagrams for the self-energy corrections to the Higgs field are mediated by top quark, W, Z and Higgs boson in the loop.

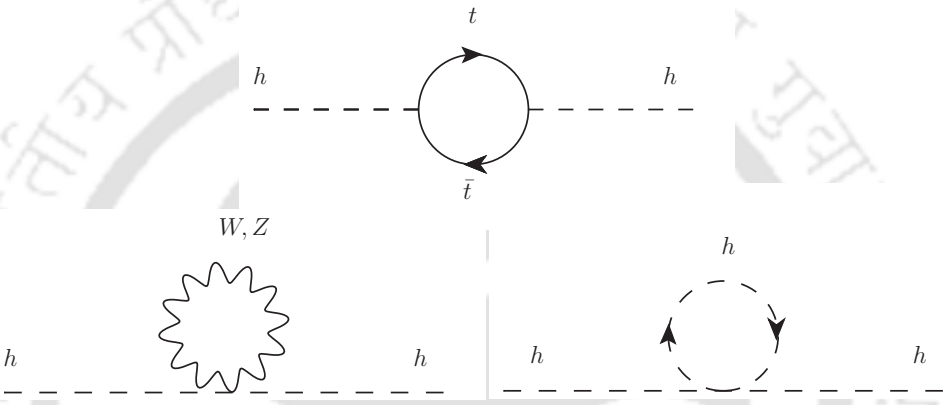

FIGURE 1.1: Loop Contributions to Higgs Mass.

Assuming that the SM is valid up to an energy scale of Λ, the contributions become [3]

$$m_h^2 = -2\mu^2 + \frac{3\Lambda^2}{8\pi^2}\left[-\lambda_t^2 + \frac{g^2}{6} + \frac{\lambda^2}{6}\right], \tag{1.1}$$

where λ_t is Yukawa coupling of top quark with the Higgs boson, g is the $SU(2)_L$ gauge coupling, λ is the Higgs self-coupling. The above expression clearly shows quadratically divergent behavior with respect ot the cut-off scale (Λ), if we choose Λ to be the GUT scale ($\sim 10^{16}$ GeV) or the Planck Scale ($\sim 10^{19}$ GeV). It requires a fine-tuning of the order of $10^{-14} - 10^{-17}$ of the couplings in order to get the required Higgs mass of 125 GeV. The problem of fine-tuning arises because of the hierarchy between the EW scale and the scale of new physics. This difficulty is popularly known as hierarchy problem and the SM is blind to this issue.

5. Gravity -: The SM is constructed on the basis of a flat space-time, so there is no intention of including gravity in its domain. On the other hand, there are recent development in the elementary particle dynamics to include gravity at EW scale, assuming higher spatial dimension.

It is a fact that the nature has different scales and the SM is not constructed to explain the dynamics in the entire range of energy. The physics beyond the SM (BSM) can be probed through presence of new particle(s) or through the influence of the BSM dynamics in the interactions of the SM particles. The latter can be established through precise measurement of the couplings.

The top quark presents an ideal place to perform these studies. For example, being the heaviest of all elementary particles, it couples the strongest to the Higgs boson. Any new physics effect related to Higgs couplings is expected to show up in its interactions with the top quark. Similarly gauge couplings especially the neutral gauge couplings and possible flavor changing couplings of the top quark can illuminate possible new dynamics. Below we discuss the SM interactions of top quark, including its productions and decay measurements at colliders including small notes on its polarization measurement. Further we discuss the FCNC interactions in the top quark sector, which is the main focus of the thesis.

1.1 Brief Introduction to TOP quark

The top quark is the heaviest fundamental particle within the SM of particle physics. Experimental conformation of its mass by TeVatron and later by LHC sets top quark to be the most massive among the known fundamental particles. Although the top quark is as heavy as a gold atom; it seems to behave as a point like particle. So far the TeVatron and LHC results are in accord with expectations and predictions of top quark properties within the SM of particle physics [4]. The mass of this particle has already been precisely measured by different groups at both TeVatron and LHC. But other properties like production and decay dynamics could however, not been investigated in great detail so far. In view of its large mass, the top quark can be an excellent probe of the mechanism that breaks the electroweak gauge symmetry and therefore play a key role in clarifying the nature of the interactions responsible for this phenomenon. The top quark is also a good probe for possible new parity-violating and/or non-SM CP-violating interactions [5]. So far, experimental data are consistent with the SM prediction that $t \to Wb$ is the dominant mode but its branching ratio and the structure of the tbW vertex has to be measured with high accuracy.

Including the above properties and any signature of New Physics (NP) if present in the top quark sector will be in the focus of the future experiments at High Luminosity LHC (HL-LHC).

Let us begin the discussion with the top quark mass measurement by TeVatron and LHC. At each of the high energy particle colliders starting from its discovery to till date the different group consider the different final states into account to calculate the top quark mass with theory and experimental errors to it. The combination of results of TeVatron for $\sqrt{s} = 1.96$ TeV and LHC for $\sqrt{s} = 7$ TeV, measures its mass to be $m_t = 173.34 \pm 0.27\ (Sta) \pm 0.71\ (Sys)$ [6]. The latest top quark mass measurement from ATLAS for $\sqrt{s}$ =8 TeV with $\mathcal{L} = 20.2\ fb^{-1}$, sets $m_t = 172.08 \pm 0.39\ (stat) \pm 0.82\ (syst)\ GeV$ [7].

The top quark has a mass above the Wb threshold, and due to the fact that $\mid V_{tb} \mid \gg \mid V_{td} \mid, \mid V_{ts} \mid$, the decay width of the top quark is expected to be dominated by the two-body decay channel $t \to Wb$ with $W-$boson being on-shell. Section 1.1 shows the Feynman diagram and the SM vertex factor of the top quark decay width at the tree level.

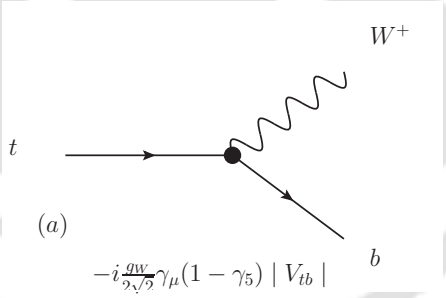

In fact the SM predicts that, the top quark decay almost exclusively into this mode. The other decay modes $t \to dW^+$ and $t \to sW^+$ are strongly CKM suppressed and are therefore negligible. Assuming unitarity of the three-generation CKM matrix one obtains $|V_{td}| = 8.74^{+0.26}_{-0.37} \times 10^{-3}$ and $|V_{ts}| = (40.7 \pm 1.0) \times 10^{-3}$ [8].

The top quark decay rate, including first order QCD corrections, is given by,

$$({\Gamma_t}^{SM})_{@NLO} = \frac{G_F {m_t}^3}{8\pi\sqrt{2}} |V_{tq}|^2 \left[1 - \frac{{M_W}^2}{{m_t}^2}\right]^2 \left[1 + 2\frac{{M_W}^2}{{m_t}^2}\right] \left[1 - \frac{2\alpha_s}{3\pi} f(y)\right] \qquad (1.2)$$

where, $y = (M_W/m_t)^2$ and $f(y) = 2\pi^2/3 - 2.5 - 3y + 4.5y^2 - 3y^2 \ln y$. This leads to $({\Gamma_t}^{SM})_{@NLO} = 1.31$ GeV while the experimental value is $\Gamma_t = 2.00^{+0.47}_{-0.43}$ GeV [9].

This leads to an extremely short life time of the top quark of the order $\mathcal{O}(10^{-25})$ sec. The top quark not forming bound state lies on the fact that its average life time is at least an order of magnitude smaller than the hadronization time, i.e.,

$$\tau_{had} \simeq \frac{1}{\Lambda_{QCD}} \approx 3 \times 10^{-24} sec, \tag{1.3}$$

which characterizes the minimum time required for an quark or anti-quark produced in some reaction to combine with other quark(s)/anti-quark(s) to form a color-neutral hadron.

The characteristics of the top quark unable to form top mesons ($t\bar{q}$) or baryons (tqq'), makes the top quark unique among the known quarks; as it gives an handle to study the properties of a bare quark. One of the advantage being free from strong interactions after its production and subsequent decay through the dominant decay mode ($t \to Wb$), which preserves the spin or polarization of the top quark. Thus its properties may be able to give insight into the spin or polarization of a bare quark in general. For this purpose we try to study the dynamics of the top quark decay particles. The angular distributions of the particles coming out of the top quark decay are sensitive to its polarization and consequently its production mechanism [10]. The detail explanation can be found in Chapter 2 of the thesis.

1.1.1 TOP Quark Productions Theory and Experiments

In this section the top quark pair productions and single top quark productions at TeVatron and LHC are discussed.

The experimental finding states that at the TeVatron, about 85% of $\sigma(t\bar{t})$ is due to $q\bar{q}$ annihilation and 15% is due to gg processes; whereas at LHC, 90(80)% is due to gg fusion at $\sqrt{s}$ =14 TeV (7 TeV) respectively and the rest due to $q\bar{q}$ annihilation [11]. At energies close to the kinematic threshold, ($s = 4{m_t}^2$), $q\bar{q}$ annihilation is the dominant process, if the incoming quarks are valence quarks. At higher energies, the gg-fusion process dominates for both $p\bar{p}$ and pp colliders. Hence the dominating channel for top pair production at LHC is due to gluon fusion.

At the TeVatron or LHC, the top quark can be produced singly via electroweak interactions involving the Wtb vertex. The Feynman diagrams corresponding to them are shown in figure Fig. 1.2. The production is categorized into three modes, *viz.,* (i) t-channel, (ii) s-channel and (iii) Wt-associated production. We consider $q = u, c$ as up-type and $q' = b, d, s$ as down type quarks.

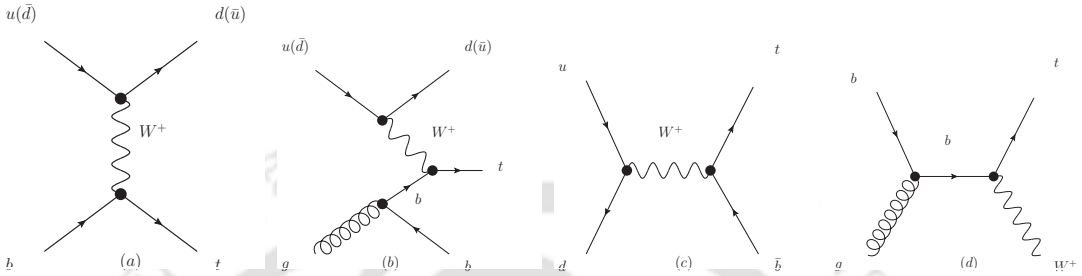

FIGURE 1.2: Feynman diagrams for the three top quark production modes via $q\bar{q}$ or gq initial state. Fig (a) and (b) show the t-channel diagrams, (c) shows the s-channel process, and (d) shows the Wt associated production channel.

I. The **t-channel** process($qb \to q't$) is possible at the TeVatron/LHC via the mediation of virtual W boson. Feynman diagrams representing this process are shown in Fig. 1.2(a),(b). The t-channel is the dominant source of single top quark production at the TeVatron and LHC both. The combined t-channel cross sections from ATLAS and CMS is 67.5 ± 5.7 pb and 87.7 ± 5.8 pb at $\sqrt{s}$=7 and 8 TeV colliders respectively [12].

II. The **s-channel** process at colliders($q\bar{q}' \to t\bar{b}$) shown in Fig. 1.2(c) is of "$Drell - Yan$" type and also called $t\bar{b}$ production channel. A time-like W-boson with ($Q^2 \geq (m_t + m_b)^2$) is produced by the fusion of two quarks. The combined ATLAS and CMS study sets the cross section to 4.9 ± 1.4 pb at $\sqrt{s}$=8 TeV [12].

III. The **associated production** of single top quark with a real W-boson requires $Q^2 = {M_W}^2$. The Feynman diagram for the process is shown in Fig. 1.2(d). The cross section is negligible at the TeVatron, but it is of considerable size at LHC energy where associated Wt-production cross section even more than the s-channel process. The combined searches from ATLAS and CMS sets cross section for tW process to be 16.3 ± 5.7 pb and 23.1 ± 3.6 pb at $\sqrt{s}$=7 and 8 TeV respectively [12]. From the ATLAS experiment alone the cross section is measured to be $94 \pm 10\ (stat.)\ ^{+28}_{-22}\ (syst.)\ \pm 2(lumi.)$ pb for the $\sqrt{s}$=13 TeV[13].

The s- and t-channels production processes can be separated kinematically. This is of particular interest because potential physics Beyond SM like, 4th generation quarks, heavy W/Z, FCNC or Charged Higgs boson would affect s- and t-channels differently [14].

A number of excellent reviews of hadronic top quark production and decay from the TeVatron and LHC are available in the literature. Coming to proposed colliders with electron(s) in its initial state, like the Large Hadron Electron Collider (LHeC) for electron-proton collision, the International Linear Collider (ILC) for electron-positron collision, both can have distinct single top channel(s) at tree level, which are possible only through FCNC interactions at the tree level of production. This provides unique possibility to study these channels as possible BSM signature including FCNC searches. The main focus of this thesis is to explain this potential to understand the possibilities in FCNC interactions of the top quark like tqZ, $tq\gamma$ and tqg, where $q = u, c$ quark. In this exposition the top quark physics perspectives at the proposed future colliders, such as LHeC and ILC will be discussed from a phenomenological point of view, in a model independent way with the help of effective FCNC couplings in the top quark sector.

1.1.1.1 Access to Top Quark Polarization

In the leading order, without any radiative corrections to the top quark decay width and in the limit of massless $b-$quark one can have three possibilities of $W-$boson helicity form factor : $\mathcal{F}_L$(longitudinal), $\mathcal{F}_+$(transverse-plus) and $\mathcal{F}_-$(transverse-minus). The contributions from different W-boson helicity fractions can be calculated from the decay rate of the top quark as [5]

$$\mathcal{F}_L : \mathcal{F}_+ : \mathcal{F}_- = \frac{m_t^2}{m_t^2+2M_W^2} : 0 : \frac{2M_W^2}{m_t^2+2M_W^2}$$

The W-bosons with positive helicity are forbidden in top-quark decays due to angular momentum conservation, assuming $m_b = 0$. With the central value of the parameters $m_t \simeq 173\ GeV$ and $M_W \simeq 80\ GeV$, we have $\mathcal{F}_L : \mathcal{F}_+ : \mathcal{F}_- = 0.7 : 0 : 0.3$. The experimentally extracted LHC data for $\sqrt{s}$=8 TeV, shows that the longitudinal, left- and right-handed polarization fractions are $\mathcal{F}_L = 0.709 \pm 0.019$, $\mathcal{F}_- = 0.299 \pm 0.015$ and $\mathcal{F}_+ = -0.008 \pm 0.014$, which is the most precisely measured W-boson polarization fractions to date [15].

In both longitudinal and transverse-minus cases the W^+ couples solely to $b-$quarks of left-handed chirality, which translates into left-handed helicity, since the $b-$quark is effectively massless compared to the energy scale set by m_t. If the b quark is emitted anti-parallel to the top-quark spin axis, the W^+ must be longitudinally polarized, i.e., helicity of W-boson is $h_W = 0$, to conserve angular momentum, which is shown in Fig. 1.3. If the $b-$quark is emitted parallel to the top quark spin axis, the W^+ boson has helicity $h_W = -1$ as shown in the figure.

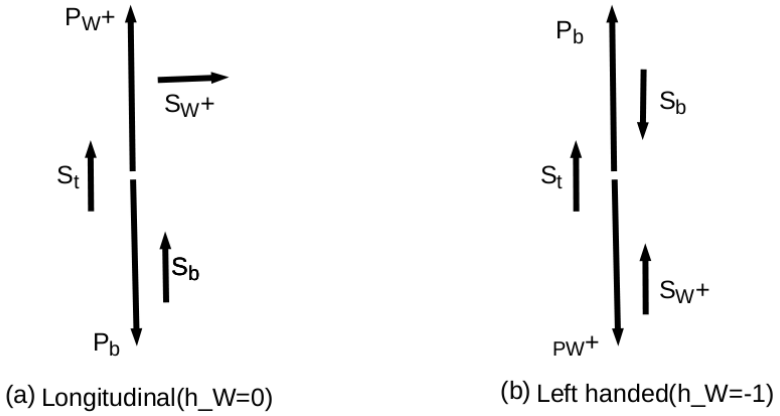

FIGURE 1.3: Fig (a) and (b) shows the two possibilities of W^+-helicity which conserves angular momentum in case of top quark decay.

The above predictions at tree level are marginally changed from these values, if we take the value of b-quark to be massive. The calculated value from NLO+NNLO in QCD for top quark [16] predicts that the value changes marginally with $\mathcal{F}_+ = \mathcal{O}(10^{-3})$, which is very much in accordance with the experimental finding as mentioned in the literature.

If any measurements reveal a significantly different value, it will be a clear indication of NP. In the case of $t \to Wb$, the top quark helicity can dictate the angular distributions of the lepton from $W-$boson decay [17, 18, 10]. The top helicity on the other hand depends on the production vertex. Thus assuming standard decay modes, we can infer the information about the interactions at the top quark production, through the angular distributions of the decay lepton. We shall make use of these observables in the analysis to understand the *Lorentz Structure* of the FCNC production vertex of the top quark.

1.2 FCNC in Top Quark Sector

The flavour dynamics in the SM is dictated by the so-called Cabibbo-Kobayash-Maskawa (CKM) matrix [19, 20, 21]. In short, this allows quarks of different generations to couple directly to the charged weak gauge boson, W. It arises due to the fact that the physical eigenstates (in the broken phase of the electroweak symmetry) are a mixture of the gauge eigenstates of different flavours. This allows top quark to couple to all the down type quark, the bottom quark, the strange quark and the down quark directly along with the charged W. CKM matrix in the SM has certain precise properties. For example, its unitarity relates the elements to each other. Deviations from these predicted properties are clear indications of dynamics beyond the SM. On the other hand, the neutral current interactions of quarks within the SM are flavour conserving at the tree-level. The celebrated GIM (Glashow-Iliopoulos-Maiani) mechanism [22] disallows any such possibility.

Thus, within the SM all decay modes other than $t \to Wb$ are rare, due to the CKM suppression factor in case of $t \to Wd$ or $t \to Ws$ having branching ratios of the $O(10^{-3})$ or less as discussed earlier. Consideration of BSM in the top quark sector can (i) change the tWb coupling and/or (ii) add new channels/exotic decay modes, which can change the decay width itself. One such possibility is to have FCNC couplings in the top quark sector.

The FCNC interactions of the top quark within the strict context of the SM are known to be extremely rare. The FCNC processes at tree level in the top quark sector are : $t \to qX^0$; where $X^0 = \gamma,\ Z,\ g,\ h$ and q=u, c quark. At higher order, they are disfavored within the framework of the SM because of the smallness of the diagonal CKM parameters appear in the loop calculation and the GIM mechanism to such an extend that any experiment(s), present and foreseeable, can measure. For instance, the branching fractions of FCNC processes at one loop level like $t \to Zu(c)$, $t \to \gamma u(c)$ and $t \to gu(c)$ are of the order of $10^{-17}(10^{-14})$, $10^{-16}(10^{-14})$ and $10^{-14}(10^{-12})$, respectively [23, 24]. Fig. 1.4 represents one such SM process.

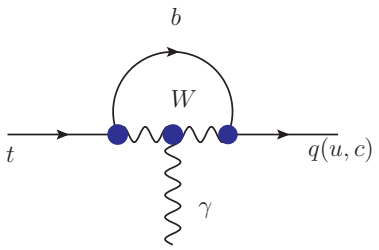

FIGURE 1.4: One loop FCNC process for $t \to q(u,c)\gamma$ within SM.

On the other hand, large presence of such FCNC interactions are part of many BSM scenarios, thus giving a clear handle to probe signatures of new physics at the collider experiments. They are hopelessly undetectable at the TeVatron and LHC due to huge QCD backgrounds and also for the case in the HL-LHC or HL_HE-LHC. Therefore, if a few of these events eventually show up in the future collider(s), we will have certainly discovered new physics.

With this motivation let us look at some of the beyond SMs which predict much better branching ratios to the FCNC's in top quark sector.

The Two Higgs Doublet Model(2HDM) -: This model is one of the simplest extensions of the SM, with an additional Higgs doublet to the SM. One of the primary motivations of the model is to explain fermion mass hierarchy within the SM. In the 2HDM, the up-type and down-type quark get masses from two different doublets, which typically address the hierarchy in more natural way. The enhanced value of $t \to Hq$ leads to the prediction that $\mathcal{B}(t \to qV) = \mathcal{O}(10^{-6})$, where $V = \gamma,\ g,\ Z - boson$ [25]. Below Fig. 1.5, represents one such diagram.

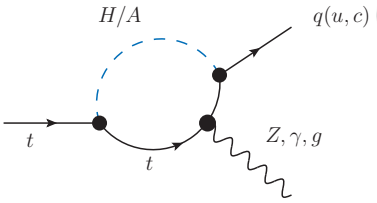

FIGURE 1.5: FCNC process for top quark in Two Higgs Doublet model. H and A are the new scalar and pseudo-scalar of the 2HDM.

The MSSM -: The minimal supersymmetric standard model(MSSM) [26, 27] is the minimal extension of standard model with the incorporation of super-symmetry. In Fig. 1.6 we have shown one such process of FCNC in top quark.

The $\mathcal{B}(t \to qV) = \mathcal{O}(10^{-7} - 10^{-5})$ [28, 29] for two different sets of benchmark value to MSSM parameter space.

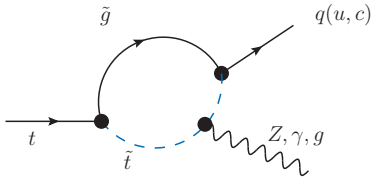

FIGURE 1.6: Feynman diagram for FCNC process for top quark in SUSY models. The $\tilde{g}$ is the fermionic partner of the gluon and $\tilde{t}$ is the scalar partner of the top quark.

The non-minimal extension of SUSY as well features the FCNC's within the quark sector.

Other Models -: Besides the above mentioned models, several other alternatives are proposed to accommodate physics beyond the SM. Among these, the most fascinating ones are the models related to Extra Dimensions (ExD) [30], which explain the hierarchy problem by bringing down the scale of gravitational interactions to the EW-scale. The idea of ExD comes from string theory. Though the presence of ExD is unclear, still the search for ExD is an alive option for experiments. Like the extension of Higgs sector of SM, extended gauge models(EGMs)[31] are also available in the market. These models not only lead to the existence of new gauge particles but also require the existence of new exotic fermions. Another popular choice among the theorists is the models those depend on dynamical symmetry breaking which can be found from [32]. All the models predict enhanced BR of FCNC decay of the quark.

For completeness we present a table showing enhanced FCNC limits on $\mathcal{B}(t \to Zq)$ calculated within different BSMs below.

Model:	SM	QS	2HDM	FC2HDM	MSSM	RPV SUSY	RS	EMF
$\mathcal{B}(t \to Zq)$:	10^{-14}	10^{-4}	10^{-6}	10^{-10}	10^{-7}	10^{-6}	10^{-5}	10^{-6}

TABLE 1.1: FCNC limits on $\mathcal{B}(t \to q(u,c)Z)$ in various BSMs.

None-the-less, some of the phenomenological studies on the production of single top quark has been carried out at different colliders. Some of which are in line with our study. For instance, a study at HERA for the process $e^- p \to e^- t$ via

tuZ interaction reveals that the cross section for $\kappa_{ut} = 0.1$, with $\Lambda = m_t = 175$ GeV and $\sqrt{s} = 318$ GeV is $\sigma^{eu\to et}_{NNLO-NLL} = 0.64^{+0.05}_{-0.04}$ pb [33]. The theoretical error comes from the scale variation from $m_t/2$ to m_t. At FCC-ee the single top quark production was performed to probe $tq\gamma$ and tqZ couplings in three different CM energies of 240, 350, 500 GeV via signal $e^-e^+ \to Z/\gamma \to t\bar{q}(\bar{t}q)$ [34]. It was shown that with 300 fb^{-1} integrated luminosity the FCC-ee would able to exclude branching ratios above $\mathcal{O}(10^{-4} - 10^{-5})$ which corresponds to couplings of the order at $\mathcal{O}(0.01 - 0.001)\%$.

1.2.1 FCNC limits from Experiments

In Table 1.2, we present the current limits and the projection on the BR of top quark FCNC at LHC (8 and 13 TeV), HL-LHC (14 TeV and 3 ab^{-1} of luminosity) and HL_HE-LHC (27 TeV and 15 ab^{-1}) searches at 95% C.L.

BR limits on 95% C.L.	8/13 TeV	3 ab^{-1}, 14 TeV	15 ab^{-1}, 27 TeV
$t \to gu$	$4.0(20) \times 10^{-5}$ [35]	3.8×10^{-6} [36]	5.6×10^{-7} [36]
$t \to gc$	..	32.1×10^{-6} [36]	10^{-7} [36]
$t \to Zq$	$1.7(2.4) \times 10^{-4}$ [37]	$2.4 - 5.8 \times 10^{-5}$ [38]	
$t \to \gamma u$	0.016(0.182)% [39]	8.6×10^{-6} [40]	
$t \to \gamma c$	..	7.4×10^{-5} [40]	
$t \to Hq$	–	10^{-4} [38]	

TABLE 1.2: The second and third column represents value of the BR of top quark for LHC(Run I, II). Projected limits on the BR for anomalous flavor changing top couplings at HL-HE LHC are presented in the third and fourth column. All limits are for the 95% C.L.

Taking into consideration all the experimental observations as discussed, we proceed to perform a phenomenological study for the e^-p and e^+e^- collider in three different chapters of the thesis. To understand the phenomenon at these colliders, we choose the model independent approach with the help of SM Effective Field Theory (SMEFT). The effective Lagrangian is accommodated with the FCNC interactions of the top quark with up and charm quarks of the SM. Below we have discussed the Lagrangian in details.

1.2.2 Effective Field Theoretical approach to FCNC Top Physics

While specific NP models with clear motivations are indeed more interestingly framed on purely theoretical point of view. On the other hand, the effects of BSM can be addressed in a phenomenological sense through the Effective Field Theory (EFT) approach. In the EFT, effects of NP are introduced through operators, defined purely in terms of the SM fields. The BSM dynamics is encoded in the coefficients of these operators. Unlike fully renormalizable gauge theories, operators of more than 4-dimensions can be accommodated here. For an elaborate description of the EFT, we refer reader to read Ref. [41, 42, 43, 44].

The phenomenon of the NP at high energy scale Λ can be described by an effective Lagrangian at the low scale. The effective Lagrangian can accommodate higher dimensional operators, which can be written as,

$$\mathcal{L}_{\text{eff}} = \mathcal{L}^{(4)} + \frac{1}{\Lambda}\mathcal{L}^{(5)} + \frac{1}{\Lambda^2}\mathcal{L}^{(6)} + \cdots , \tag{1.4}$$

where $\mathcal{L}^{(n)}$ consists of operators of dimension n made of the SM fields obeying $SU(2)_L \otimes U(1)_Y$ gauge invariance. The dimension 6 operators in the $\mathcal{L}^{(6)}$ can be parameterized as the coefficients of the effective γ^μ and $\sigma^{\mu\nu}q_\nu$ interactions for the on-shell top quark in the production or decay process. The measurement of these anomalous couplings directly gives us the opportunity to understand the properties of the NP.

In the rest of this section, we shall restrict ourself in describing the FCNC's in the top quark sector with the neutral gauge bosons of the SM. The complete Effective Lagrangian governing the top quark FCNC processes with the SM Gauge bosons is given by [44],

$$\begin{aligned} -\mathcal{L}_{\text{fcnc}} =& g_s\bar{q}\lambda^a\frac{i\sigma^{\mu\nu}q_\nu}{\Lambda}(\kappa^L_{gqt}P_L + \kappa^R_{gqt}P_R)tG^a_\mu \\ &+ e\bar{q}\frac{i\sigma^{\mu\nu}q_\nu}{\Lambda}(\kappa^L_{\gamma qt}P_L + \kappa^R_{\gamma qt}P_R)tA_\mu \\ &+ \frac{g}{2c_W}\bar{q}\gamma^\mu(X^L_{zqt}P_L + X^R_{zqt}P_R)tZ_\mu \\ &+ \frac{g}{2c_W}\bar{q}\frac{i\sigma^{\mu\nu}q_\nu}{\Lambda}(\kappa^L_{zqt}P_L + \kappa^R_{zqt}P_R)tZ_\mu + \text{H.c}, \end{aligned} \tag{1.5}$$

where $q_\nu = p_t - p_q$, is the momentum transfer between the quarks in the process, and Λ is the cut-off scale. The vector couplings are denoted by $X_{zqt}^{L,R}$ for $Z-$boson and the tensor couplings by $\kappa_{gqt}^{L,R}$, $\kappa_{\gamma qt}^{L,R}$ and $\kappa_{zqt}^{L,R}$ for gluon, photon and $Z-$boson involved processes, respectively. New physics contributions to the Effective Lagrangian in Eq. (1.5) can enhance the rates of top FCNC productions or decays by several orders of magnitude, giving observable BR's in some regions of parameter space. In the thesis we discuss the situation at high energy future colliders.

With the NP couplings in hand, let us calculate the decay width of the FCNC processes of the top quark. In the Fig. 1.7, we have shown few such processes of the top quark.

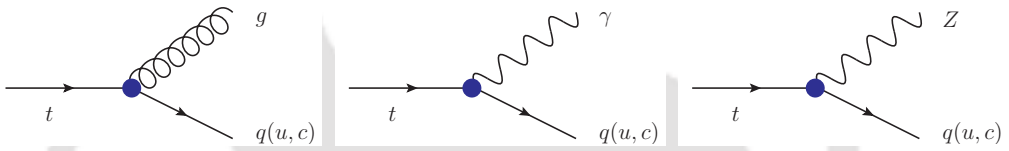

FIGURE 1.7: Non-standard FCNC vertices in top quark sector.

The decay width of the top quark governed by the Lagrangian in Eq. (1.5), assuming the presence of one of the NP couplings at a time, is given by [45],

$$\Gamma_T(t \to q\gamma) = \frac{\alpha}{2}|\kappa_{\gamma qt}^{L,R}|^2 \frac{m_t^3}{\Lambda^2}, \tag{1.6}$$

$$\Gamma_V(t \to qZ) = \frac{\alpha}{32 s_W^2 c_W^2}|X_{zqt}^{L,R}|^2 \frac{m_t^3}{M_Z^2}\Big[1 - \frac{M_Z^2}{m_t^2}\Big]^2\Big[1 + 2\frac{M_Z^2}{m_t^2}\Big], \tag{1.7}$$

$$\Gamma_T(t \to qZ) = \frac{\alpha}{16 s_W^2 c_W^2}|\kappa_{zqt}^{L,R}|^2 \frac{m_t^3}{\Lambda^2}\Big[1 - \frac{M_Z^2}{m_t^2}\Big]^2\Big[2 + \frac{M_Z^2}{m_t^2}\Big], \tag{1.8}$$

$$\Gamma_T(t \to qg) = \frac{2\alpha_s}{3}|\kappa_{gqt}^{L,R}|^2 \frac{m_t^3}{\Lambda^2}, \tag{1.9}$$

where, Γ_V and Γ_T represents the decay width involving either a vector or a tensor coupling, respectively.

1.3 Future Colliders and their Advantages

The advancement of the high energy colliders proved to be boon for Physics beyond the SM. As per the current knowledge of data from LHC, no new particle

has been discovered. It seems that the new particle(s) are heavier than the reach of LHC to discover or we may need better techniques to disentangle signal from background. The better could be expected further at HL-LHC.

Coming to the detailed and precise measurement of the couplings, the experiments performed earlier at the TeVatron and now at the LHC have failed to give us any interesting observation of FCNC sector. Some of the difficulties arises due to the presence of huge and unwanted backgrounds, which cover the tiny signal in most of the cases. But it is more or less clear that for the study of such rare processes, we need a cleaner environment than the higher energy frontiers.

As mentioned earlier, colliders with electron beams are at advantage here. Firstly, unlike LHC, single top production is not possible at ILC without top FCNC interactions. In the case of the proposed LHeC, the single top quark production is possible in association with an electron flavored neutrino through the t-channel process, mediated by a W-boson, while the FCNC process will be through a neutral current interactions in association with an electron, in the final state. The latter requires that the production of top quark via tqZ or $tq\gamma$ FCNC vertices.

The **LHeC** proposed to have electron beam of energy of $E_e = 60$ GeV, along with the available proton beam of energy $E_p = 7$ TeV [46]. It would provide a center of mass energy of $\sqrt{s} \approx 1.3$ TeV for the machine. The LHeC would have advantage over the LHC or the Future Circular Collider for proton-proton (FCC-pp) [47] due to the fact that,

- it provides a clean environment with suppressed backgrounds from strong interaction processes and free from issues like pile-ups, multiple interactions, which are plenty at LHC,
- with an electron in its initial state, such machines are known for high precision measurements of the dynamical properties of the proton allowing simultaneous tests of EW and QCD effects.
- nonetheless the collider will have asymmetric initial states, providing handle to disentangle the forward and backward scattering.

A detailed report on the physics and detector design concepts can be found in the Ref. [46].

The **ILC** [48] on the other hand is a linear collider for polarized e^-e^+-beam. The initial run for ILC is proposed to have c.m. energy of 250 GeV. The collider is suitable for study of particle physics phenomena in cleaner environment than any other collider running today or proposed to be built in future. Most of the ILC studies focus on Higgs couplings measurement through ZH or $\nu\nu H$ production which are within the reach of c.m. energy of 250 GeV. On the other hand the study of top quark is minimized due to insufficient c.m. energy available to produce it, within the SM mechanism. The c.m. available to the initial run of ILC is not sufficient to produce $t\bar{t}$-pair, nevertheless the single top quark production at the lowest leading order is not possible with the e^+e^- initial state. However, if the NP allows FCNC interactions through the γ or Z-boson we can certainly produce an on-shell single top quark along with a light quark jet. Except cleaner environment, one of the major advantage of this collider lies in the fact that both the beams can be polarized to a certain value, which could be useful in the study of NP interactions.

As discussed in the previous sections, we shall focus our attention in understanding the top quark FCNCs through different processes at the LHeC as well as the ILC. We shall adopt a model independent study with the help of FCNC effective couplings like tZq, $t\gamma q$ and tgq, parameterized in terms of 4-D and 5-D operators involving the corresponding fields Eq. (1.5). We shall develop methodology to distinguish different types of couplings. Unlike the analysis typically carried out by the LHC experiments, we shall consider presence of multiple variables to obtain simultaneous limits on the couplings.

1.4 Outline Of Chapters

A brief outline of the chapters in the thesis are the following.

In **Chapter 2**, the purpose is to discuss tools including necessary theoretical framework, analysis techniques and software used in detail. The various tools including model file used for the study of FCNC processes involving the top quark, the event generator, detector simulator and the analysis softwares for the study are introduced in brief. This chapter also helps the reader to set the tone for further reading with a better understanding of the rest of the thesis.

In **Chapter 3**, we present a study of the top quark FCNC interactions with the Z-boson in the proposed LHeC of beam energies, $E_{e(p)} = 60$ (7000) GeV. Contrary to LHC searches where the decay of the top quark processes are via FCNC interactions, we consider the production of the top quark itself via the FCNC vertex. For the analysis, we consider the effective theory where the anomalous FCNC couplings are of vector and tensor in nature. The effect of these couplings is probed in the single top production along with the scattered electron via the t-channel process ($e^- p \to e^- t$). The polar angle of the electron in the lab frame, along with the top quark polarization asymmetries constructed from the angular distribution of the secondary lepton (arising from the top decay), calculated in the top quark rest frame allows to distinguish the Lorentz structure of the coupling. We conclude the chapter with the multi-parameter statistical analysis by considering the cross section and asymmetries values used to set limits on the NP couplings. Our study shows that a reach of $\mathcal{O}(10^{-2})$ in the case of Ztu and Ztc couplings at an integrated luminosity of 2 ab^{-1} at 95% C.L can be obtained, assuming presence of all NP couplings simultaneously.

In **Chapter 4**, we try to emphasize the possibility of single top quark production at Run I of the ILC with $\sqrt{s}$=250 GeV. The top quark physics has not drawn much interest in the ILC community due to the low c.m. energy available to it. We propose the production of single top quark along with a light quark jet, through top quark FCNC interactions at tree level. The only possible single top production process $e^- e^+ \to tj$, $(t \to \ell\nu_\ell b)$, with j=light quark jet is studied against a complete set of background processes provided by the ILD group at KEK, Japan. In the analysis we consider both possible polarization of the initial electron and positron beam along with the projected Luminosity. The significance of signal samples for different Lorentz structures, (tensor structure for the $tq\gamma$ and vector and tensor structure tqZ couplings) has been studied. We show that a significance of 2.7σ can be achieved through the leptonic decay of the produced top quark.

In **Chapter 5**, we complete our study with the strong FCNC interactions in the top quark sector through tqg-anomalous coupling along with the FCNC via $tq\gamma$ couplings. The process under study is considered at the FCC-he collider with beam energy $E_{e(p)} = 60$ $(50,000)$ GeV through the process of $e^- p \to e^- tj$, with j being a light quark jet. We have shown that this is the best process for the study of tqg vertex and can probe the couplings to the level of $\mathcal{O}(10^{-2})$ with moderate Luminosity.

In **Chapter 6**, we conclude with our remark on the *Study Of Single Top Quark FCNC Coupling at Future Colliders* with some of the future prospective along the line.

भारतीय प्रौद्योगिकी संस्थान गुवाहाटी
Indian Institute of Technology Guwahati

– Modern science follows three fundamental principles of scientific cognition, i.e., the principle of determinism, the principle of correspondence, and the principle of complementarity.

Book: Research Methodology

2

Software and Analysis Strategy

In this chapter, I will discuss various tools including softwares and techniques used in the projects during thesis work. For a collider study one requires a complete software framework including event generators, detector simulations, reconstructions and analysis tools. Moreover, simulation, reconstruction and analysis are independent applications which have to share a common detector geometry at run time to ensure their coherence. We discuss various asymmetries used in the projects, which are useful in distinguishing *Lorentz structure* of the couplings and hence sensitive to the polarization of the top quark. We discuss the technique used to get their numerical values towards the end of the chapter.

2.1 A Brief Summary of The Tools Used

We start with the MadGraph5 [49]; a *Monte Carlo* (MC) event generator used to produce event cross-sections with knowledge of the initial conditions of the beam energies at particle colliders. It is a framework which provides a common platform for various different packages to perform the duty. In the following I list out those packages.

The Helicity Amplitude subroutine (HELAS) [50] is part of the MadGraph5 used to generate the code for the evaluation of the matrix-elements based on Helicity amplitude formalism. The package called Automatic Libraries Of Helicity Amplitudes (ALOHA) [51] writes the Feynman rules for quantum field theory Lagrangian. MadEvent [52] allows the computation of the cross-section at

leading-order (LO) accuracy as well as the generation of events. The model file called the Universal FeynRules Output (UFO) [53] is used to incorporate the dynamics as dictated by the specific Lagrangian and/or model used. If instructed aMC@NLO [49] can allow us to simulate processes at next-to-leading order (NLO) accuracy in QCD. Other specific modules like MadSpin [54] is used to decay unstable particles with full spin-correlation, MadDarkMatter [55] is used to compute the relic density, MadWeight [56] is used to estimate the weights of the matrix element method, MadLoop [57] allows automatic one loop QCD corrections and MadWidth [58] allows automatically evaluate the width of all particles for a given set of input parameters.

We had performed out study in the context of the LHeC and FCC-he, both are $e^{-}p$ colliders and the ILC, an $e^{+}e^{-}$ collider. Different simulation and background events generation are adopted for these two colliders. For the LHeC and FCC-he, the details of the detector are yet to be finalized, whereas that of ILC is better established.

For the LHeC processes, the generated events (both signal and background) output by MadGraph5, were passed to a customized PYTHIA-PGS [59], to perform showering, fragmentation and hadronization on the events. The events thus generated are passed through FASTJET [60] for jet formation and DELPHES [61] to simulate the detector effects where an appropriately customised detector card being used. We adopted the detector card available with the LHeC working group and modified various parameters for particle identification, selection efficiency, isolation criteria for leptons. This was done in close discussion with the working group with valuable inputs from many members of the group. The detail of the detector is described in the Technical Detailed Report (TDR) for LHeC [46].

Similarly for the ILC, the concept of detector simulator for ILD is available in great detail. Most of the SM backgrounds generated with all collider and detector architector are available in ILD repository. We have made ample use of this in our study. The signal processes were generated with the MadGraph5 and passed the events to PYTHIA8 [62] for showering, fragmentation and hadronization. The events were then passed to MOKKA a GEANT4 [63, 64, 65] based detector simulation. The output of MOKKA/GEANT4 have the information of hits due to the passage of particles in various different parts of the ILD [66, 67]. The full simulation of background processes for ILC at 250 GeV is taken from the ILD group at KEK, Japan. Further the data from MOKKA/GEANT4 is passed to

Marlin [68, 69, 70, 71, 72] for reconstruction of particles/objects. The *Marlin* stands for *ModularAnalysis and Reconstruction for the LINear Collider* is a *C++* application framework for the analysis and reconstruction of LCIO(Linear Collider I/O) data. It consists of various software modules called the "Processor" which takes care of particle identification, Event selections, Particle Flow Algorithm, Jet clustering from the data collected after detector simulation. LCIO is a persistence framework and event data model for linear collider detector analysis studies. The Marlin framework uses a well defined geometry definition for reconstruction which is flexible with different detector concepts.

The output of the Delphes simulation (for LHeC and FCC-he projects) and Marlin simulation (for ILC project) are analyzed in the ROOT [73] framework in each of the cases differently. The MadAnalysis5 [74] is extensively used for analysis purpose for the LHeC and FCC-he projects.

We have used the UFO model file developed *in-house* encoding the $\mathcal{L}_{eff}$ as discussed in Section 1.2.2 of Chapter 1. For this purpose, the Mathematica based package called FeynRules-v2.0 [75] was used. We made use of Mathematica and FORM programming tools to calculate the analytical expressions for cross section, whenever necessary.

2.2 Analysis Strategy

The ultimate goal of physics analysis in collider phenomenology is to extract some signal from a usually swamping background, so that one could study the properties with better significance. The reconstruction and analysis software framework offers the possibility to tag a specific event sample as a background or the signal sample. This quantity is recomputed after each of the different selection cuts implemented by the user. With these pieces of information available, optimizing selection cuts consequently becomes easier, which allows us to investigate in a fast and efficient way whether a given signature could be observed at colliders or not. In the following, we discuss the analysis strategy used in probing polarization of the top quark produced.

Because the weak interaction violate parity, the collider processes that can involve the weak interactions typically exhibit asymmetries in various kind of distributions in the final state particles. Some of them are typically sensitive to the

interactions of particle and anti particle while other sensitive to left handed and right handed chirality/helicity. The specific choice of some of the asymmetries can give better handle to probe the *Lorentz structure* of the couplings as well. Thus these asymmetries can be used as sensitive observables in the NP interactions, which is discussed below for a generic point of view.

2.2.1 Top quark Polarization observables

In this section, we discuss method to extract the polarization observables of a spin-$\frac{1}{2}$ particle (top quark) in a generic production process from the distribution of its decay products. The polarization of the top quark depends on the nature of the production vertex. The angular distributions of the decay products give information of the top quark polarization. Partially integrating the angular distributions, one can construct several asymmetries to probe polarization of the top quark. Note that the angles of the leptons from the decay of top quark are reconstructed in the rest frame of the top quark. In the following we present a generic process of single top quark production along with a fermion(s) (either a light quark or lepton) and the subsequent semi-leptonic decay of the top quark. The leptons from top quark decay termed as secondary leptons. For details of the formalism one may consult Ref. [10, 18, 76].

Consider a process such as : $A + B \to tX \to b\ell\nu_\ell X$, with X being the associated fermion(s) in the production process. The cross section of the process is given by,

$$d\sigma_{\rm tot} = \frac{\overline{|\mathcal{M}|^2}}{F} d\Pi \tag{2.1}$$

where $F = \sqrt{[\hat{s} - (m_A + m_B)^2][\hat{s} - (m_A - m_B)^2]}$ is the flux and the phase space is given by,

$$d\Pi = \frac{d^3p_X}{(2\pi)^3 2E_X} \frac{d^3p_b}{(2\pi)^3 2E_b} \frac{d^3p_\ell}{(2\pi)^3 2E_\ell} \frac{d^3p_\nu}{(2\pi)^3 2E_\nu} (2\pi)^4 \delta^4(K_A + K_B - p_X - p_b - p_\ell - p_\nu) \tag{2.2}$$

where, K_A and K_B are the initial four momentum of particle A and B respectively. In the Narrow Width Approximation (NWA), we have the top quark propagator

factor,

$$\left|\frac{1}{p_t^2 - m_t^2}\right|^2 = \frac{\pi}{\Gamma_t m_t}\delta(p_t^2 - m_t^2) \tag{2.3}$$

and hence the invariant amplitude square of the full process can be written as a product of the production and decay density matrices in the helicity basis of the top quark as

$$\overline{|\mathcal{M}|^2} = \frac{\pi\delta(p_t^2 - m_t^2)}{\Gamma_t m_t}\sum_{\lambda,\lambda'}\rho(\lambda,\lambda')\Gamma(\lambda,\lambda') \tag{2.4}$$

where, p_t and m_t represent the four momentum and mass of the top quark produced with Γ_t being the total decay width of the top quark. The production and decay density matrices of the process are,

$$\rho(\lambda,\lambda') = M_P(\lambda)M_P^*(\lambda') \tag{2.5}$$

$$\Gamma(\lambda,\lambda') = M_D(\lambda)M_D^*(\lambda') \tag{2.6}$$

with λ, λ' the helicity indices of the top quark.

The total phase space can be separated in production and decay part for the process which is discussed in detail in Appendix C. The total differential cross section of the considered process at parton level is given by,

$$d\sigma_{\rm tot} = \sum_{\lambda,\lambda'} d\hat{\sigma}_{\rm prod}(\lambda,\lambda').\frac{1}{\Gamma_t m_t}.d\Gamma_D(\lambda,\lambda') \tag{2.7}$$

where,

$$d\hat{\sigma}_{\rm prod}(\lambda,\lambda') = \left[\frac{(2\pi)^4}{2F}\rho(\lambda,\lambda')\delta^4(K_A + K_B - p_X - p_t)\frac{d^3p_X}{2E_X(2\pi)^3}\frac{d^3p_t}{2E_t(2\pi)^3}\right]$$

and

$$d\Gamma_D(\lambda,\lambda') = \left[\frac{(2\pi)^4}{2}\Gamma(\lambda,\lambda')\delta^4(p_t - P_b - P_\nu - P_\ell)\frac{d^3P_b}{2E_b(2\pi)^3}\frac{d^3P_\nu}{2E_\nu(2\pi)^3}\frac{d^3P_\ell}{2E_\ell(2\pi)^3}\right] \tag{2.8}$$

where Γ_t represents the total decay width of the top quark, so that the BR($t \to Wb$)=$\frac{\Gamma_D}{\Gamma_t}$. The differential production cross section in the c.m. frame is given by,

$$d\hat{\sigma}_{\rm prod}(\lambda,\lambda') = \frac{\beta}{16\pi^2\hat{s}}\rho(\lambda,\lambda').d\hat{\Omega} \tag{2.9}$$

where $\beta = \sqrt{1 - \frac{4m_t^2}{\hat{s}}}$. The analytical expression of the $\rho(\lambda, \lambda')$ and $\Gamma(\lambda, \lambda')$ is calculated in Appendix C. The normalized production cross-section for different helicity combination of the top quark can be parametrized in terms of a 2×2 hermitian matrix as discussed below.

$$\frac{\hat{\sigma}_{\rm prod}(\lambda, \lambda')}{\hat{\sigma}_{\rm prod}} = \frac{1}{2}\begin{bmatrix} 1 + P_z & P_x - iP_y \\ P_x + iP_y & 1 - P_z \end{bmatrix} \tag{2.10}$$

Here (P_x, P_y, P_z) represents the components of the polarization vector ($\mathbf{P}$). Thus the polarization parameters are given by,

$$P_x = \frac{\hat{\sigma}_{\rm prod}(+,-) + \hat{\sigma}_{\rm prod}(-,+)}{\hat{\sigma}_{\rm prod}} \tag{2.11}$$

$$-iP_y = \frac{\hat{\sigma}_{\rm prod}(+,-) - \hat{\sigma}_{\rm prod}(-,+)}{\hat{\sigma}_{\rm prod}} \tag{2.12}$$

$$P_z = \frac{\hat{\sigma}_{\rm prod}(+,+) - \hat{\sigma}_{\rm prod}(-,-)}{\hat{\sigma}_{\rm prod}} \tag{2.13}$$

or,

$$\frac{\hat{\sigma}_{\rm prod}(+,+)}{\hat{\sigma}_{\rm prod}} = \frac{1}{2}(1 + P_z), \tag{2.14}$$

$$\frac{\hat{\sigma}_{\rm prod}(-,-)}{\hat{\sigma}_{\rm prod}} = \frac{1}{2}(1 - P_z), \tag{2.15}$$

$$\frac{\hat{\sigma}_{\rm prod}(+,-)}{\hat{\sigma}_{\rm prod}} = \frac{1}{2}(P_x + iP_y) \tag{2.16}$$

$$\frac{\hat{\sigma}_{\rm prod}(-,+)}{\hat{\sigma}_{\rm prod}} = \frac{1}{2}(P_x - iP_y). \tag{2.17}$$

The normalized decay density matrix elements for the process $t \to W^+ b \to b\ell^+\nu_\ell$ may be written in terms of the polar (θ_ℓ) and azimuthal (ϕ_ℓ) angles of the secondary lepton in the top rest frame as discussed in Appendix C,

$$\begin{aligned} \Gamma'(+,+) &= \frac{1}{2}(1 + \cos\theta_\ell), \\ \Gamma'(-,-) &= \frac{1}{2}(1 - \cos\theta_\ell), \\ \Gamma'(+,-) &= \frac{1}{2}\sin\theta_\ell e^{i\phi_\ell}, \\ \Gamma'(-,+) &= \frac{1}{2}\sin\theta_\ell e^{-i\phi_\ell}. \end{aligned} \tag{2.18}$$

where $\Gamma'(\lambda,\lambda') = \frac{\Gamma_D(\lambda,\lambda')}{\Gamma_t}$ is the fraction of BR of top quark for the particular combination of (λ,λ'). The above equations can be written in 2×2 matrix form. Thus the decay density matrix for the process $t \to W^+b \to b\ell^+\nu_\ell$ in the top quark rest frame is given by,

$$\Gamma'(\lambda,\lambda') = \frac{1}{2}\begin{bmatrix} 1+\cos\theta_\ell & \sin\theta_\ell e^{i\phi_\ell} \\ \sin\theta_\ell e^{-i\phi_\ell} & 1-\cos\theta_\ell \end{bmatrix} \tag{2.19}$$

Here θ_ℓ and ϕ_ℓ are the polar angle and azimuthal orientation of the final state fermion(b-quark or ℓ^+ or ν_ℓ), in the rest frame of top quark.

Combining the production and decay density matrices from Eqs. (2.10) and (2.19), the total rate for the process with top quark and $W-$boson to be on shell, is given by

$$\begin{aligned} \frac{1}{\sigma_{\rm tot}}\frac{d\sigma_{\rm tot}}{d\Omega} &= \frac{1}{4\pi}Tr\big[P(\lambda,\lambda')\Gamma'(\lambda,\lambda')\big] \\ &= \frac{1}{4\pi}[1+P_z\cos\theta_\ell + P_x\sin\theta_\ell\cos\phi_\ell + P_y\sin\theta_\ell\sin\phi_\ell], \end{aligned} \tag{2.20}$$

where $\sigma_{\rm tot} = \sigma_{\rm prod} \times {\rm BR}(t \to b\ell\nu)$ is the cross section of the entire process. This provides an effective handle for experimentally obtaining information about the top quark spin. Using partial integration of the differential cross section given in Section 2.2.1, with respect to θ_ℓ and ϕ_ℓ of the secondary lepton in the top quark rest frame, one can construct observables like asymmetries to get the value of the polarization parameters. The following asymmetries computed in the rest frame of the top quark are directly related to the top polarization.

$$\begin{aligned} A_x &= \frac{1}{\sigma_{\rm tot}}\int_{-1}^{1} d{\rm c}_{\theta_\ell}\left[\int_{-\frac{\pi}{2}}^{\frac{\pi}{2}} d\phi_\ell \frac{d\sigma}{d{\rm c}_{\theta_\ell}d\phi_\ell} - \int_{\frac{\pi}{2}}^{\frac{3\pi}{2}} d\phi_\ell \frac{d\sigma}{d{\rm c}_{\theta_\ell}d\phi_\ell}\right] \\ &= \frac{\sigma({\rm c}_{\phi_\ell}>0)-\sigma({\rm c}_{\phi_\ell}<0)}{\sigma({\rm c}_{\phi_\ell}>0)+\sigma({\rm c}_{\phi_\ell}<0)} \equiv \frac{1}{2}P_x, \end{aligned} \tag{2.21}$$

$$\begin{aligned} A_y &= \frac{1}{\sigma_{\rm tot}}\int_{-1}^{1} d{\rm c}_{\theta_\ell}\left[\int_{0}^{\pi} d\phi_\ell \frac{d\sigma}{d{\rm c}_{\theta_\ell}d\phi_\ell} - \int_{\pi}^{2\pi} d\phi_\ell \frac{d\sigma}{d{\rm c}_{\theta_\ell}d\phi_\ell}\right] \\ &= \frac{\sigma({\rm s}_{\phi_\ell}>0)-\sigma({\rm s}_{\phi_\ell}<0)}{\sigma({\rm s}_{\phi_\ell}>0)+\sigma({\rm s}_{\phi_\ell}<0)} \equiv \frac{1}{2}P_y, \end{aligned} \tag{2.22}$$

$$\begin{aligned} A_z &= \frac{1}{\sigma_{\rm tot}}\int_{0}^{2\pi} d\phi_\ell\left[\int_{0}^{1} d{\rm c}_{\theta_\ell} \frac{d\sigma}{d{\rm c}_{\theta_\ell}d\phi_\ell} - \int_{-1}^{0} d{\rm c}_{\theta_\ell} \frac{d\sigma}{d{\rm c}_{\theta_\ell}d\phi_\ell}\right] \\ &= \frac{\sigma({\rm c}_{\theta_\ell}>0)-\sigma({\rm c}_{\theta_\ell}<0)}{\sigma({\rm c}_{\theta_\ell}>0)+\sigma({\rm c}_{\theta_\ell}<0)} \equiv \frac{1}{2}P_z, \end{aligned} \tag{2.23}$$

where $s_{\theta_\ell} = \sin_{\theta_\ell}$, $c_{\theta_\ell} = \cos_{\theta_\ell}$, $s_{\phi_\ell} = \sin_{\phi_\ell}$ and $c_{\phi_\ell} = \cos_{\phi_\ell}$ in the above equations.

The value of the asymmetries are calculated numerically to understand (1) the polarization state of the top quark produced and (2) to set limits on the couplings due to its distinguishability potential to the types of couplings as well. In the following Section 2.2.1.1, we have discussed the procedure followed in the numerical calculation of the asymmetries.

2.2.1.1 Numerical Calculation of P_x, P_y and P_z

After the detector simulation the output has been written in a ROOT file format, which contains the information of transverse momentum(P_T), psudorapidity(η), azimuthal angle(ϕ) and energy(E) of the outgoing particles. The reconstruction of missing momentum and subsequently the top quark momentum is described in Appendix A for reference. With the reconstructed particles in hand, we calculate the numerical value of the asymmetries by the following steps. Note that the important point is to get the polar angle (θ_ℓ) and azimuthal angle (ϕ_ℓ) of the lepton in the top (anti) quark rest frame.

1 Identify $Z - axis$ as the initial direction of, the proton beam (in case of e^-p collider) or the electron beam (in case of e^-e^+ collider).

2 Get the reconstructed particles, top quark $[P_T(t),\ \eta_t,\ \phi_t,\ E_t]$ and lepton $[P_T(\ell),\ \eta_\ell,\ \phi_\ell,\ E_\ell]$ from the decay of W-boson.

3 Rotate $\ell^\pm$, along the $Z - axis$ through the negative of the azimuthal angle of the top quark $[-\phi_t]$. Then rotate the top quark itself by $[-\phi_t]$ along the $Z - axis$.

4 Further, rotate $\ell^\pm$ along the $Y - axis$ through negative of the polar angle of the top quark $[-\theta_t]$. Then rotate the top quark by $[-\theta_t]$ along the $Y - axis$,

5 Provide a negative boost (β_t) of the top quark to ℓ,

6 Now we have the parameters of the lepton as measured from the rest frame of the top quark. We measure the value of the azimuthal and polar orientation of the ℓ as θ_ℓ and ϕ_ℓ to calculate the value of the asymmetries as discussed in Eq. (2.23).

– My success will not depend on what A or B thinks of me. My success will be what I make of my work.

Homi J. Bhabha

3

Top quark FCNC interaction via tqZ couplings at LHeC

A study of the top quark *Flavor Changing Neutral Current* (FCNC) through Z-boson has been performed for the proposed future e^-p collider for the energy, $E_{e(p)} = 60$ (7000) GeV. We considered an effective theory where the anomalous FCNC couplings are of vector and tensor nature. The effect of these couplings is probed in the single top production along with the scattered electron. The polar angle θ of the electrons coming out of the primary vertex in association with the top quark polarization asymmetries constructed from the angular distribution of the secondary lepton arising from the top decay, allow to distinguish the Lorentz structure of the coupling. From a multi-parameter analysis, we obtain a reach of $\mathcal{O}(10^{-2})$ in the case of Ztu and Ztc couplings at an integrated luminosity of 2 ab^{-1} at 95% C.L.

3.1 Introduction

In the aftermath of the top quark discovery at the TeVatron, its properties like spin, charge, couplings with the other Standard Model (SM) particles etc. conform to the SM values. Further, the Large Hadron Collider (LHC) measured these values very precisely Ref. [77, 78]. All these measurements over the years have established the top quark as the most interesting chapter of the SM. Particularly, its mass around 173.1 GeV makes the top quark the heaviest among the SM

chapters and as a result allows it to decay much before the hadronization sets in. This behavior single it out from other known quarks and gives us a probe of new physics, Ref. [79, 80, 81, 82].

The FCNC processes (involving top quark) are completely absent at the tree level and barely show up, even at the one loop level. Due to the GIM (Glashow-Iliopoulos-Maiani) suppression Ref. [22], the SM predictions for the branching fractions of FCNC processes like $t \to Zu(c)$ and $t \to \gamma u(c)$ are of the order of $10^{-17}(10^{-14})$ and $10^{-16}(10^{-14})$, respectively Ref. [23]. Experiments performed earlier at the TeVatron and now at the LHC have failed to give us any interesting observation of FCNC. The bounds on such couplings from those experiments are very strong.

Here, we intend to study the possible BSM signature in the FCNC of the top quark sector in the proposed powerful high energy e^-p collider, the *Large Hadron Electron Collider* (LHeC). With a choice of electron energy of $E_e = 60$ GeV, along with an available energy of LHC proton of $E_p = 7$ TeV, it would provide a center of mass energy of $\sqrt{s} \approx 1.3$ TeV at the LHeC. Its design is such that the e^-p and pp colliders will operate simultaneously. Thus in addition to its advantages discussed in Section 1.3 of Chapter 1, it also provide a cost effective alternative to all the future proposed colliders.

This chapter is arranged as follows. In Section 3.2, we describe in detail the formalism used in this study. Section 3.2.1 describes the FCNC effect in the top quark sector through the Effective Field Theory (EFT) approach and its experimental status. In Section 3.2.2, we detail the mechanism to construct asymmetries specific to top quark, whereas Section 3.2.3 describes angular asymmetry of the primary electron. Section 3.3 gives the thorough analysis of the FCNC couplings from various aspects. Section 3.3.1 gives the cut-based analysis and various distributions. Section 3.3.2 gives the bounds arrived at form the multi-parameter analysis and likelihood analysis. Finally, we draw our inferences in Section 3.4.

3.2 Formalism

3.2.1 The Process

The most general effective Lagrangian describing interactions of the top quark with light quarks $q = u, c$ and Z boson allowing FCNC processes is described in Eq. (1.5) of Chapter 1, as,

$$\mathcal{L}_{Ztq} = -\frac{g}{2c_W}\bar{q}\gamma^{\mu}(X^{L}_{zqt}P_L + X^{R}_{zqt}P_R)t\ Z_{\mu} - \left[\frac{g}{2c_W}\bar{q}\frac{i\sigma^{\mu\nu}(p_t - p_q)_{\nu}}{\Lambda}(\kappa^{L}_{zqt}P_L + \kappa^{R}_{zqt}P_R)t\ Z_{\mu} + \text{h.c}\right], \quad (3.1)$$

where $(p_t - p_q)$ is the momentum transfer between the quarks in the process, and Λ is the cut-off scale, which we set as the top quark mass ($\Lambda = m_t$). The vector couplings are denoted by $X^{L,R}_{zqt}$ and the tensor couplings by $\kappa^{L,R}_{zqt}$. The choice of scale m_t is motivated from the minimum energy required to produce at least one *on-shell* top quark. As we can see the vector couplings are independent of Λ, whereas its effect on the tensor couplings can be derived easily by using the substitution $\kappa^{L,R}_{zqt} \to \kappa^{L,R}_{zqt}\, m_t/\Lambda$.

The single top-quark production process at $e^{-}p$ collider (a detailed study through charged-current top-quark production is performed in Refs. [83, 84]) enabled by these interactions is a t-channel exchange of Z boson coupling with the quarks and the leptons, $e^{-}p \to e^{-}t, (t \to W^{+}b, W^{+} \to \ell^{+}\nu_{\ell})$, where $\ell = e,\ \mu$, the Feynman diagram of which is shown in Fig. 3.1. We consider the leptonic decay of the top quark keeping in mind the spin-correlation study and the top polarization asymmetries that might be useful in the investigation of the Ztq anomalous couplings.

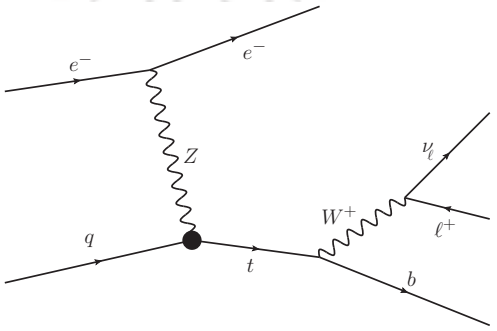

FIGURE 3.1: Signal processes: The Ztq anomalous vertex at production channel of top and decay of top via SM coupling vertex only. The final state charge lepton is ℓ^{+} in our study to make proper distinction between charged lepton (e^{-}) coming out of the $e^{-}Ze^{-}$-primary vertex and decay of the top it self.

Note that, there is no SM analogue of this process, thus we expect the backgrounds can be reduced without difficulty.

A few comments are in order before we get into the details of the analyses.

1. At the first look, the scattered electron (as opposed to the electron or muon produced in the W decay) is a spectator, not connected with the top quark production vertex. However, notice that the Z boson coupling to the top quark is sensitive to its state of polarization. This in turn can reflect in the polarization state of it, and consequently the angular distribution of the scattered electron. We shall exploit this situation in our analyses, and construct observables based on the kinematic distribution of the scattered electron.

2. The second observation is that the top quark polarization is directly affected by the nature of the coupling. That is, whether it is a vector coupling or a tensor coupling, and whether it couples to the left-handed or the right-handed quarks. It is well known that the spin information of the top quark will be carried forward to the decay products, and will be reflected in the angular and energy distribution of the secondary leptons. We shall make use of this fact in constructing multiple observables, a combination of which could discriminate the type of Ztq couplings.

In the following section we shall elaborate on the top quark spin analysis and various asymmetries making use of this information, which would be employed in the study.

3.2.2 Polarization of the top quark

As explained in the previous section, the motivation for the spin analysis of top quark comes from the fact that the angular distributions of top quark decay products give access to the Lorentz structure of the production vertex through the information of top quark polarization. The technique employed in this section is already explained in Section 2.2.1 of Chapter 1, for a generic $2 \to 2$ process at any collider.

The production and decay density matrices of the full process ($eq \to et \to eb\ell\nu$) are $\rho(\lambda, \lambda')$ and $\Gamma(\lambda, \lambda')$, respectively. The measurement of the polar (θ_ℓ)

and azimuthal (ϕ_ℓ) angles of the secondary lepton in the top rest frame, enable us tp write the differential cross section of the process as the function of the top quark polarization vector (in its rest frame), written as

$$\frac{1}{\sigma_{\rm tot}}\frac{d\sigma}{d\Omega_\ell} = \frac{1}{4\pi}\Big(1+ P_z\cos\theta_\ell + P_x\sin\theta_\ell\cos\phi_\ell + P_y\sin\theta_\ell\sin\phi_\ell\Big), \tag{3.2}$$

The θ_ℓ is measured with respect to the top quark boost direction, and the top production plane is taken as the x-z plane. These choices of reference do not cost us generality of the analysis as shown in Ref. [10]. This enables one to define angular asymmetries of the secondary leptons, and connect those directly to the top quark polarization. The three asymmetries out of which, two defined in terms of the azimuthal angle, and one in terms of the polar angle of the decay lepton can be referred from Eq. (2.23) of Chapter 2.

Note that the angles in the asymmetries are defined in the rest frame of the top quark, and thus require full reconstruction of the top quark momentum. In the present case this leads to the following relations between the components of the missing momentum (neutrino in this case) denoted by $p_{x\nu}$, $p_{y\nu}$, $p_{z\nu}$, and those of the visible final chapters. The detailed explanation with mathematical derivation can be found from Appendix A of the thesis.

$$\begin{aligned} p_{x\nu} &= -\sum_{k=e,\ell,b} p_{xk}, \qquad p_{y\nu} = -\sum_{k=e,\ell,b} p_{yk}, \\ (p_{z\nu})_\pm &= \frac{1}{p_{T\ell}^2}\Big[\Delta\times p_{z\ell} \mp E_\ell\sqrt{\Delta^2 - p_{T\nu}^2 p_{T\ell}^2}\Big], \end{aligned} \tag{3.3}$$

where $\Delta = \frac{m_W^2}{2} + p_{x\ell}p_{x\nu} + p_{y\ell}p_{y\nu}$ and $p_{Ti}^2 = p_{xi}^2 + p_{yi}^2$. Out of the above two solutions for $p_{z\nu}$, the one for which $|\sum_j p_j^2 - m_t^2|$ is minimum, where p_j is the four momentum of the corresponding particle, with $j = \ell, b, \nu$, will be considered as the correct choice for the z-component. The missing momentum thus obtained is used to reconstruct the top quark momentum. The reader may note that the accuracy of this reconstruction of the top momentum depends on the precise measurements of the lepton and jet momenta and energy. In our numerical analysis we take into account of all these effects through an assumed systematic uncertainty.

3.2.3 Angular asymmetry of the recoiled electron

As mentioned in the introduction, the angular distribution of the scattered electron is indirectly sensitive to the Lorentz structure of the Ztq interaction. Exploiting this unique feature of LHeC, we define forward-backward asymmetry (in the lab frame) of the e^- coming out of the primary vertex

$$A_e^{FB} = \frac{\sigma(\cos\theta_e > 0) - \sigma(\cos\theta_e < 0)}{\sigma(\cos\theta_e > 0) + \sigma(\cos\theta_e < 0)}. \tag{3.4}$$

Notice that the other lepton coming from the decay of the top quark is positively charged, and we assume identifying the charge of the leptons is possible.

In the rest of the chapter we shall demonstrate that these asymmetries along with the cross section itself could be effectively employed to identify and distinguish the Ztq couplings.

3.3 Simulation and Analysis

We perform the analyses with events generated using Monte Carlo event generator MadGraph5 Ref. [49], using the model for signal events implemented using FeynRules Ref. [75] package. Showering, fragmentation and hadronization are performed with customized Pythia-PGS Ref. [59]. The events thus generated are passed through FastJet Ref. [60] for jet formation within $\Delta R = 0.4$, and Delphes Ref. [61] to emulate the detector effects where an appropriately customised detector card being used. To generate the signal events CTEQ6L1 PDF set is used fixing the factorization and renormalization scale to be the threshold value of the top quark mass, $\mu = \mu_F = \mu_R = m_t$. However, for all background events these scales are set to be of a dynamical scale based on events. As preliminary selection criteria at the event generation level we considered $p_T > 10$ GeV and $|\eta| < 5$ for all light jets, b-jets and leptons, $\not{E}_T > 10$ GeV and the separation of $\Delta R_{ij} > 0.4$ between all possible jets and leptons or photons.

In Table 3.1, we show the parton level cross section taking one coupling at a time. These numbers are for demonstration of the relative effect each of the couplings have in the cross section. For this purpose we have taken each coupling to be unity. Furthermore, we have shown the effects of the polarization of the initial

electron on the cross section. We have considered initial electron polarization to be -80%, 0% and $+80\%$ for this purpose. The cross section shows an enhanced

Coupling	Cross section σ in fb		
	0%	-80%	+80%
X^L_{zut}	1563.76	1957.58	1168.56
X^R_{zut}	1502.00	1642.47	1360.00
κ^L_{zut}	706.00	706.77	702.00
κ^R_{zut}	780.00	1038.68	522.00
X^L_{zct}	106.00	136.76	74.41
X^R_{zct}	100.00	103.82	94.00
κ^L_{zct}	32.50	26.37	40.00
κ^R_{zct}	40.20	60.00	20.00

TABLE 3.1: The partonic cross section of the signal process for different anomalous $tqZ, (q = u, c)$ couplings at beam energies, $E_{e^-} = 60$ GeV and $E_p = 7$ TeV for electron polarization 0%, -80% and $+80\%$. The value of the couplings are set to unity here.

value for the -80% polarization case. On the other hand a lower value of the cross section is accumulated for a $c-$quark involved coupling due to the PDF suppression. In our further analysis, we consider the case of events samples with -80% polarized electron beam. The cutflow table for signal events for different FCNC couplings taken one at a time are given in Table 3.2 for initial electron beam polarization of -80%. The corresponding cross section for the other values of e^- beam polarization, $\sigma_{\rm pol}$ can be obtained using the formula $\sigma_{\rm pol} = \sigma_{\rm unpol} \times (1 - P_e)$. The main background processes and the corresponding cross sections are given in Table 3.3. Notice that there are no backgrounds mimicking the same final state at the parton level. However, we considered all probable cases that could arise due to misidentification of chapters leading to background emerging at the detector level. These include (i) charged current processes like $ep \to ejW \to ejjj$, $ep \to eWj \to ej\ell\nu$, $ep \to \nu_e Wb \to \nu_e \ell\nu b$, , (ii) neutral current processes like $ep \to eZb \to ebbb$, $ep \to eZb \to eb\ell\ell$, $ep \to eZb \to ebjj$ and (iii) photo-processes like $p\gamma \to \ell\ell b$, $p\gamma \to \nu\nu\ell\ell b$.

Coupling g_{Ztq}	Cross section σ in fb for $P_e = -80\%$			
	Basic Cuts	$N_{e^-} = 1$	$N_{e^-,b} = 1$	$N_{e^-,b,\ell^+} = 1$
X^L_{zut}	1957.57	1763.82	799.65	745.57
X^R_{zut}	1642.47	1485.97	706.09	629.54
κ^L_{zut}	706.77	636.65	304.56	279.13
κ^R_{zut}	1038.68	933.47	474.90	427.77
X^L_{zct}	136.76	122.54	66.90	62.84
X^R_{zct}	103.82	93.05	51.26	47.65
κ^L_{zct}	26.37	23.65	12.96	12.09
κ^R_{zct}	60.00	53.33	29.70	27.45

TABLE 3.2: The signal cross sections for different anomalous $Ztq, (q = u, c)$ couplings, g_{Ztq}, at beam energies, $E_{e^-} = 60$ GeV and $E_p = 7$ TeV for polarized electron beam of -80%. The cross section can be obtained from the above table as $\sigma = |g_{Ztq}|^2[\sigma(pe^- \to e^-t, t \to W^+b, W^+ \to \ell^+\nu_\ell)]$. In the case of tensor couplings, the scale $\Lambda = m_t$.

For further selection of events, in addition to the basic cuts (BC) employed at the generation level preliminary selection, we demand that the event contain exactly one e^-, one b-jet and one ℓ^+. The signal and background cross sections, for -80% polarization of the initial e^- beam, after this selection is presented in Table 3.2 and Table 3.3, respectively. A p_T dependent b-tagging efficiency of about 70% is considered as expected. A mistagging rate of 1%(0.1%) is also considered for $c(u)$ quark (behave as $b-$jet). Most of the backgrounds are eliminated at this stage, with the remaining background cross section totalling to about 2.3 fb. We consider this remaining background throughout our analysis.

Bkg processes	Cross section σ in fb for $P_e = -80\%$			
	Basic Cuts	$N_{e^-} = 1$	$N_{e^-,b} = 1$	$N_{e^-,b,\ell^+} = 1$
Charged Current int.	67441.71	477.50	154.26	0.63
Neutral Current int.	339289.52	293361.77	8110.97	$< 10^{-3}$
Photo Production int.	29091.31	1339.20	435.45	1.64

TABLE 3.3: The SM background cross sections at beam energies, $E_{e^-} = 60$ GeV and $E_p = 7$ TeV for electron polarization -80%.

3.3.1 Asymmetries

In this section we study the asymmetries as defined in **??** and Eq. (3.4). To study these asymmetries we plot the angular distribution of the scattered electron as shown in Fig. 3.2 for three different polarized electron beam sample. Here, the forward direction is defined as the direction of the proton beam.

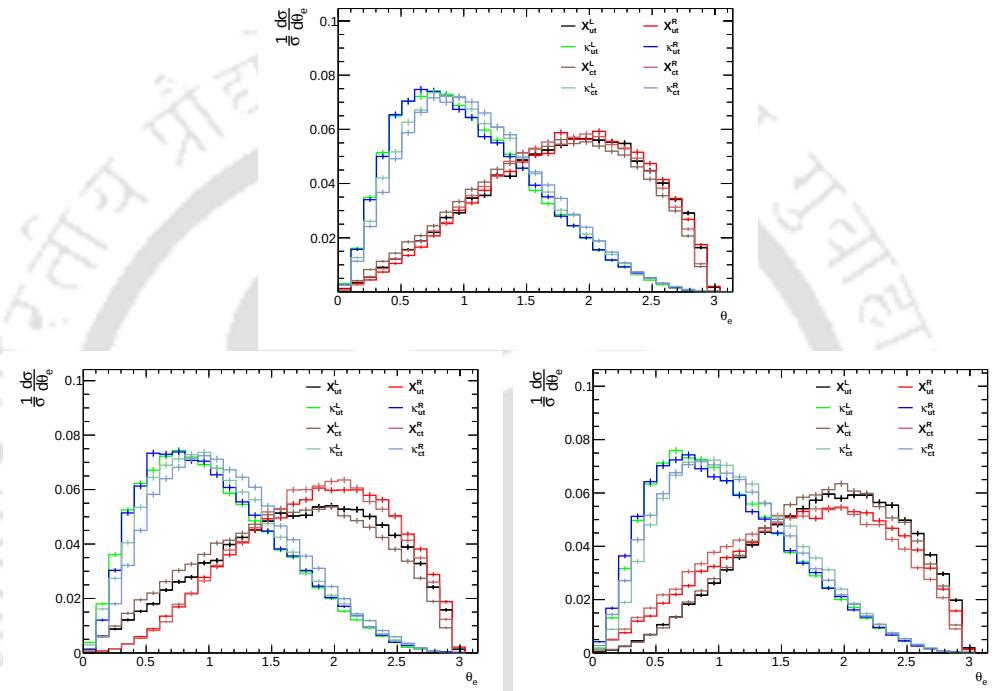

FIGURE 3.2: Polar angle distributions of the scattered e^- in the final state for (a) unpolarized, (b) -80% polarization and (c) $+80\%$ polarization of electron beam. Note that X and κ denote the vector and tensor couplings respectively.

We can observe that the distributions are irrespective of the initial beam polarization. Thus the asymmetry in the distributions of the primary electron can be due to the fact that the different polarization of the mediating Z-boson in Fig. 3.1 carry signature of the Lorentz structure of tqZ vertex, which may leads to a considerable distinction in the angular distributions of final state electron.

Notice that the vector couplings prefer electrons coming opposite to the proton direction (or along the incoming electron beam direction), which corresponds to smaller fraction of backward scattering. On the other hand, all the tensor couplings exhibit large backward scattering of the electron, indicating the requirement of larger momentum transfer. This is expected from the nature of the coupling, which is proportional to the momentum transfer. Moreover, vector couplings allow slight

discrimination between the left- and right-handed couplings. We may caution the reader that this distinguishability is limited by statistics, and perhaps not possible for Ztc couplings even with very large luminosity. However, the possibility is quite realistic in the case of Ztu couplings. This asymmetry, along with the top quark polarization asymmetry are given in Table 3.4, assuming that only one type of coupling is present (in each case). Note that the asymmetries (when only one type of couplings is present) are independent of the actual value of the coupling, as the dependence gets cancelled between its numerator and the denominator. On the other hand, if more than one type of couplings contribute, then this cancellation does not occur due to their interference, and the asymmetry depends on the actual value of the coupling. We shall discuss the multi-parameter case and the analyses in the next subsection. The correlated dependence of the A_e^{FB} asymmetry on the left/right-handed couplings and the beam polarization is quite clearly indicated as well in Table 3.4. Larger asymmetries are present when the electron beam polarization and the handedness of the couplings are opposite in the case of vector couplings.

Left-polarised e-beam

A_x	A_z	A_e^{FB}	Coupling
-0.16	-0.43	-0.18	X^L
-0.17	-0.46	$+0.63$	κ^L
$+0.07$	$+0.32$	-0.33	X^R
$+0.04$	$+0.37$	$+0.65$	κ^R

Right-polarised e-beam

A_x	A_z	A_e^{FB}	Coupling
-0.06	-0.43	-0.34	X^L
-0.01	-0.46	$+0.64$	κ^L
$+0.16$	$+0.32$	-0.17	X^R
$+0.16$	$+0.37$	$+0.65$	κ^R

Unpolarised e-beam

A_x	A_z	A_e^{FB}	Coupling
-0.12	-0.43	-0.24	X^L
-0.12	-0.46	$+0.64$	κ^L
$+0.11$	$+0.32$	-0.26	X^R
$+0.08$	$+0.36$	$+0.65$	κ^R

TABLE 3.4: Asymmetries for one fixed value of coupling at a time. It shows the distinction among X^L_{zqt}, X^R_{zqt}, κ^L_{zqt} and κ^R_{zqt} by just looking at the sign of A_z (Top quark rest frame observable) and A_e^{FB} (Lab frame observable) as discussed in the equations for asymmetries.

Among the top polarization asymmetries, $A_y = P_y$ is identically zero owing

to the CP symmetry of the interactions considered. When only one type of coupling is present both $\sigma(+,+)$ and $\sigma(-,-)$ are expected to be the same leading to $A_z = \frac{P_z}{2} = \frac{1}{2}$. However, we notice a small deviation from the value of $\frac{1}{2}$ in the Table 3.4 which might be due to the effects like that of the detector simulation, chapter identification efficiency, etc. As expected, the left-handed couplings and right-handed couplings give rise to negative and positive asymmetries, respectively, thus giving a handle to discriminate the type of couplings. With unpolarised electron beam, A_x is close to 10% for all cases of couplings, except for left-handed tensor couplings for which it is negligible. With the beam polarization, this features the distinguishing ability, with the asymmetry vanishing for the opposite combination of polarization. That is, A_x is negligible for right-handed couplings, when the electron beam is left-polarised, and vice versa. Thus, a combination of the asymmetries measured with left-polarised, right-polarised and unpolarised electron beam provide clear indication of the type of the coupling present.

3.3.2 Multi-parameter Analysis

Going beyond the single parameter case, we shall now consider simultaneous presence of more than one parameter and the reach on their values that may be obtained at an $e^- p$ collider through single top production being considered in this discussion. We shall restrict to the case when either of u or c quark is considered at a time. The cross section can be written as a second order polynomial in the relevant parameters, as follows

$$\begin{aligned}\sigma_{\rm tot}(fb) \;=\; & 745.57\ {X^L_{zut}}^2 + 629.54\ {X^R_{zut}}^2 + 279.13\ {\kappa^L_{zut}}^2 \\ & +427.77\ {\kappa^R_{zut}}^2 - 7.96\ X^L_{zut}\,\kappa^R_{zut} + 0.97\ X^R_{zut}\,\kappa^L_{zut} \\ & +62.84\ {X^L_{zct}}^2 + 47.65\ {X^R_{zct}}^2 + 12.09\ {\kappa^L_{zct}}^2 \\ & +27.45\ {\kappa^R_{zct}}^2 - 0.91\ X^L_{zct}\,\kappa^R_{zct} - 2.48\ X^R_{zct}\,\kappa^L_{zct} \end{aligned} \tag{3.5}$$

The normalised top-polarization asymmetries may similarly be written as

$$A_i = \frac{A_i^N}{\sigma_{\rm tot}}, \qquad i = x, z, e(FB), \tag{3.6}$$

where $A_i^N \times \mathcal{L}$, with $\mathcal{L}$ denoting the integrated luminosity, will give the asymmetric number of events. A_i^N can also be expressed as a polynomial function of the coupling parameters as given below. The coefficients in this case are obtained by

a numerical fit.

$$\begin{aligned} A_x^N &= -119.90\ {X_{zut}^L}^2 + 44.02\ {X_{zut}^R}^2 - 45.68\ {\kappa_{zut}^L}^2 \\ &\quad +16.86\ {\kappa_{zut}^R}^2 + 3.89\ X_{zut}^L\ \kappa_{zut}^R - 3.20\ X_{zut}^R\ \kappa_{zut}^L \\ &\quad -13.85\ {X_{zct}^L}^2 + 1.08\ {X_{zct}^R}^2 - 2.45\ {\kappa_{zct}^L}^2 \\ &\quad -0.36\ {\kappa_{zct}^R}^2 + 1.61\ X_{zct}^L\ \kappa_{zct}^R - 3.61\ X_{zct}^R\ \kappa_{zct}^L \end{aligned} \tag{3.7}$$

$$\begin{aligned} A_z^N &= -320.27\ {X_{zut}^L}^2 + 199.36\ {X_{zut}^R}^2 - 125.51\ {\kappa_{zut}^L}^2 \\ &\quad +151.95\ {\kappa_{zut}^R}^2 + 5.36\ X_{zut}^L\ \kappa_{zut}^R + 11.65\ X_{zut}^R\ \kappa_{zut}^L \\ &\quad -25.97\ {X_{zct}^L}^2 + 14.28\ {X_{zct}^R}^2 - 6.18\ {\kappa_{zct}^L}^2 \\ &\quad +7.76\ {\kappa_{zct}^R}^2 + 3.57\ X_{zct}^L\ \kappa_{zct}^R + 8.41\ X_{zct}^R\ \kappa_{zct}^L \end{aligned} \tag{3.8}$$

$$\begin{aligned} A_e^{FB^N} &= -134.93\ {X_{zut}^L}^2 - 206.87\ {X_{zut}^R}^2 + 170.14\ {\kappa_{zut}^L}^2 \\ &\quad +269.34\ {\kappa_{zut}^R}^2 - 2.85\ X_{zut}^L\ \kappa_{zut}^R + 3.57\ X_{zut}^R\ \kappa_{zut}^L \\ &\quad -6.85\ {X_{zct}^L}^2 - 15.81\ {X_{zct}^R}^2 + 6.30\ {\kappa_{zct}^L}^2 \\ &\quad +16.00\ {\kappa_{zct}^R}^2 + 2.81\ X_{zct}^L\ \kappa_{zct}^R - 2.37\ X_{zct}^R\ \kappa_{zct}^L \end{aligned} \tag{3.9}$$

We tried to include all the possible terms irrespective of their significance. Terms with smaller coefficients are less significant. This means that the quadratic couplings give the dominant contributions. Similarly, the tensor couplings are subleading compared to the vector couplings, when considered together. In the rest of this section, we shall make use of the above information on the cross section and the asymmetries to obtain the reach of the e^-p collider in extracting the anomalous FCNC couplings.

Apart from the single parameter analysis, where one assumes that only one of the couplings is present at a time, we shall also investigate the possibilities when more than one couplings present simultaneously. For single and two parameter cases we shall employ χ^2 analysis, whereas considering simultaneous presence of all couplings, we shall perform a likelihood analysis to extract the information regarding reach of the collider at 2 ab^{-1} luminosity.

3.3.2.1 χ^2 Analysis

We perform a χ^2 analysis with the integrated cross section and the asymmetries considered as the observables $\mathcal{O}_i$, with

$$\chi^2\left(\mathbf{f}\right) = \sum_i \frac{\left(\mathcal{O}_i(\mathbf{f})\right)^2}{\delta\mathcal{O}_i^2}, \tag{3.10}$$

where $\mathbf{f}$ collectively denoting the anomalous couplings considered. $\delta\mathcal{O}$ is the estimated error in the measurement of $\mathcal{O}$, which is $\delta(\sigma) = \sqrt{\frac{\sigma_{BG}}{\mathcal{L}} + (\epsilon\sigma_{BG})^2}$ when cross section is considered as the observable, where σ_{BG} denote the total background cross section (after final selection this is 2.3 fb in our case as shown in Table 3.3), and ϵ (taken to be 10% in our numerical analysis) represents the systematic error in the calculation of cross section. When asymmetry is considered as the observable, we have $\delta(A^i) = \sqrt{\frac{1-A^i_{BG}}{\mathcal{L}\ \sigma_{BG}} + \epsilon_A^2}$, where A^i_{BG} is the corresponding asymmetry arising purely from the background (once again, this is 2.3 fb in our case), and ϵ_A (again, taken to be 10% in our numerical analysis) represents the systematic error in the calculation of asymmetries. Taking the cross sections σ_{tot} and asymmetries, A_x, A_z and A_e^{FB} as our observables we compute χ^2 for single and multi-parameter cases. To distinguish the use of asymmetries used in this analysis in setting the limits of various couplings, we did the χ^2 analysis with σ as the only observable, which is represented in Fig. 3.3 and Fig. 3.4. The single parameter case for an integrated luminosity of 2 ab^{-1} is presented in Fig. 3.3. The vector couplings for the right-handed (left-handed) Ztu case yield a 3σ limit of about ±0.032 (±0.034), whereas for the right-handed (left-handed) tensor couplings it is ±0.042 (±0.052). The corresponding values in the case of Ztc couplings are ±0.11 (±0.12) and ±0.16 (±0.24) for the right-handed (left-handed) vector and tensor couplings, respectively. The limits on the couplings looks different in case of u(c)-quark, due to the fact that the c-quark initiated process gives rise to very low cross-section than the u-quark initiated processes, Ref. Table 3.2. In Fig. 3.4, we perform the same exercise for two parameter case.

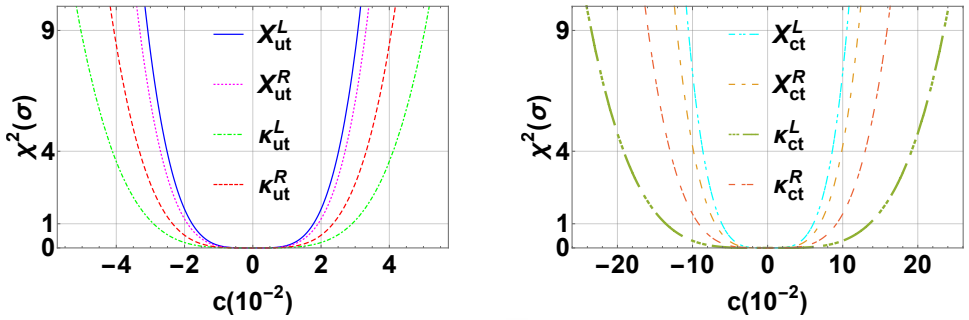

FIGURE 3.3: Single parameter reach with an integrated luminosity of 2 ab^{-1}.

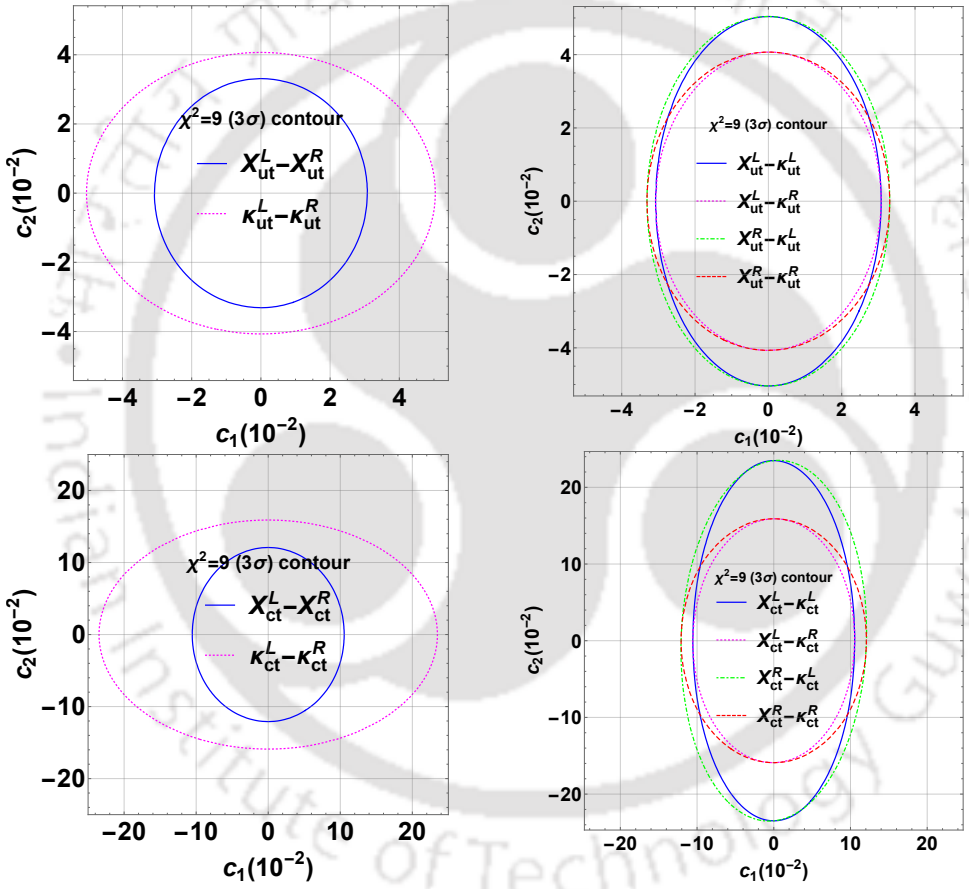

FIGURE 3.4: Two parameter reach with an integrated luminosity of 2 ab^{-1}.

3.3.2.2 Likelihood mapping of the parameter space

In this section we perform a likelihood analysis using the events available after the final selection. The likelihood of a given point **f** in the parameter space is given by

$$\mathcal{L} = \exp\left[-\frac{\chi^2(\mathbf{f})}{2}\right] \tag{3.11}$$

where χ^2 is defined in Eq. (3.10). We apply the Markov Chain Monte Carlo (MCMC) method to map the likelihood of the parameter space for each of the couplings. We make use of the publicly available GetDistRef. [85] package to obtain the single and multi-parameter bounds using MCMC chain. Table 3.5 shows the simultaneous limits on the anomalous couplings at 68%, 95% and 99% C.L's obtained from the MCMC analysis considering an integrated luminosity of 2 ab^{-1}.

Vector	Obtainable reach (in part of 10^3)		
Coupling	at C.L. = 68%	95%	99%
X^L_{zut}	$\in [-9.8, 9.7]$	$\in [-16.4, 16.4]$	$\in [-20.0, 20.1]$
X^R_{zut}	$\in [-13.7, 13.6]$	$\in [-20.8, 20.9]$	$\in [-24.4, 24.4]$
X^L_{zct}	$\in [-30.8, 31.1]$	$\in [-52.8, 52.7]$	$\in [-65.7, 65.5]$
X^R_{zct}	$\in [-48.0, 47.3]$	$\in [-73.0, 72.7]$	$\in [-85.9, 86.8]$

Tensor	Obtainable reach (TeV $^{-1}$)		
Coupling	at C.L. = 68%	95%	99%
κ^L_{zut}/Λ	$\in [-0.06, 0.06]$	$\in [-0.10, 0.10]$	$\in [-0.13, 0.13]$
κ^R_{zut}/Λ	$\in [-0.07, 0.07]$	$\in [-0.12, 0.12]$	$\in [-0.16, 0.15]$
κ^L_{zct}/Λ	$\in [-0.23, 0.23$	$\in [-0.40, 0.40]$	$\in [-0.50, 0.50]$
κ^R_{zct}/Λ	$\in [-0.31, 0.31]$	$\in [-0.57, 0.56]$	$\in [-0.71, 0.72]$

Table 3.5: The list of simultaneous limits on FCNC parameters obtained from MCMC analysis including the cross-section and all other asymmetries for e^-p collider at $E_{e(p)} = 60$ (7000) GeV with integrated luminosity of 2 ab^{-1}.

For direct comparison with the experimental observations, 95% branching fraction of FCNC decays of the top quark corresponding to the couplings quoted in Table 3.5 are given in Table 3.6. While these limits are at best comparable to that of the HL-LHC reach [38], one may notice that our limits do not assume the absence of other couplings, unlike those quoted in the case of LH-LHC study.

	BR % $(t \to Zu)$		BR % $(t \to Zc)$
$X^L_{zut} = 0.016$	0.009	$X^L_{zct} = 0.053$	0.095
$X^R_{zut} = 0.021$	0.015	$X^L_{zct} = 0.073$	0.181
$\frac{\kappa^L_{zut}}{\Lambda} = 0.10$ TeV^{-1}	0.004	$\frac{\kappa^L_{zct}}{\Lambda} = 0.40$ TeV^{-1}	0.068
$\frac{\kappa^R_{zut}}{\Lambda} = 0.12$ TeV^{-1}	0.006	$\frac{\kappa^R_{zct}}{\Lambda} = 0.57$ TeV^{-1}	0.133

TABLE 3.6: Limiting values of the couplings that can be reached (refer Table 3.5), and the branching fractions of the corresponding top quark decays.

In Fig. 3.5 the 2-dimensional projections of the hyperspace of the 4-dimensional (four couplings for u/c quark each) parameter space region limited by the 95% and 99% C.L. regions obtained assuming an integrated luminosity of 2 ab^{-1}. Limits of the order of 0.02 can be reached at 99% C.L. on all the Ztu couplings, whereas these are around 0.06-0.12 for the Ztc couplings.

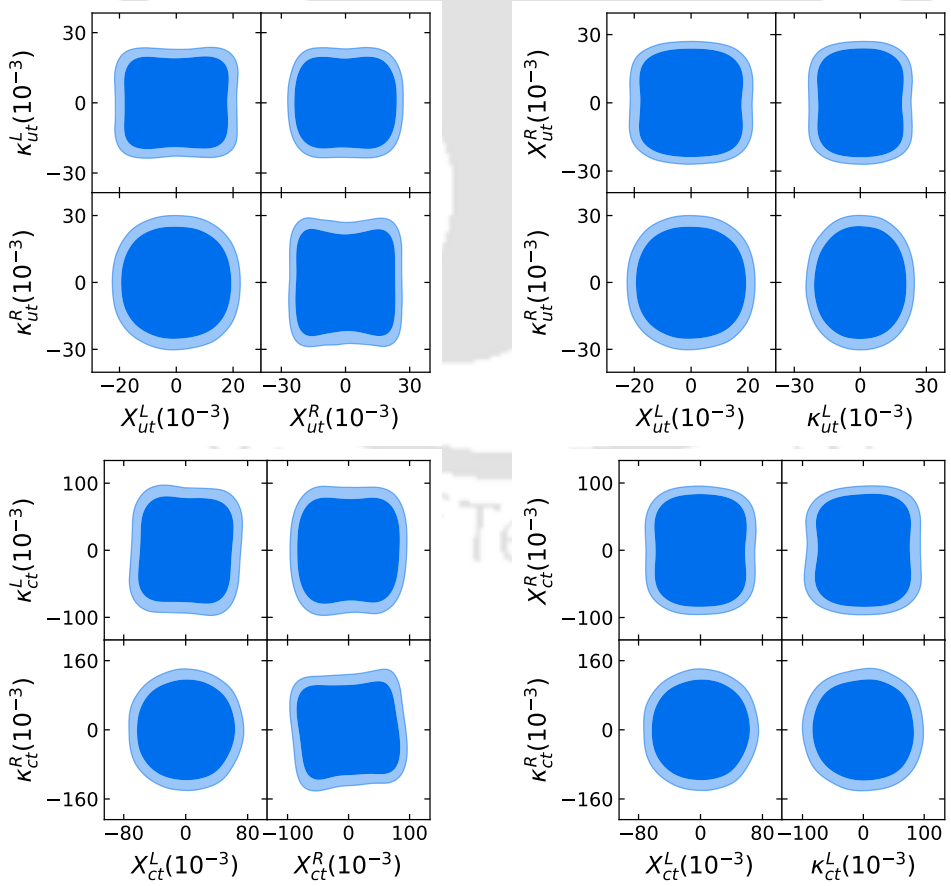

FIGURE 3.5: MCMC two parameter contour at 95% (deep blue), 99% (light blue) C.L. integrated luminosity of 2 ab^{-1} is used. The tensor couplings are considered at $\Lambda = m_t$.

3.4 Discussion and conclusion

Top quark, being the only quark that reveals direct information of the weak couplings through its decay without adding complication of hadronic bound states, has a special place to play in our understanding of the elementary chapter dynamics. The fact that it is the heaviest of the known fundamental chapters, consequently having the strongest coupling with the Higgs boson, makes the properties of the top quark a unique window to understand the electroweak symmetry breaking mechanism. In this chapter we have focused our attention on the FCNC couplings of the top quark with the Z boson. Noting that the SM prediction of these couplings are about 10^{-15} to 10^{-12} orders of magnitude smaller than the present experimental bounds, there are ample opportunities in probing new physics effects in these couplings. However, extracting information regarding the FCNC couplings of top quark in the standard processes involving its rare decay (enabled by the new couplings) has limitations of statistics, as the decays are expected to be a few in a million of the standard decay process at the best. On the other hand, we may look at possibilities in the rare production, which are not possible in the absence of the FCNC couplings. Such rare single top productions at the LHC are harder to probe, as the standard single production processes overshadow these rare processes. Colliders with leptonic initial state like the electron-proton collider (LHeC) have definite advantage here, where it is possible to have $e^-p \to e^-t$ produced in the presence of Ztq vertex, where q denotes either u or c quark. There is no SM analogue of this process, and therefore expected to be relatively free from the background. We consider such a situation in a projected e^-p collider of beam energies of 60 GeV (electron) and 7 TeV (proton) equivalent to a center of mass energy of 1.3 TeV. We note that the presence of scattered (spectator) electron in this case is quite advantageous, and discuss exploiting it to distinguish the Lorentz structure of the anomalous coupling. We consider the leptonic decay of the top quark, and define angular asymmetries of the decay lepton that can be easily constructed. These angular asymmetries reflect the polarization state of the top quark decayed. We have given a detailed discussion on the top-quark polarization states, and the transition of the spin information to the decay leptons. Along with the integrated cross section, these additional observables are made use of in extracting the reach of the couplings. Anticipating small cross section as expected from couplings of the order of 10^{-3}, we require large luminosity in the inverse attobarn

range to have sufficient statistics for this investigation. Apart from single parameter analysis considering the presence of one coupling alone at a time, we perform a multi-parameter analysis, where χ^2 minimisation and likelihood analysis methods are employed. MCMC technique is used for these analyses, with the cross section and asymmetries considered as observables. Correlations of the couplings in extracting the reach is obtained in a 4-dimensional hyperspace of the parameters, and the 2-dimensional slices of this in all combinations of two-parameter plane are presented. At an integrated luminosity of 2 ab^{-1} we consistently obtain a reach of $\mathcal{O}(10^{-2})$ in the case of Ztu and Ztc vector couplings by both χ^2 analysis and MCMC analysis at LHeC of $\sqrt{s} \approx 1.3$ TeV, whereas the reach of tensor couplings are about $0.1 - 0.5$ TeV^{-1}. While these limits sound approximately similar to those projected in the case of HL-LHC (which assumes presence of single coupling at a time), note that our analysis considered the simultaneous presence of all the relevant couplings. We believe that this study has clearly brought out the advantages of the e^-p collider in probing the top quark FCNC couplings with Z boson, which would not only complement the information that could be extracted from the LHC, but also is capable of providing additional information like the Lorentz structure of the couplings. Finally, we note that the scope of the present study is limited to the BSM scenarios leading to anomalous Ztq vertices. Another class of models like the non-universal Z' models [86, 87, 88] with tree-level FCNC couplings could lead to the same process through Z' exchange channels. Analysis of these models and a comparison with the framework considered in the present work is an interesting project in itself.

– Gases are distinguished from other forms of matter, not only by their power of indefinite expansion so as to fill any vessel, however large, and by the great effect heat has in dilating them, but by the uniformity and simplicity of the laws which regulate these changes.

James Clerk Maxwell

4

Investigating FCNC anomalous top quark coupling through $e^-e^+ \to tj$ at the ILC

The proposed International Linear Collider (ILC) is at advantage in probing the Flavour Changing Neutral Current (FCNC) in many ways. First of all, the clean environment and a good handle on beam polarization along with the fixed partonic center of mass energy of the ILC make it an ideal laboratory to do precision measurements. With relatively smaller number of events, it is expected to study the details of the Lorentz structure of the interaction exploiting top quark spin correlations and cleverly designed observables possible in such a set up. The presently approved baseline design with center of mass energy of 250 GeV is sufficient to investigate the anomalous top quark couplings through rare single top production channels. We may note here that the standard top quark production is not possible at 250 GeV ILC, disfavoring standard top quark studies.

4.1 Introduction

In this chapter, we shall consider a model independent approach to understand the FCNC interactions in the top quark with the light quark and neutral Standard Model (SM) gauge bosons. We consider effective Lagrangian with anomalous

couplings of top quark with the SM gauge bosons and lighter quarks as described in Eq. (1.5) of Chapter 1 for the $tq\gamma$ and tqZ interactions,

$$\begin{aligned}-\mathcal{L}_{\text{fcnc}} =& e\bar{q}\frac{i\sigma^{\mu\nu}q_\nu}{\Lambda}(\kappa^L_{\gamma qt}P_L + \kappa^R_{\gamma qt}P_R)tA_\mu + \frac{g}{2c_W}\bar{q}\gamma^\mu(X^L_{zqt}P_L + X^R_{zqt}P_R)tZ_\mu \\ &+ \frac{g}{2c_W}\bar{q}\frac{i\sigma^{\mu\nu}q_\nu}{\Lambda}(\kappa^L_{zqt}P_L + \kappa^R_{zqt}P_R)tZ_\mu + \text{h.c}, \end{aligned} \tag{4.1}$$

where $q_\nu = p_t - p_q$ is the momentum transfer between the quarks in the process, and Λ is the cut-off scale. The parameters $X^{L(R)}_{zqt}$, $\kappa^{L(R)}_{zqt}$ represent the left(right)-handed vector and tensor couplings, respectively, of tqZ interactions, whereas $\kappa^{L(R)}_{\gamma qt}$ is the left(right)- handed tensor couplings of $tq\gamma$ interaction. The experimental constraints on the rare decay branching fractions of the top quark enabled by these couplings arising from LHC are discussed in Section 1.2.1 . As we discussed there, LHC limits are derived considering the presence of one coupling at a time. Moreover, it is very unlikely that LHC would be able to decipher the details of the couplings like its Lorentz structure. On the other hand, colliders with leptonic initial states can study processes with single top quark in the final state, which are forbidden in the SM, and therefore are expected to have relatively small irreducible backgrounds. For example, in e^+e^- collisions, single top quark produced in association with a light quark is realised with the presence of flavour changing tqZ and/or $tq\gamma$ couplings. One advantage here is the involvement of the anomalous coupling at the production level itself. We shall show that this can be exploited to distinguish the Lorentz structure of the coupling with the kinematic observables involving the light jet emerging from the production vertex. We shall consider the baseline configuration of ILC with center of mass energy of 250 GeV. We shall also make use of polarised electron and positron beams as another advantage to our study to disentangle various couplings. Unlike the proton beam, here one can prepare polarised beams. The degree of polarization of a beam is defined as

$$P_e = \frac{N_R - N_L}{N_R + N_L}, \tag{4.2}$$

where $N_{R(L)}$ is the number of right(left)-handed electrons in the beam. Thus, if the beam is 100% right-polarised, all the electrons in the beam are right-handed. Similarly for the left-polarised beam. When $N_R = N_L$, the beam is unpolarised. A similar expression can be thought up for the degree of polarization of the positron beam as well. We shall denote this by P_p here. We may denote the cross section for 100% left-polarised electron beam and 100% right-polairsed positron beam as

σ_{LR}, and, similarly, as σ_{RL} for the other opposite polarization combination, and σ_{LL} and σ_{RR} for the same polarization combinations. With this, we can write the cross section for a particular degree of polarization combination $(P_e,\ P_p)$ as

$$\begin{aligned}\sigma(P_e,\ P_p) \ = \frac{1}{4}\ \big\{&(1+P_e)(1+P_p)\ \sigma_{RR} + (1-P_e)(1-P_p)\ \sigma_{LL} \\ &+ (1+P_e)(1-P_p)\ \sigma_{RL} + (1-P_e)(1+P_p)\ \sigma_{LR}\big\}. \end{aligned} \tag{4.3}$$

The signal process ($e^+e^- \to tq$) goes through the s-channel mediation of γ and Z. Thus, only the opposite combinations of σ_{RL} and σ_{LR} are non-zero for this process. ILC is expected to have $\pm 80\%$ polarization for electron beams and $\pm 30\%$ for the positron beam. We shall therefore consider the two cases of $(P_e,\ P_p) = (-80\%,\ +30\%)$ and $(+80\%,\ -30\%)$ in our study.

Information on the polarization of top quark produced is another very useful input to understand the nature of the couplings. It is clear from the parametrisation of the couplings given in the Lagrangian that the difference in the left- or right-handed couplings will result in the asymmetric production of left- or right-handed top quark. This will naturally affect the angular distribution of the top quark produced, and further the angular distribution of the decay products as well. As discussed in Section 2.2.1, one may construct angular asymmetries of the decay leptons, which are proportional to the top quark polarization. Notice, that such couplings at the production level will control the handedness of the light quark produced, and consequently the angular distribution of the jets followed. In addition to the handedness of the top quark, the Lorentz structure of the couplings; if vector coupling or tensor coupling, would also affect the angular distribution of the jet, as well as the top decay leptons. We shall make use of these facts in constructing angular asymmetries of jets and top decay products as a discriminator of different types of couplings.

We organize this chapter with details of the process, including the cross-section and analysis strategy presented in Section 4.2. In Section 4.3 the details of the numerical study and the results for 250 GeV ILC are presented. In Section 4.5 we discuss the projected results at higher energy ILC and finally conclude in Section 4.6.

4.2 Event Generation, Detector Simulation and Reconstruction

Single top production at e^+e^- collision is not possible through standard couplings. However with the top FCNC, $tq\gamma$ or tqZ, electron-positron annihilation to tq, where q is a light quark is allowed through the s-channel process mediated by photon or Z boson. With t we shall denote both the top quark or top antiquark (unless mentioned), with q denoting light anti-quark or quark, respectively. We shall further consider the leptonic decay of the top quark, $t \to bW \to b\ell\nu$, where $\ell = e,\ \mu$ of either charge. The Feynman diagram corresponding to the process is shown in Fig. 4.1.

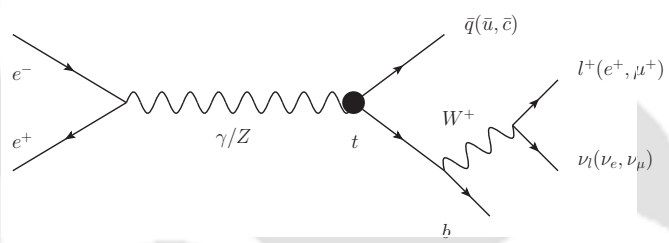

FIGURE 4.1: Signal process: The Feynman diagram corresponding to single top production at ILC enabled by the anomalous $tq\gamma(Z)$, with the leptonic decay of top quark.

Thus our signal has a light jet, a $b-$jet and a lepton (either electron or muon) of either charge along with missing energy in the final state. The total cross section is expected to be insensitive to the handedness of the top FCNC coupling. On the other hand, we shall see that some of the angular distributions would discriminate these couplings. Considering one type of couplings to be present at a time, the cross sections at $\sqrt{s} = 250$ GeV ILC are given in Table 4.1 for the unpolarised beams, as well as for the two different combinations of beam polarization of $(-80\%,\ +30\%)$ and $(+80\%,\ -30\%)$. In the rest of this Chapter, unless otherwise specified, we shall use σ^{LR} and σ^{RL} to denote cross section corresponding to the above mentioned polarization combination. The couplings are set to unity for the values of cross sections quoted in Table 4.1. The cross section being proportional to the square of the couplings (we consider real couplings), the cross section for any value of the coupling can be obtained by a single scaling.

	$\kappa_{\gamma qt}^{L(R)}$	$X_{zqt}^{L(R)}$	$\kappa_{zqt}^{L(R)}$
σ_{unpol} (fb)	253.3	107.9	179.0
$\sigma^{LR} \equiv \sigma(-80\%, +30\%)$ (fb)	313.0	155.9	263.4
$\sigma^{RL} \equiv \sigma(+80\%, -30\%)$ (fb)	313.0	107.3	178.4

TABLE 4.1: The partonic cross section of the signal process : $e^-e^+ \to tq$, $(t \to Wb,\ W \to \mu\nu_\mu\ (e\nu_e))$ for different anomalous $tq\gamma(Z)$ couplings at $\sqrt{s}$=250 GeV. The values of the couplings are set to unity in all cases.

The variation of the total cross section against the center of mass energy $\sqrt{s}$ is shown in Fig. 4.2 for the three types of couplings, and for the two polarization combinations. The vector couplings show the usual behavior of decrease of cross section for higher center of mass energies, whereas the case of tensor couplings saturates to a stable value. Here again, the relevant coupling is taken to be unity. One may also notice the insensitivity of the photon coupling to the handedness of the electron, and consequently independent of the beam polarization. On the other hand, the left-handed electron polarization spares better in the case of Z-couplings. The graph for the tensor couplings in γqt overlap each other for RL or LR beam samples.

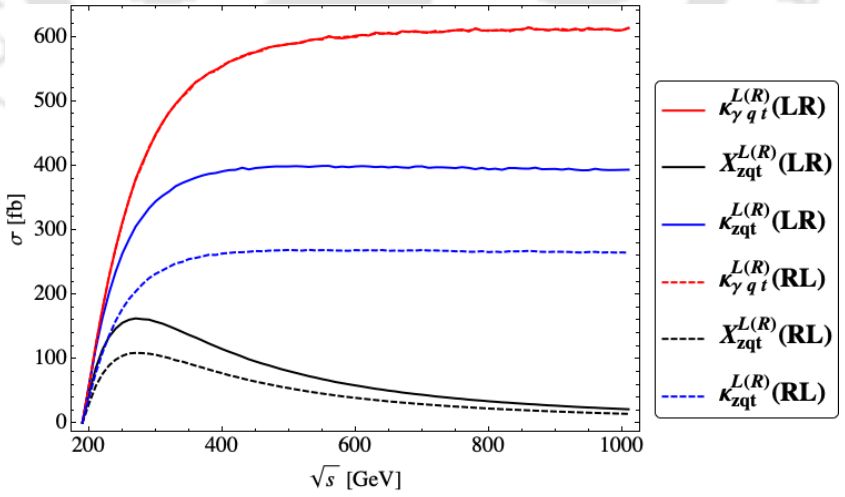

FIGURE 4.2: Cross section of signal process : $e^-e^+ \to tj$, $(t \to W^+b,\ W^+ \to \mu^+\nu_\mu\ (e^+\nu_e))$ at different $\sqrt{s}$ values. The superfix in the legends represents the handedness of the couplings. The solid(dashed) lines represents the LR(RL) samples. The graph of $\kappa_{\gamma qt}^{L(R)}$ for LR and RL samples overlap each other.

We may express the cross section including the leptonic branching fraction of the top quark as a function of the anomalous couplings for the signal process $e^-e^+ \to tj, (t \to Wb,\ W \to \mu^+\nu_\mu\ (e^+\nu_e))$ for the two polarization combination as

$$\begin{aligned}\sigma_{tot}^{LR}(fb) &= 156.5\left[(\kappa_{\gamma qt}^{L})^2 + (\kappa_{\gamma qt}^{R})^2\right) + 78.0\left[(X_{zqt}^{L})^2 + (X_{zqt}^{R})^2\right] \\ &+ 131.5\left[(\kappa_{zqt}^{L})^2 + (\kappa_{zqt}^{R})^2\right] + 260.9\left(\kappa_{\gamma qt}^{L}\kappa_{zqt}^{L} + \kappa_{\gamma qt}^{R}\kappa_{zqt}^{R}\right) \\ &- 188.6\left(\kappa_{\gamma qt}^{L}X_{zqt}^{R} + \kappa_{\gamma qt}^{R}X_{zqt}^{L}\right) - 190.6\left(X_{zqt}^{L}\kappa_{zqt}^{R} + X_{zqt}^{R}\kappa_{zqt}^{L}\right), \qquad (4.4)\\ \sigma_{tot}^{RL}(fb) &= 156.5\left[(\kappa_{\gamma qt}^{L})^2 + (\kappa_{\gamma qt}^{R})^2\right) + 53.6\left[(X_{zqt}^{L})^2 + (X_{zqt}^{R})^2\right] \\ &+ 89.2\left[(\kappa_{zqt}^{L})^2 + (\kappa_{zqt}^{R})^2\right] - 202.2\left(\kappa_{\gamma qt}^{L}\kappa_{zqt}^{L} + \kappa_{\gamma qt}^{R}\kappa_{zqt}^{R}\right) \\ &- 128.6\left(\kappa_{\gamma qt}^{L}X_{zqt}^{R} + \kappa_{\gamma qt}^{R}X_{zqt}^{L}\right) - 190.6\left(X_{zqt}^{L}\kappa_{zqt}^{R} + X_{zqt}^{R}\kappa_{zqt}^{L}\right). \qquad (4.5)\end{aligned}$$

The signal final state consists of one isolated lepton, one isolated light jet and one isolated $b-$jet along with missing energy. Major SM background process for this final state are

1. $e^+e^- \to WW \to (2\ell 2\nu,\ 2j\ell\nu,\ 4j)$,
2. $e^+e^- \to ZZ \to (2\ell 2\nu,\ 4\ell,\ 2\ell 2j,\ 4j)$,
3. $e^+e^- \to Z \to (2\ell,\ 2j,\ 2b)$,
4. $e^+e^- \to ffh$.

Our strategy to investigate the presence of the signal at ILC250 is the following. Signal events are simulated using MadGraph5 [49] with the Pythia8 [62] used for hadronisation and showering of the hard processes. The background samples available with ILC repository for 100% beam polarizations are mixed with appropriate weight factors as per Eq. (4.3) to get the cross sections corresponding to $(P_e,\ P_p) = (-80\%,\ +30\%)$ or $(+80\%,\ -30\%)$, as the case considered.

The events were simulated in the environment of International Large Detector (ILD) [89], the detector concept for the ILC. It consists of a high precision silicon vertex detector, a large time projection chamber, additional silicon strip tracking detectors, and highly granular electromagnetic, hadronic, and forward calorimeters, all placed within the 3.5 T field of a solenoid whose iron flux return yoke is instrumented with muon detectors. Simulation of the *ILD-01-v05* detector model [89] was performed using the GEANT-4-based MOKKA toolkit [63, 64, 65].

The simulated energy deposits were digitized and reconstructed using MARLINRECO [68, 69, 70, 71, 72] and other software tools of ILCsoft [68] (*version v01-16-02*). The output of event reconstruction is a collection of Particle Flow Objects (PFOs), each containing zero, one or more reconstructed tracks and calorimeter clusters, corresponding to individual final state particles. The output of MARLIN containing the final state events is analysed through ROOT [73] data processing toolkit for the analysis.

While for the background events, we obtained the processed events samples, we performed a similar processing on our signal events to include the effects of ILD and reconstruct the events.

4.3 Events Selection and Numerical Analysis

We shall discuss the criteria considered for event selection and the analysis in this section.

4.3.1 Preselection of events:

The events prepared through MOKKA and MARLINRECO are analysed through ROOT. As pre-selection criteria, we demand our sample (both signal and background) to have two jets, tagged with b-tagging probability. Further we demand to have one isolated lepton (muon/electron). These events are scrutinised for further analysis considering their particle content and kinematic distributions. We shall ignore the charge identification of the leptons, and consider ℓ^+ and ℓ^- together. However we shall analyse the case of $e^\pm$ and $\mu^\pm$ in the final state separately to get the values of asymmetries. We perform our analysis for two beam polarizations of $(-80\%, +30\%)$ and $(+80\%, -30\%)$.

4.3.2 Case 1: Beam polarization of $(-80\%, +30\%)$

We shall first consider the case of $(-80\%, +30\%)$ beam polarization below, for the signal process with $e^+e^- \to t\bar{q} \to \bar{q}bW^+ \to \bar{q}b\mu^+\nu$ and $e^+e^- \to \bar{t}q \to q\bar{b}W^- \to q\bar{b}\mu^-\bar{\nu}$ together. Following this the final state with $e\nu jb$, again combined case of both charge combinations, shall be taken up.

4.3.2.1 Event Selection: Muonic final state

As the first level of selection of events, we demand that every event contains one isolated muon (or either charge) and two jets, satisfying the preselection criteria. Out of the two jets, the one with higher b-tagging efficiency is tagged as the $b-$jet (no charge identification), while the other one is tagged as the light-jet. Considering the $(-80\%, +30\%)$ beam polarization, we plot different distributions of both the signal and background events in Fig. 4.3. For clarity of the plots we have included only those backgrounds which remain after all the event selection criteria are imposed as described in Table 4.2. The major backgrounds at this stage are $e^+e^- \to WW \to 2j\ell\nu$ (W-pair), $e^+e^- \to We\nu \to 2j\ell\nu$ (single W), $e^+e^- \to ZZ \to 2j2\ell + 2j2\nu$ (Z-pair) and $e^+e^- \to Zee \to 2j2\ell$ (single Z) events in the semi-leptonic category; $e^+e^- \to ZZ \to 2\ell2\nu$, $e^+e^- \to Zee \to 2\nu2\ell$ and $e^+e^- \to We\nu \to 2\ell2\nu$ in the leptonic caterogy; $e^+e^- \to ZZ \to 2j2b$ in the hadronic category and $e^+e^- \to ffh$ with all possible decays of the Higgs boson(h), included. Before proceeding to apply kinematic cuts, we select events with a b-tagging efficiency of less than 0.4 for the light jet, while it is required to be larger than 0.8 for the $b-$jet. The former reduces the background slightly, affecting the semi-leptonic and hadronic backgrounds mediated through ZZ and the ffh background somewhat, leaving all other backgrounds and signal events practically untouched. On the other hand, the latter one with $b-$jets practically eliminates the single W and single Z semi-leptonic events, the single Z leptonic events and the $2e\gamma$ events, while reducing all other background events considerably. This, on the other hand, retains close to 65% of the signal events. The events after each selection are presented in the Table 4.2.

In this analysis we assume a total integrated luminosity of 2 ab^{-1} at a center-of-mass energy of 250 GeV, distributed among the different polarization sign combinations for $[e^-_Le^+_R,\ e^-_Re^+_L,\ e^-_Le^+_L,\ e^-_Re^+_R]$ as [45, 45, 5, 5]%, corresponding to the 250 GeV portion of the "H20-staged" ILC running scenario proposed in [90]. The $e^-_Le^+_R$ portion, for example, has a dominantly lefthanded electron beam and dominantly righthanded positron beam. The detailed plan and accelerator design for the 250 GeV stage of the ILC is described in [91].

From the distributions in Fig. 4.3 it is clear that energies of the jets, E_j and E_b and the invariant mass of $\ell\nu$ (denoted as M_W, as it corresponds to the reconstructed W mass in the case of signal), and the invariant mass of $b\ell\nu$ system

(denoted as M_t, as it corresponds to the reconstructed t mass in the case of signal) can be exploited to enhance the signal significance by suitable selection. We optimised the selected regions of these observables so as to enhance the signal significance. Notice that the light jet in the signal originates from the the quark emitted in association with the top quark. At 250 GeV ILC, at parton level, its energy is fixed to be close to 65 GeV. The first kinematic selection that we employ is, therefore, $55 < E_j < 75$ GeV, reducing the backgrounds considerably. The major backgrounds comes from semi-leptonic category with 10791 events, followed by the hadronic and ffh backgrounds with 3505 and 763 events, respectively, and finally 380 events from leptonic background. For further selection we consider the restricted regions of $40 < E_b < 105$ GeV, $65 < M_W < 95$ GeV and $140 < M_t < 185$ GeV, along with a selection of invariant mass of b and light jets, $M_{bj} \notin [65, 95]$ GeV. This reduces the total background from 14676 to its less than one-tenth, 1181 events. The signal, on the other hand, retains between 70 and 75% of the events with this latest set of selection. As the last set of cuts we considered a lower cut on the missing momentum, $|p_\nu| > 30$ GeV, angular cuts $\cos\theta_\mu < .95$, $|\cos\theta_\nu| < .95$, $\Delta\theta_{j\mu} < 1.5$, where θ_μ, θ_ν and $\Delta\theta_{j\mu}$ are the polar angles of the muon and the missing momentum, and the angular separation of the jet and the muon, respectively. Finally, we employed $50 < |p_j| < 70$ GeV and $\sqrt{(p_j + p_b)^2} > 20GeV$, bringing the background to ∼300 events. To start with, the signal events with $N_j = N_b = N_\mu = 1$ for coupling value set equal to unity is $\sim 27 \times 10^4$ in the case of $tq\gamma$ couplings, while it is $\sim 23 \times 10^4$ and $\sim 13.5 \times 10^4$ in the case of tqZ tensor and vector couplings, respectively. After the event selection, detailed above, this goes down to $\sim 8.2 \times 10^4$ ($tq\gamma$), $\sim 7.1 \times 10^4$ (tensor tqZ coupling) and $\sim 4 \times 10^4$ (vector tqZ coupling), respectively.

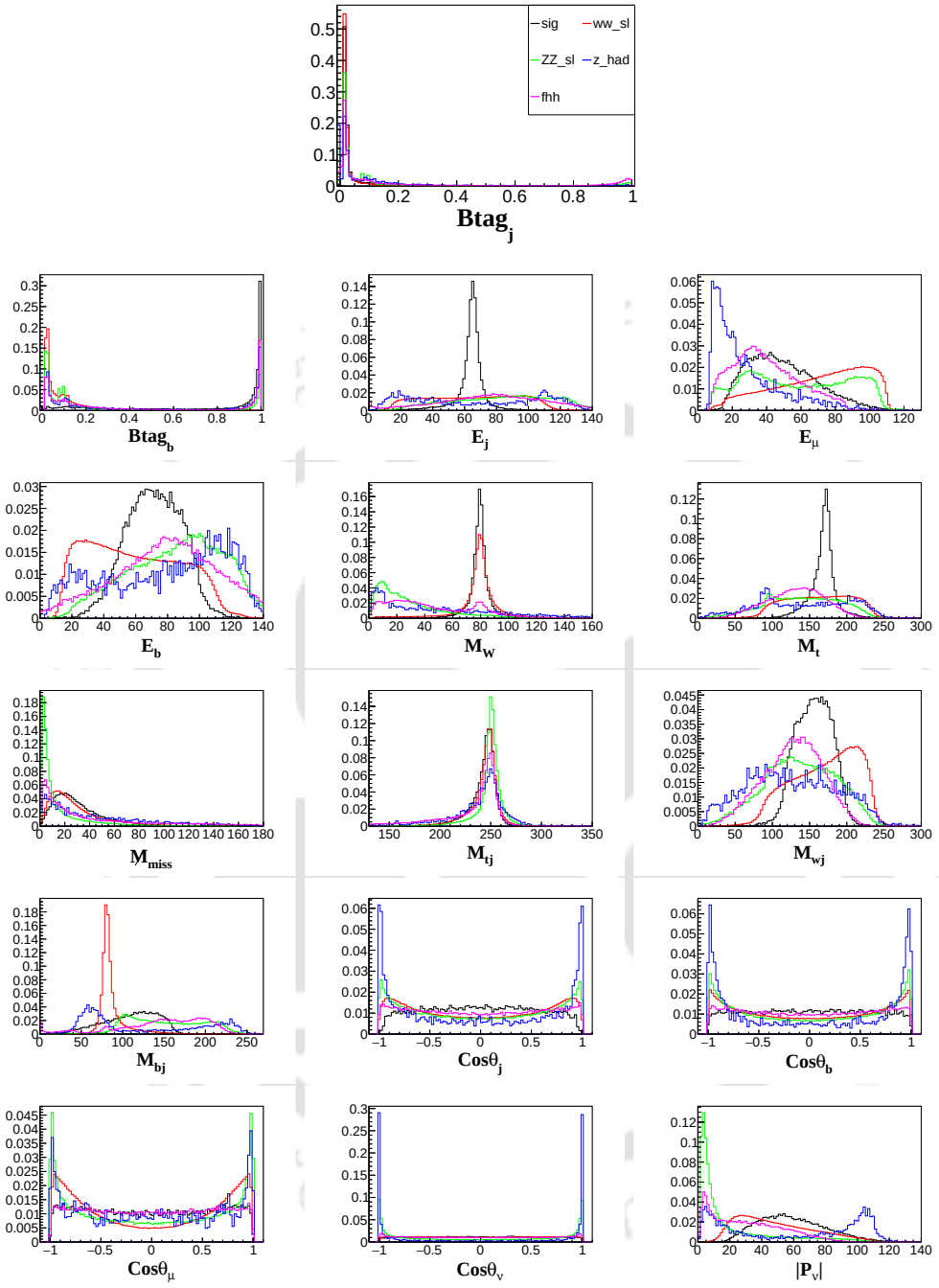

FIGURE 4.3: Distributions after the events are identified with one light-jet, one $b-$jet and one μ of either charge. The beam polarizations combination of $(-80\%, +30\%)$ is assumed. Signal corresponds to the coupling $\kappa^L_{\gamma qt}$, and the backgrounds are (a) $e^-e^+ \to WW \to l\nu_l 2j$ (b) $e^-e^+ \to ZZ \to 2l2j + 2\nu_l 2j$ (c) $e^-e^+ \to Z \to 2j + 2b$ (d) $e^-e^+ \to ffh$

Process	$N_{simulated}$	$\sigma_{-.8,+.3}[fb]$	N_{eve}	N_μ=N_j=N_b=1	$Btag_j < 0.4$	$Btag_b > 0.8$	$55 < E_j < 75$	$40 < E_b < 105$	$65 < m_W < 95$	$140 < m_t < 185$	$M_{bj\not{p}} \epsilon [65, 95]$	$\lvert p_\nu \rvert > 30$	$\cos\theta_\mu < .95$, $\lvert\cos\theta_\nu\rvert < .95$, $\Delta\theta_{j,\mu} < 1.5$	$\lvert P_j \rvert \epsilon [50, 70]$, $\sqrt{(p_j + p_b)^2} > 20$
SIGNAL: $e^-e^+ \to t, q(t \to Wb, W \to \mu\nu_\mu)$														
$\kappa_{\gamma qt}^{L(R)}(\gamma)$	20000	312.59	281331	272735	270794	175690	152128	148274	140241	132605	107411	100687	86967	82479
$X_{zqt}^{L(R)}$	20000	156.16	140544	136685	135828	88943	77565	75633	71993	68016	57320	54116	48698	46147
$\kappa_{zqt}^{L(R)}$	19000	263.63	237267	230111	228437	148928	129609	126412	120169	113301	91671	85477	74263	70679
BACKGROUND(Type: semileptonic):														
$e^-e^+ \to WW \to l\nu_l 2j$	1962649	10992.9	9893624	5150518	5148930	30138	6667	5996	4861	4140	716	504	396	288
$e^-e^+ \to Z\nu\nu \to 2j\nu\nu$	147517	271.805	244624	593	509	167	12	4	0	0	0	0	0	0
$e^-e^+ \to ZZ \to 2l2j + 2\nu_l 2j$	535103	856.927	771234	194230	176686	18258	4112	1930	447	390	347	127	54	35
$e^-e^+ \to W^\pm e^\mp \nu \to 2je\nu$	121492	5898.17	5308351	953	953	0	0	0	0	0	0	0	0	0
$e^-e^+ \to Ze^-e^+ \to 2je^-e^+$	325217	378.281	340452	73	71	3	0	0	0	0	0	0	0	0
BACKGROUND(Type: leptonic):														
$e^-e^+ \to WW \to l\nu_l 2l$	409207	915.577	824018	626490	626327	2538	55	20	8	6	6	6	2	2
$e^-e^+ \to Z\nu\nu \to 2l\nu\nu$	80000	114.137	102722	23841	23841	13	3	0	0	0	0	0	0	0
$e^-e^+ \to ZZ \to 2l2l + 2\nu_l 2l$	70000	95.8895	86300	43097	42954	233	42	22	6	6	6	2	2	2
$e^-e^+ \to W^\pm e^\mp(\bar{\nu_e})\nu_e \to 2le^\mp(\bar{\nu_e})\nu_e$	865717	1966.97	1770274	445623	445621	105	16	0	0	0	0	0	0	0
$e^-e^+ \to Ze^-e^+ \to 2le^-e^+$	1036137	1053.45	948101	75199	75199	20	0	0	0	0	0	0	0	0
$e^-e^+ \to Z \to 2l + 2\nu_l$	2962831	12993.9	11694480	4544242	4544006	3557	227	62	7	7	7	0	0	0
$e^-e^+ \to ZZ/WW \to 2l2\nu_l$	430208	958.97	863072	317845	317822	312	37	2	2	0	0	0	0	0
$e^-e^+ \to Z/W \to 2e2\nu_e$	255052	550.666	495599	0	0	0	0	0	0	0	0	0	0	0
BACKGROUND(Type: hadronic):														
$e^-e^+ \to WW \to 4j$	114038	8706.23	7835603	15779	15779	98	0	0	0	0	0	0	0	0
$e^-e^+ \to ZZ/WW \to 4j$	176000	7252.1	6526889	15027	15027	163	0	0	0	0	0	0	0	0
$e^-e^+ \to Z \to 2j + 2b$	3015395	78046.5	70241816	138488	127112	38869	3410	1174	278	103	6	6	0	0
$e^-e^+ \to ZZ \to 2j(b) + 2b(j)$	237330	841.376	757238	3771	3088	1361	95	0	0	0	0	0	0	0
BACKGROUND(Type: misceleneous):														
$e^-e^+ \to 2e\gamma$	1996718	25183.4	22665024	79	79	0	0	0	0	0	0	0	0	0
$e^-e^+ \to ffh$	849373	312.937	281642	24750	19569	3295	763	339	115	95	94	78	62	34

TABLE 4.2: Signal with *muonic* final state (coupling values set equal to unity) and background events at different stages of selection. The beam polarizations of $(-80\%, +30\%)$ are assumed.

4.3.2.2 Event Selection: Electronic final state

In this case we demand that every event contains one electron (of either charge) and two jets, satisfying the preselection criteria. Out of the two jets, the one with higher b-tagging efficiency is tagged as the $b-$jet (no charge identification), while the other one is tagged as the light-jet. The distributions are plotted in Fig. 4.4. The distributions consists of one signal events and all other background events, which remain non zero after implication of cuts as described in Table 4.3.

We employ the same selection criteria as that considered for the muonic case in Section 4.3.2.1, except the muon replace by electron in this case. The signal events remain at the same level of $3 - 7 \times 10^4$, whereas the corresponding background events total to $\sim$512. The detailed cut-flow chart for different backgrounds separately are presented in Table 4.3.

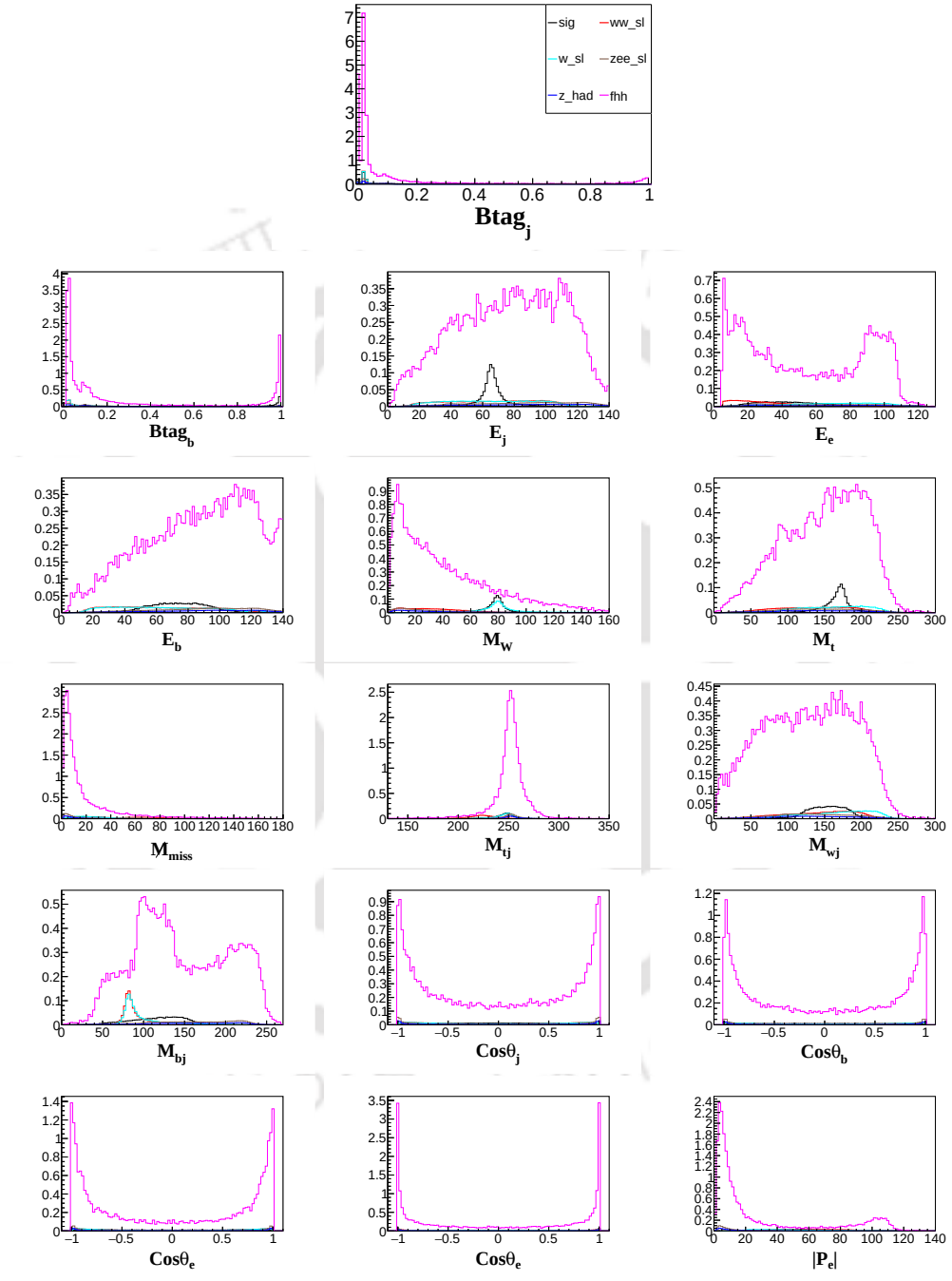

FIGURE 4.4: Distributions after the events are identified with as containing one light-jet, one $b-$jet and one *electron* of either charge. The beam polarizations of $(-80\%, +30\%)$ are assumed. Signal corresponds to the coupling $\kappa^L_{\gamma qt}$, and the backgrounds are (a) $e^-e^+ \to WW \to l\nu_l 2j$ (b) $e^-e^+ \to W^\pm e^\mp \nu \to 2je\nu$ (c) $e^-e^+ \to Ze^-e^+ \to 2je^-e^+$ (d) $e^-e^+ \to Z \to 2j + 2b$ (e) $e^-e^+ \to ffh$

Process	$N_{simulated}$	$\sigma_{-.8,+.3}[fb]$	N_{eve}	N_e=N_j=N_b=1	$Btag_j < 0.4$	$Btag_b > 0.8$	$55 < E_j < 75$	$40 < E_b < 105$	$65 < m_W < 95$	$140 < m_t < 185$	$M_{bj\not{e}} \epsilon [65, 95]$	$\lvert p_\nu \rvert > 30$	$\cos\theta_e < .95$, $\lvert\cos\theta_\nu\rvert < .95$, $\Delta\theta_{j,e} < 1.5$	$\lvert P_j \rvert \epsilon [50, 70]$, $\sqrt{(p_j + p_b)^2} > 20$
SIGNAL: $e^-e^+ \to t, q(t \to Wb, W \to e\nu_e)$														
$\kappa_{\gamma qt}^{L(R)}$	20000	313.01	281709	265368	263481	171193	137642	132107	120781	113753	91710	86132	77680	73637
$X_{zqt}^{L(R)}$	20000	156.13	140517	132372	131445	85272	68382	65270	59269	55335	43784	40672	34556	32869
$\kappa_{zqt}^{L(R)}$	19000	263.51	237159	221517	219870	144316	115221	109953	100555	93789	77038	72494	62619	59373
BACKGROUND(Type: semileptonic):														
$e^-e^+ \to WW \to l\nu_l 2j$	1962649	10992.9	9893624	545138	544922	3154	731	638	61	46	20	20	15	15
$e^-e^+ \to Z\nu\nu \to 2j\nu\nu$	147517	271.805	244624	929	824	159	10	6	2	0	0	0	0	0
$e^-e^+ \to ZZ \to 2l2j + 2\nu_l 2j$	535103	856.927	771234	24761	22312	2269	535	313	16	10	8	6	2	2
$e^-e^+ \to W^\pm e^\mp \nu \to 2je\nu$	121492	5898.17	5308351	4982370	4981561	29515	6174	4966	2941	2406	533	533	399	399
$e^-e^+ \to Ze^-e^+ \to 2je^-e^+$	325217	378.281	340452	320186	304663	23771	4721	1744	498	434	405	131	44	23
BACKGROUND(Type: leptonic):														
$e^-e^+ \to WW \to l\nu_l 2l$	409207	915.577	824018	22008	22008	10	2	0	0	0	0	0	0	0
$e^-e^+ \to Z\nu\nu \to 2l\nu\nu$	80000	114.137	102722	3045	3045	10	0	0	0	0	0	0	0	0
$e^-e^+ \to ZZ \to 2l2l + 2\nu_l 2l$	70000	95.8895	86300	5660	5633	61	6	2	0	0	0	0	0	0
$e^-e^+ \to W^\pm e^\mp(\bar{\nu_e})\nu_e \to 2le^\mp(\bar{\nu_e})\nu_e$	865717	1966.97	1770274	1154121	1154012	3171	157	102	18	8	4	4	4	2
$e^-e^+ \to Ze^-e^+ \to 2le^-e^+$	1036137	1053.45	948101	764449	764288	1118	120	56	11	10	10	3	1	1
$e^-e^+ \to Z \to 2l + 2\nu_l$	2962831	12993.9	11694480	983610	983189	4897	239	121	8	1	0	0	0	0
$e^-e^+ \to ZZ/WW \to 2l2\nu_l$	430208	958.97	863072	76945	76933	323	4	0	0	0	0	0	0	0
$e^-e^+ \to Z/W \to 2e2\nu_e$	255052	550.666	495599	479953	479953	101	16	8	4	4	0	0	0	0
BACKGROUND(Type: hadronic):														
$e^-e^+ \to WW \to 4j$	114038	8706.23	7835603	34809	34809	197	0	0	0	0	0	0	0	0
$e^-e^+ \to ZZ/WW \to 4j$	176000	7252.1	6526889	32346	32346	272	54	0	0	0	0	0	0	0
$e^-e^+ \to Z \to 2j + 2b$	3015395	78046.5	70241816	608835	556591	71837	12723	5389	1675	1498	1103	439	177	42
$e^-e^+ \to ZZ \to 2j(b) + 2b(j)$	237330	841.376	757238	4743	3925	1172	90	6	0	0	0	0	0	0
BACKGROUND(Type: misceleneous):														
$e^-e^+ \to 2e\gamma$	1996718	25183.4	22665024	21204083	21203986	2230	246	111	0	0	0	0	0	0
$e^-e^+ \to ffh$	849373	312.937	281642	26602	21030	3396	740	314	95	79	79	63	52	33

TABLE 4.3: Signal with *electronic* final state (coupling values set equal to unity) and background events at different stages of selection. The beam polarizations of $(-80\%, +30\%)$ are assumed.

4.3.2.3 Further analysis: making use of asymmetries

As described in Section 4.1, the Lorentz structure of the anomalous couplings could leave its distinct feature in the angular distributions of the light-jet emitted along with the top quark, as well as the decay products of the top quark. We investigate the angular distributions of light jet, $b-$jet, decay lepton and the missing momentum (arising from ν) in the c.m. frame, for the different choices of tensor and vector couplings in Fig. 4.5. Clearly, the tensor and vector couplings have different forward-backward asymmetry in the case of light-jet. While the right-handed vector coupling corresponds to a forward peak, the left-handed vector coupling leaves most of the events in the backward hemisphere. On the other hand, the tensor couplings have the opposite behaviour. However, there is no clear distinction between the Z or γ couplings. The distribution of the decay product, $b-$jet, on the other hand, gives a slightly different perspective. Generally, the asymmetries as against the handedness is reversed compared to the case of light-jet. This is expected, as the $b-$jet emerges from the top quark which has a momentum opposite to that of the light-jet. With the top quark decay on-flight, the asymmetries are less pronounced, with the asymmetry in the tensor couplings is somewhat washed out.

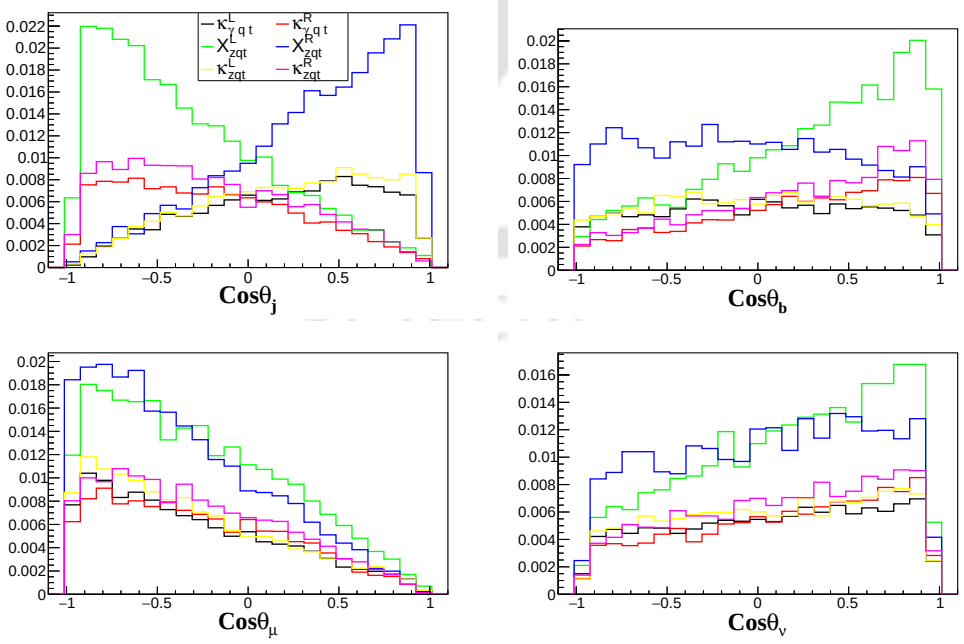

FIGURE 4.5: Normalized angular distributions of the final state particles (reconstructed) in the case of *top quark, muonic* decay, for different type of couplings, taken one at a time. Beam polarizations of $(-80\%, +30\%)$ is assumed.

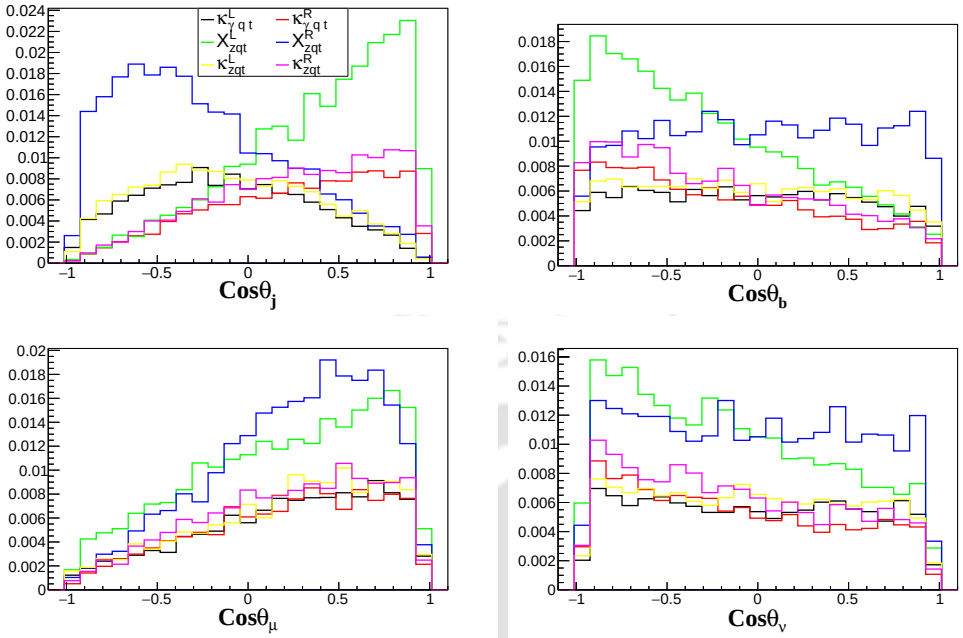

FIGURE 4.6: Normalised angular distributions of the final state particles (reconstructed) in the case of *anti-top quark, muonic* decay, for different type of couplings, taken one at a time. Beam polarizations of $(-80\%, +30\%)$ is assumed.

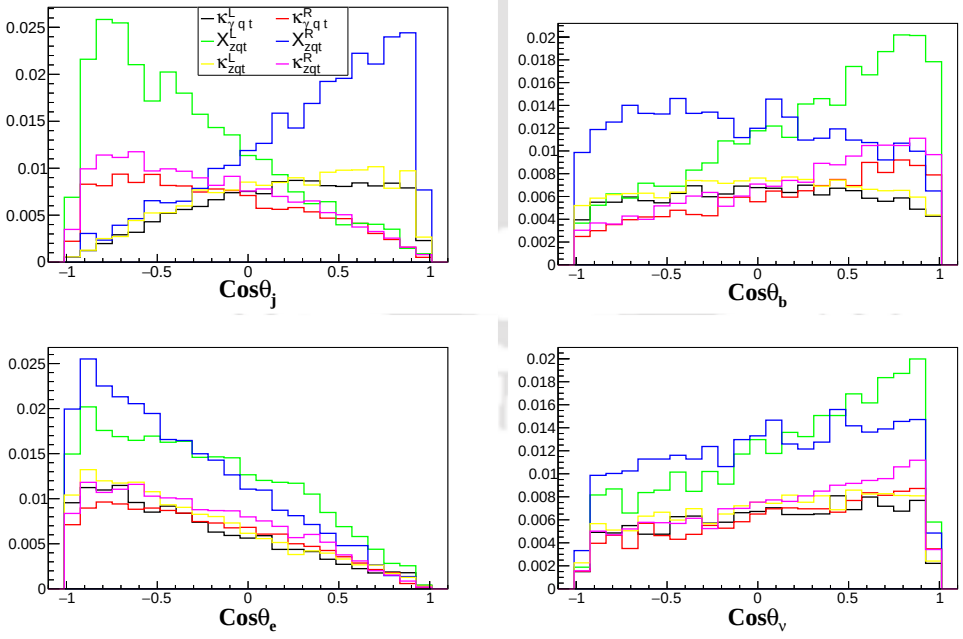

FIGURE 4.7: Normalised angular distributions of the final state particles (reconstructed) in the case of *top quark, electronic* decay, for different type of couplings, taken one at a time. Beam polarizations of $(-80\%, +30\%)$ is assumed.

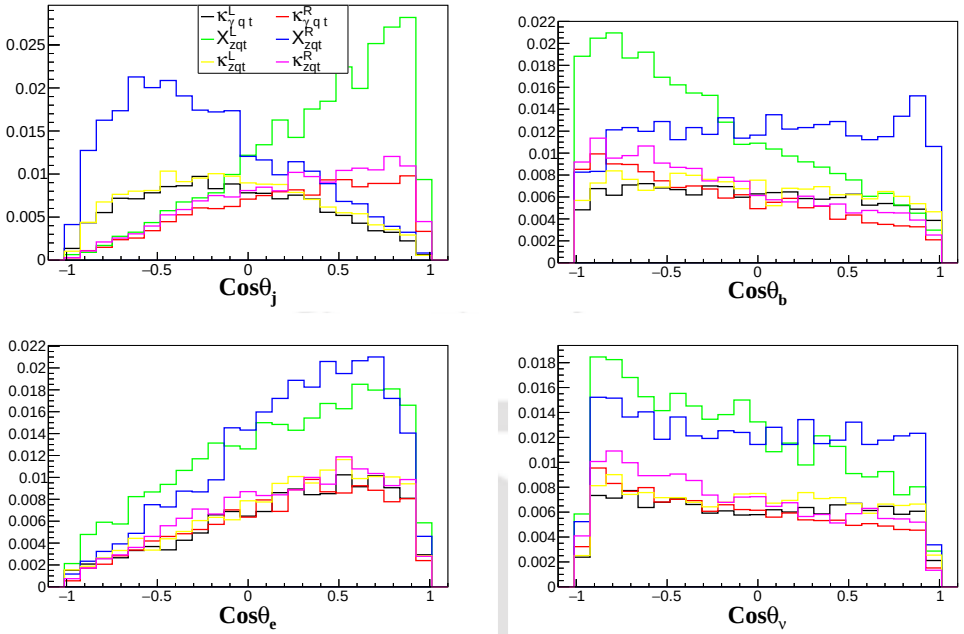

FIGURE 4.8: Normalised angular distributions of the final state particles (reconstructed) in the case of *anti-top quark, electronic* decay, for different type of couplings, taken one at a time. Beam polarizations of $(-80\%, +30\%)$ is assumed.

Both the μ and ν distributions in the c.m. frame are somewhat insensitive to the nature of the couplings. The case of electron in the final state has a similar behavior. We plot the distributions in Figs. 4.7 and 4.8 for muonic decay and Figs. 4.7 and 4.8 for electronic decay of top/antitop quark respectively.

The top quark polarization is expected to be a helpful observable in deciphering the structure of the interactions at the production level. As discussed in the Chapter 2 of the thesis, the top quark polarization can be parameterized in terms of the quantities, P_x, P_y, P_z defined in Section 2.2.1. The polarization of the top quark will be reflected in the angular distribution of the decay products. The polar angle (θ_ℓ) and azimuthal angle (ϕ_ℓ) of the top decay lepton (muon or electron, as the case may be) measured in the top rest frame with z-axis along the top boost direction, and the top production plane defining the xz-plane. The three asymmetries defined in the top quark rest frame, out of which, two defined in terms of the azimuthal angle, and one in terms of the polar angle of the decay lepton can be referred from Eq. (2.23) of Chapter 2. As discussed earlier, by definition P_y vanishes in the case of CP-symmetric interactions, as considered in our case. In Tables 4.4 and 4.5 we present the value of above asymmetries, along with the forward-backward asymmetry of the light-jet (A_j^{FB}), $b-$jet (A_b^{FB}) and μ/e (A_ℓ^{FB})

defined in the lab frame. First of all, the asymmetries help distinguishing the signal from irreducible background remaining after the final selection. Further suitable combinations of the asymmetries have the potential to disentangle the Lorentz structure, viz, if the coupling is vector type or tensor type; left-handed or right-handed. A_x, for example is vanishingly small for all the backgrounds, whereas it is between $30 - 40\%$ for the signal, depending on the type of the coupling.

Coupling	top - muonic final state					top - electonic final state				
	A_x	A_z	A_j^{FB}	A_b^{FB}	A_μ^{FB}	A_x	A_z	A_j^{FB}	A_b^{FB}	A_μ^{FB}
$\kappa^L_{\gamma qt}$	0.41	-0.19	0.30	0.02	-0.47	0.39	-0.19	0.31	0.02	-0.46
$\kappa^R_{\gamma qt}$	0.40	-0.18	-0.32	0.30	-0.42	0.41	-0.14	-0.30	0.25	-0.41
X^L_{zqt}	0.34	-0.47	-0.49	0.36	-0.42	0.33	-0.44	-0.53	0.34	-0.37
X^R_{zqt}	0.36	0.12	0.53	-0.04	-0.54	0.35	0.14	0.53	-0.06	-0.54
κ^L_{zqt}	0.39	-0.17	0.32	0.02	-0.49	0.43	-0.19	0.30	0.04	-0.50
κ^R_{zqt}	0.42	-0.17	-0.33	0.32	-0.43	0.41	-0.11	-0.33	0.28	-0.40
$e^-e^+ \to WW \to l\nu_l 2j$	0.02	0.09	0.14	0.00	-0.02	-0.17	0.17	-0.50	-0.17	0.50
$e^-e^+ \to ZZ \to 2l2j + 2\nu_l 2j$	-0.65	-0.76	-0.41	0.35	-0.47	–	–	–	–	–
$e^-e^+ \to ffh$	0.14	-0.27	0.2	-0.12	-0.25	0.46	-0.75	0.68	-0.67	-0.59

TABLE 4.4: **After Detector:** top quark case. The mean value of the asymmetries at $\sqrt{s}$=250 GeV with beam polarizations of $(-80\%, +30\%)$. All coupling values are set to unity.

Coupling	anti-top - muonic final state					anti-top - electonic final state				
	A_x	A_z	A_j^{FB}	A_b^{FB}	A_μ^{FB}	A_x	A_z	A_j^{FB}	A_b^{FB}	A_μ^{FB}
$\kappa_{\gamma qt}^L$	-0.30	-0.32	-0.19	-0.02	0.32	-0.31	-0.34	-0.17	-0.05	0.32
$\kappa_{\gamma qt}^R$	-0.32	-0.13	0.39	-0.26	0.31	-0.34	-0.13	0.39	-0.30	0.35
X_{zqt}^L	-0.25	-0.44	0.58	-0.37	0.31	-0.26	-0.42	0.59	-0.37	0.30
X_{zqt}^R	-0.28	0.01	-0.40	0.04	0.41	-0.25	0.03	-0.44	0.09	0.40
κ_{zqt}^L	-0.31	-0.33	-0.17	-0.04	0.35	-0.32	-0.33	-0.16	-0.06	0.34
κ_{zqt}^R	-0.31	-0.12	0.39	-0.27	0.30	-0.34	-0.12	0.39	-0.30	0.30

TABLE 4.5: **After Detector:** anti-top quark case. The mean value of the asymmetries at $\sqrt{s}$=250 GeV with beam polarizations of $(-80\%, +30\%)$. All coupling values are set to unity.

The sign of the values for A_x is $+ve$ for top quark and $-ve$ for anti-top quark events. The combination of $(A_j^{FB},\ A_\mu^{FB})$ is $(+ve,\ -ve)$ for the left-handed tensor couplings and right-handed vector coupling for the signal events. In the case of the remaining backgrounds, the A_y is between $30-60\%$, which clearly disentangle backgrounds from the remaining events samples. Similarly, A_x is negligible for the WW-semi-leptonic background. In practice, one will be left with background and signal events. This means, that these asymmetries will vanish if the signal with the above coupling is present along with the irreducible background.

On the other hand, if the coupling is either right-handed tensor type or left-handed vector type, $(A_j^{FB},\ A_\mu^{FB}) \equiv (-ve,\ -ve)$ with an enhanced value. Notice also that the asymmetries, unlike the cross section does not depend on the quantitative information on the coupling. Rather, with relatively smaller number of events, one can unambiguously establish the presence of asymmetry, and further distinguish one class of couplings from the another. We emphasis the importance in Tables 4.11 and 4.12 to give a clear idea of distinguishing various different couplings by just looking in to the sign of the asymmetries values.

4.3.3 Case 2: Beam polarization of $(+80\%, \ -30\%)$

We shall now take up the case of $(+80\%, -30\%)$ beam polarization combination. The preliminary selection identified events with one muon or electron as the case may be. The distributions in the muonic case after the preliminary selection are given in Fig. 4.9. We notice that there is no considerable difference in the qualitative nature of the distributions with the left-handed electron dominated polarization combination considered previously. For event selection, we shall follow the same strategy as described in detail in Section 4.3.2.1. The cut-flow listed in Table 4.6 gives the signal and background events at every stage of selection. About $2.5 - 8.3 \times 10^4$ signal events survive the selection depending on the type of coupling considered (taken to be unity), whereas the background events total to 21 in the semi-leptonic category and 29 from ffh channel.

On the other hand, in the case of signal with $jbe\nu$ final state, we have $2-7\times10^4$ signal events as in the left-handed electron dominated polarization combination, while the background is reduced to 46 events in semi-leptonic case and 25 events in the ffh channel. The cut-flow with detailed event selection is given in Table 4.7.

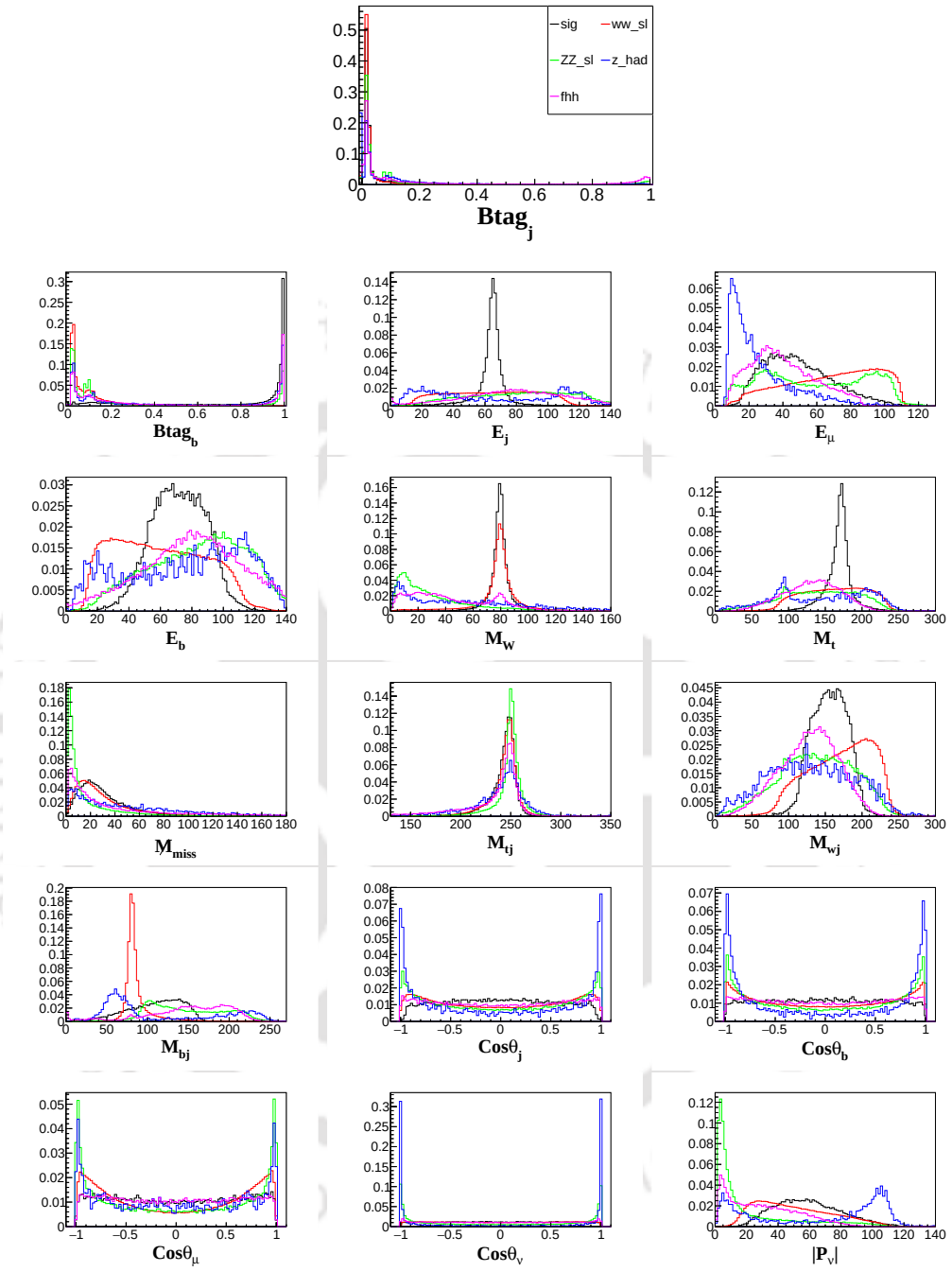

FIGURE 4.9: Distributions after the events are identified with as containing one light-jet, one $b-$jet and one μ of either charge. The beam polarization combinations of $(+80\%, -30\%)$ are assumed. Signal corresponds to the coupling $\kappa^L_{\gamma qt}$, and the backgrounds are (a) $e^-e^+ \to WW \to l\nu_l 2j$ (b) $e^-e^+ \to ZZ \to 2l2j + 2\nu_l 2j$ (c) $e^-e^+ \to Z \to 2j + 2b$ (d) $e^-e^+ \to ffh$

Process	$N_{simulated}$	$\sigma_{+.8,-.3}[fb]$	N_{eve}	N_μ=N_j=N_b=1	$Btag_j < 0.4$	$Btag_b > 0.8$	$55 < E_j < 75$	$40 < E_b < 105$	$65 < m_W < 95$	$140 < m_t < 185$	$M_{bj\ell}\epsilon[65,95]$	$\lvert p_\nu\rvert > 30$	$\cos\theta_\mu < .95$, $\lvert\cos\theta_\nu\rvert < .95$, $\Delta\theta_{j,\mu} < 1.5$	$\lvert P_j\rvert\epsilon[50,70]$, $\sqrt{(p_j+p_b)^2} > 20$
SIGNAL: $e^-e^+ \to t, q(t \to Wb, W \to \mu\nu_\mu)$														
$\kappa_{\gamma qt}^{L(R)}$	20000	313.47	282123	273843	271994	175962	151756	148371	140584	132811	108378	101170	87486	83354
$X_{zqt}^{L(R)}$	20000	106.13	95517	92899	92298	59938	52207	50912	48674	46037	38082	36082	32398	30640
$\kappa_{zqt}^{L(R)}$	20000	178.5	160650	155852	154865	101429	87742	85630	81614	76891	62575	58864	50841	48238
BACKGROUND(Type: semileptonic):														
$e^-e^+ \to WW \to l\nu_l 2j$	1962649	758.383	682544	355641	355536	2105	485	437	352	299	44	32	23	17
$e^-e^+ \to Z\nu\nu \to 2j\nu\nu$	147517	92.4996	83249	236	208	88	10	2	0	0	0	0	0	0
$e^-e^+ \to ZZ \to 2l2j + 2\nu_l 2j$	535103	467.188	420469	112252	102617	10658	2486	1141	255	225	207	74	15	4
$e^-e^+ \to W^\pm e^\mp \nu \to 2je\nu$	121492	445.424	400881	84	84	0	0	0	0	0	0	0	0	0
$e^-e^+ \to Ze^-e^+ \to 2je^-e^+$	325217	299.684	269715	56	54	4	0	0	0	0	0	0	0	0
BACKGROUND(Type: leptonic):														
$e^-e^+ \to WW \to l\nu_l 2l$	409207	63.342	57007	43267	43255	178	3	1	0	0	0	0	0	0
$e^-e^+ \to Z\nu\nu \to 2l\nu\nu$	80000	29.7478	26772	7037	7037	1	1	0	0	0	0	0	0	0
$e^-e^+ \to ZZ \to 2l2l + 2\nu_l 2l$	70000	63.7397	57365	28911	28834	142	26	16	5	5	1	1	1	0
$e^-e^+ \to W^\pm e^\mp(\bar{\nu_e})\nu_e \to 2le^\mp(\bar{\nu_e})\nu_e$	865717	148.905	134014	34281	34280	16	2	0	0	0	0	0	0	0
$e^-e^+ \to Ze^-e^+ \to 2le^-e^+$	1036137	1017.64	915872	71976	71976	22	0	0	0	0	0	0	0	0
$e^-e^+ \to Z \to 2l + 2\nu_l$	2962831	10377.9	9340094	3569950	3569780	2905	152	49	5	0	0	0	0	0
$e^-e^+ \to ZZ/WW \to 2l2\nu_l$	430208	88.8252	79942	27415	27413	22	2	0	0	0	0	0	0	0
$e^-e^+ \to Z/W \to 2e2\nu_e$	255052	55.4048	49864	0	0	0	0	0	0	0	0	0	0	0
BACKGROUND(Type: hadronic):														
$e^-e^+ \to WW \to 4j$	114038	600.369	540331	1134	1134	7	0	0	0	0	0	0	0	0
$e^-e^+ \to ZZ/WW \to 4j$	176000	564.949	508454	1167	1167	9	0	0	0	0	0	0	0	0
$e^-e^+ \to Z \to 2j + 2b$	3015395	46214.8	41593316	86464	80173	24032	2144	1118	383	320	105	105	0	0
$e^-e^+ \to ZZ \to 2j(b) + 2b(j)$	237330	402.98	362682	1843	1489	652	42	2	0	0	0	0	0	0
BACKGROUND(Type: misceleneous):														
$e^-e^+ \to 2e\gamma$	1996718	24605.9	22145318	103	103	0	0	0	0	0	0	0	0	0
$e^-e^+ \to ffh$	849373	205.277	184748	16525	12986	2243	515	235	84	71	70	54	42	29

TABLE 4.6: Signal with *muonic* final state (coupling values set equal to unity) and background events at different stages of selection. The beam polarizations of $(+80\%, -30\%)$ are assumed.

Similarly the electronic samples are considered for distributions in the following.

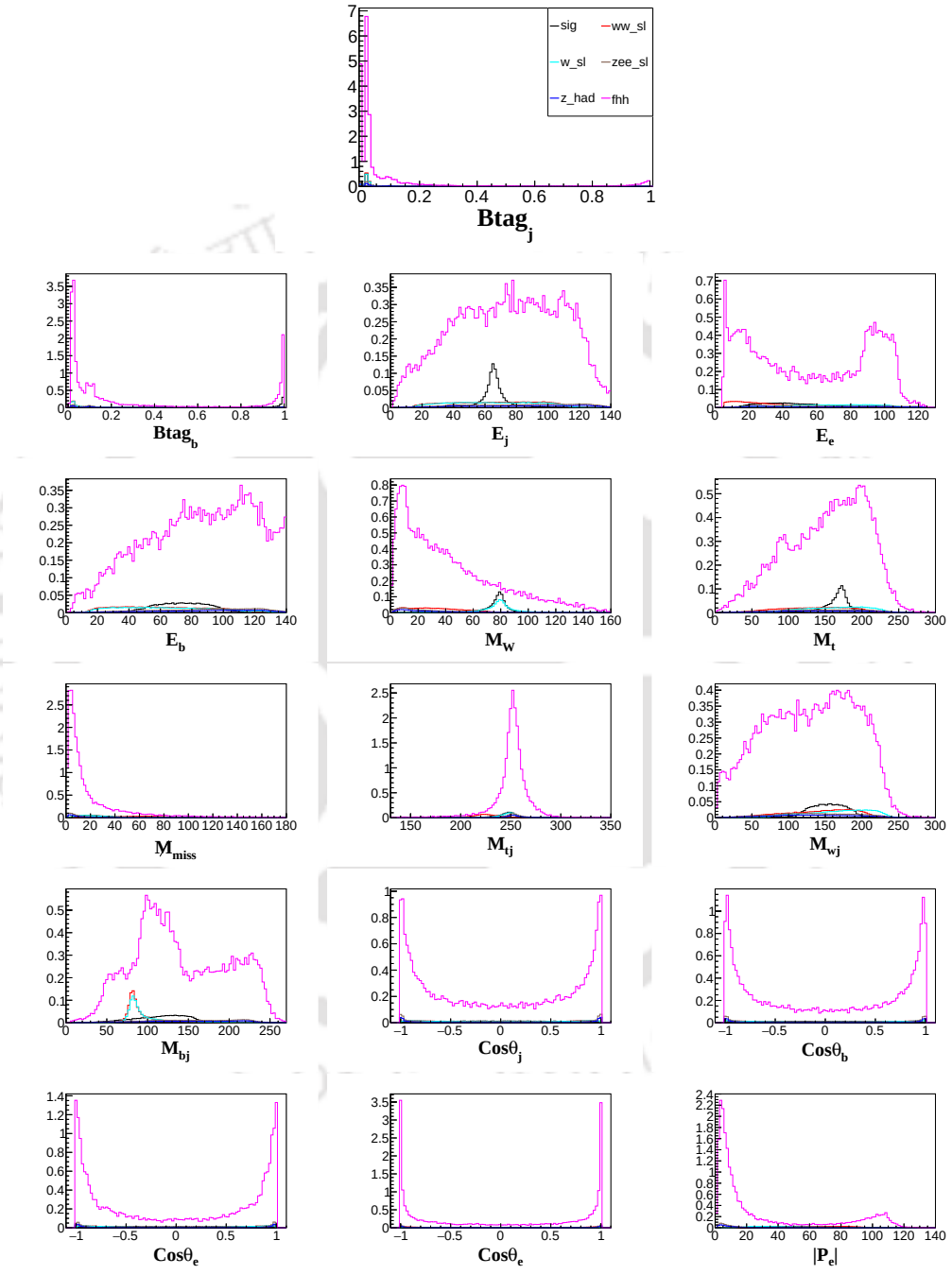

FIGURE 4.10: Distributions after the events are identified with one light-jet, one $b-$jet and one *electron* of either charge. The beam polarizations of $(+80\%, -30\%)$ are assumed. Signal corresponds to the coupling $\kappa^L_{\gamma qt}$, and the backgrounds are (a) $e^-e^+ \to WW \to l\nu_l 2j$ (b) $e^-e^+ \to W^\pm e^\mp \nu \to 2je\nu$ (c) $e^-e^+ \to Ze^-e^+ \to 2je^-e^+$ (d) $e^-e^+ \to Z \to 2j + 2b$ (e) $e^-e^+ \to ffh$.

Process	$N_{simulated}$	$\sigma_{+.8,-.3}[fb]$	N_{eve}	N_e=N_j=N_b=1	$Btag_j < 0.4$	$Btag_b > 0.8$	$55 < E_j < 75$	$40 < E_b < 105$	$65 < m_W < 95$	$140 < m_t < 185$	$M_{bj\not{e}} \epsilon [65, 95]$	$\lvert p_\nu \rvert > 30$	$\cos\theta_e < .95$, $\lvert\cos\theta_\nu\rvert < .95$, $\Delta\theta_{j,e} < 1.5$	$\lvert P_j \rvert \epsilon [50, 70]$, $\sqrt{(p_j + p_b)^2} > 20$
SIGNAL: $e^-e^+ \to t, q(t \to Wb, W \to e\nu_e)$														
$\kappa_{\gamma qt}^{L(R)}$	20000	312.86	281574	265145	263427	169676	136240	130721	119640	111671	91172	85765	77670	73151
$X_{zqt}^{L(R)}$	20000	105.1	94590	88413	87792	56984	45885	44177	40885	38540	31602	30140	27128	25619
$\kappa_{zqt}^{L(R)}$	19500	178.01	160209	151246	150295	96220	77378	73943	68048	63671	51949	48742	43953	41536
BACKGROUND(Type: semileptonic):														
$e^-e^+ \to WW \to l\nu_l 2j$	1962649	758.383	682544	37447	37434	213	49	44	3	2	1	1	0	0
$e^-e^+ \to Z\nu\nu \to 2j\nu\nu$	147517	92.4996	83249	323	285	46	0	0	0	0	0	0	0	0
$e^-e^+ \to ZZ \to 2l2j + 2\nu_l 2j$	535103	467.188	420469	13301	12038	1137	285	171	3	2	2	2	0	0
$e^-e^+ \to W^\pm e^\mp \nu \to 2je\nu$	121492	445.424	400881	370726	370644	2187	465	375	227	183	40	38	29	29
$e^-e^+ \to Ze^-e^+ \to 2je^-e^+$	325217	299.684	269715	250594	240699	16856	3373	1236	327	265	250	88	29	17
BACKGROUND(Type: leptonic):														
$e^-e^+ \to WW \to l\nu_l 2l$	409207	63.342	57007	1513	1513	0	0	0	0	0	0	0	0	0
$e^-e^+ \to Z\nu\nu \to 2l\nu\nu$	80000	29.7478	26772	1069	1069	2	0	0	0	0	0	0	0	0
$e^-e^+ \to ZZ \to 2l2l + 2\nu_l 2l$	70000	63.7397	57365	3668	3653	32	5	1	0	0	0	0	0	0
$e^-e^+ \to W^\pm e^\mp(\bar{\nu_e})\nu_e \to 2le^\mp(\bar{\nu_e})\nu_e$	865717	148.905	134014	85213	85205	234	9	6	1	0	0	0	0	0
$e^-e^+ \to Ze^-e^+ \to 2le^-e^+$	1036137	1017.64	915872	737183	737060	1061	117	53	10	10	9	3	1	1
$e^-e^+ \to Z \to 2l + 2\nu_l$	2962831	10377.9	9340094	740631	740305	3838	228	139	29	23	11	11	11	0
$e^-e^+ \to ZZ/WW \to 2l2\nu_l$	430208	88.8252	79942	6277	6276	24	1	0	0	0	0	0	0	0
$e^-e^+ \to Z/W \to 2e2\nu_e$	255052	55.4048	49864	47780	47780	8	2	1	0	0	0	0	0	0
BACKGROUND(Type: hadronic):														
$e^-e^+ \to WW \to 4j$	114038	600.369	540331	2429	2429	15	0	0	0	0	0	0	0	0
$e^-e^+ \to ZZ/WW \to 4j$	176000	564.949	508454	2466	2466	22	3	0	0	0	0	0	0	0
$e^-e^+ \to Z \to 2j + 2b$	3015395	46214.8	41593316	393790	362848	49180	8862	3861	938	823	641	235	115	2
$e^-e^+ \to ZZ \to 2j(b) + 2b(j)$	237330	402.98	362682	2258	1829	625	63	8	0	0	0	0	0	0
BACKGROUND(Type: misceleneous):														
$e^-e^+ \to 2e\gamma$	1996718	24605.9	22145318	20702738	20702700	2384	249	99	0	0	0	0	0	0
$e^-e^+ \to ffh$	849373	205.277	184748	17833	13961	2295	508	216	70	56	56	44	38	25

TABLE 4.7: Signal with *electronic* final state (coupling values set equal to unity) and background events at different stages of selection. The beam polarizations of $(+80\%, -30\%)$ are assumed.

The angular distributions of light-jet, $b-$jet, ℓ and the missing momentum are plotted in Figs. 4.11 and 4.12 for muonic decay and Figs. 4.13 and 4.14 for electronic decay, of top/anti-top quark respectively.

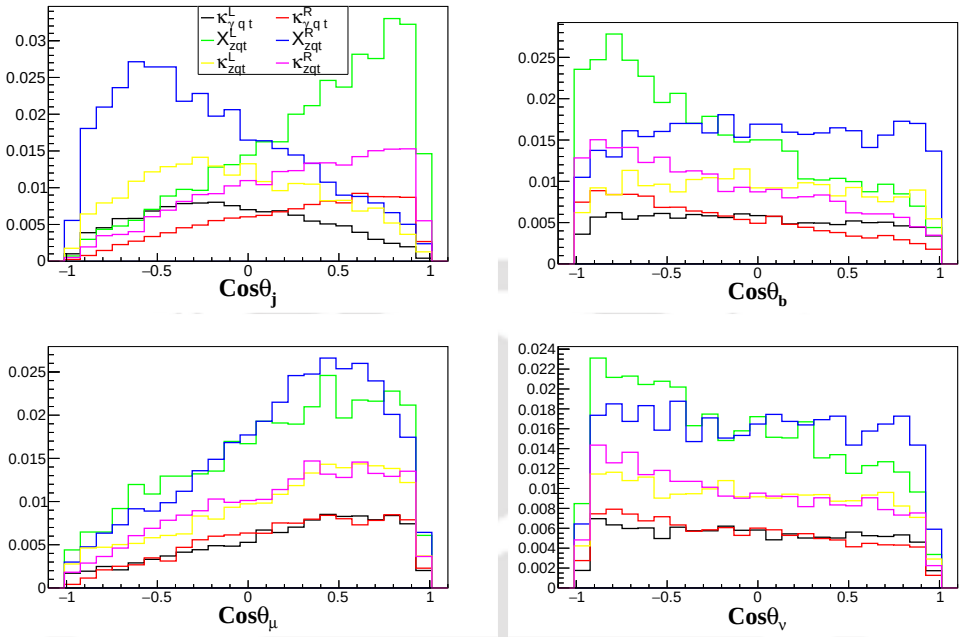

FIGURE 4.11: Normalised angular distributions of the final state particles (reconstructed) in the case of *top quark, muonic* decay, for different type of couplings, taken one at a time. Beam polarizations of $(+80\%, -30\%)$ is assumed.

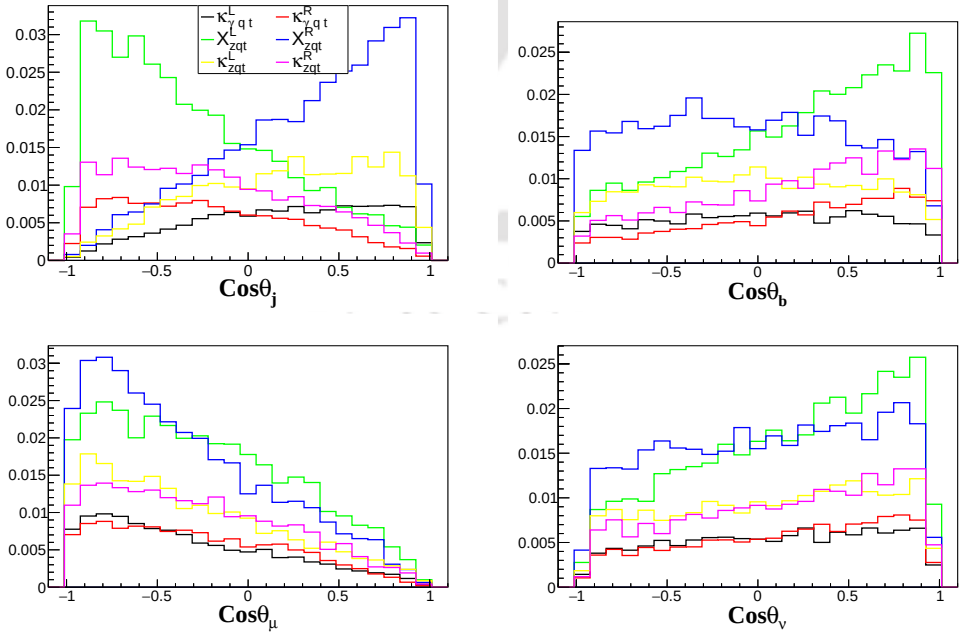

FIGURE 4.12: Normalised angular distributions of the final state particles (reconstructed) in the case of *anti-top quark, muonic* decay, for different type of couplings, taken one at a time. Beam polarizations of $(+80\%, -30\%)$ is assumed.

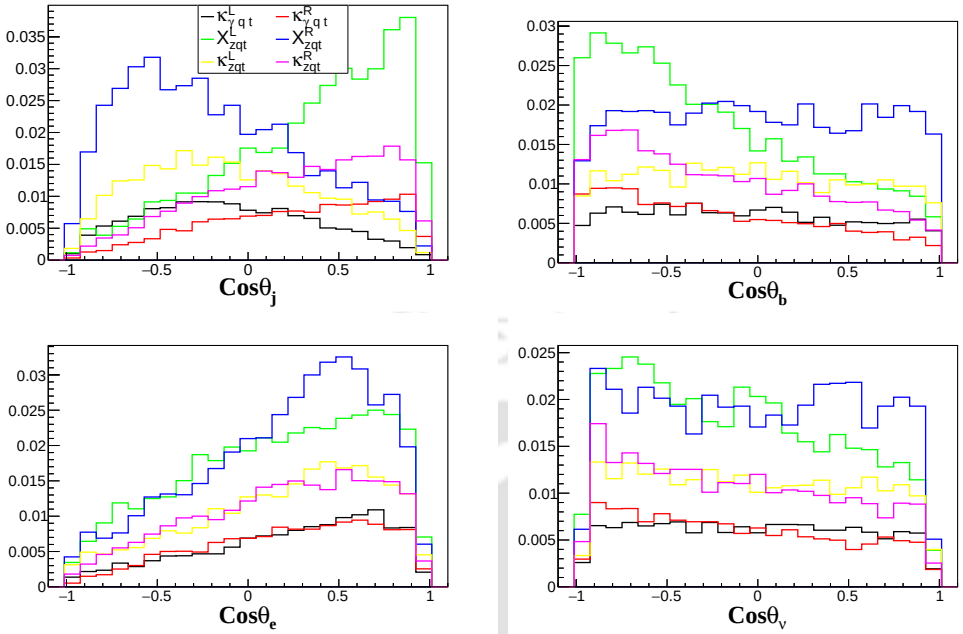

FIGURE 4.13: Normalised angular distributions of the final state particles (reconstructed) in the case of *top quark, electronic* decay, for different type of couplings, taken one at a time. Beam polarizations of $(+80\%, -30\%)$ is assumed.

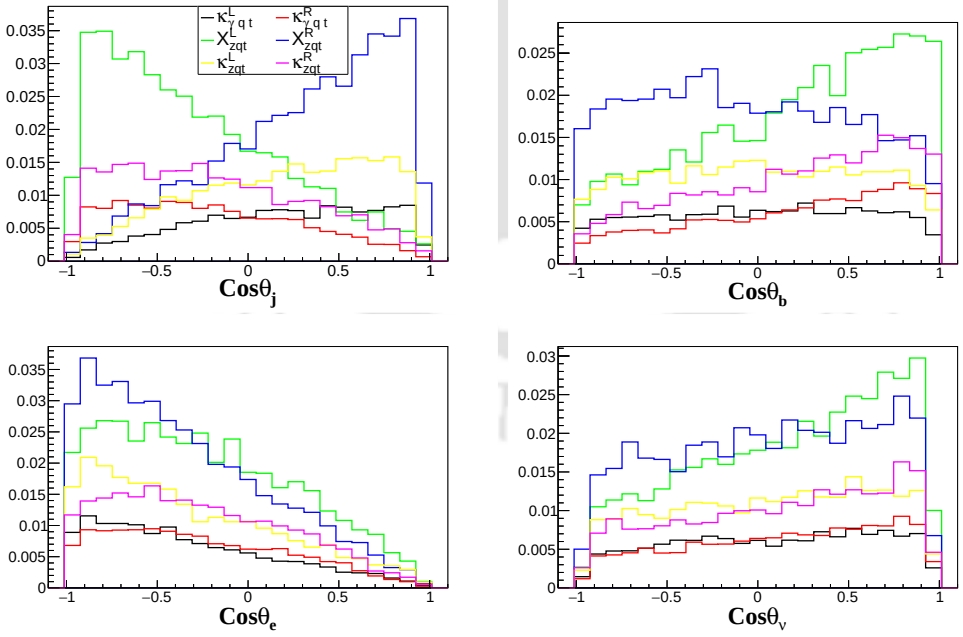

FIGURE 4.14: Normalised angular distributions of the final state particles (reconstructed) in the case of *anti-top quark, electronic* decay, for different type of couplings, taken one at a time. Beam polarizations of $(+80\%, -30\%)$ is assumed.

Distinct from the case of $(-80\%, +30\%)$ polarization, here, the light-jets are forward peaked in the case of left-handed tensor couplings and right-handed vector

coupling, while backward peaked in the case of opposite handedness. Similarly the value of A_x changes sign opposite to that considered in the case of $(-80\%, +30\%)$ polarization.

In Tables 4.8 and 4.9 we present the value of asymmetries defined in the top quark rest frame or lab frame.

Coupling	top - muonic final state					top - electonic final state				
	A_x	A_z	A_j^{FB}	A_b^{FB}	A_μ^{FB}	A_x	A_z	A_j^{FB}	A_b^{FB}	A_μ^{FB}
$\kappa_{\gamma qt}^L$	-0.32	-0.33	-0.14	-0.07	0.36	-0.27	-0.31	-0.19	-0.07	0.33
$\kappa_{\gamma qt}^R$	-0.38	-0.11	0.37	-0.29	0.35	-0.33	-0.11	0.34	-0.27	0.32
X_{zqt}^L	-0.23	-0.43	0.50	-0.30	0.26	-0.21	-0.43	0.49	-0.32	0.24
X_{zqt}^R	-0.22	0.04	-0.34	0.03	0.37	-0.20	0.05	-0.32	0.01	0.33
κ_{zqt}^L	-0.29	-0.29	-0.14	-0.04	0.31	-0.26	-0.34	-0.16	-0.03	0.32
κ_{zqt}^R	-0.32	-0.14	0.34	-0.24	0.27	-0.29	-0.15	0.37	-0.24	0.30
$e^-e^+ \to WW \to l\nu_l 2j$	0.02	0.09	0.14	0.00	-0.02	-0.17	0.17	-0.50	-0.17	0.50
$e^-e^+ \to ZZ \to 2l2j + 2\nu_l 2j$	-0.65	-0.76	-0.41	0.35	-0.47	—	—	—	—	—
$e^-e^+ \to ffh$	0.14	-0.27	0.20	-0.12	-0.25	0.46	-0.75	0.68	-0.67	-0.59

TABLE 4.8: **After Detector:** top quark case. Table showing the mean value of the asymmetric observables at $\sqrt{s}$=250 GeV with beam polarizations of $(+80\%, -30\%)$. All coupling values are set to unity.

Coupling	anti-top - muonic final state					anti-top - electonic final state				
	A_x	A_z	A_j^{FB}	A_b^{FB}	A_μ^{FB}	A_x	A_z	A_j^{FB}	A_b^{FB}	A_μ^{FB}
$\kappa^L_{\gamma qt}$	0.38	-0.18	0.27	0.05	-0.46	0.41	-0.20	0.27	0.03	-0.49
$\kappa^R_{\gamma qt}$	0.38	-0.16	-0.31	0.28	-0.40	0.37	-0.17	-0.30	0.29	-0.40
X^L_{zqt}	0.31	-0.47	-0.47	0.33	-0.38	0.31	-0.50	-0.46	0.32	-0.38
X^R_{zqt}	0.34	0.14	0.49	-0.04	-0.51	0.32	0.13	0.48	-0.09	-0.51
κ^L_{zqt}	0.39	-0.18	0.29	0.01	-0.46	0.41	-0.18	0.29	0.01	-0.45
κ^R_{zqt}	0.39	-0.15	-0.30	0.27	-0.39	0.38	-0.13	-0.29	0.27	-0.39

TABLE 4.9: **After Detector:** anti-top quark case. Table showing the mean value of the asymmetric observables at $\sqrt{s}$=250 GeV with beam polarizations of $(+80\%, 30\%)$. All coupling values are set to unity.

In the case of $b-$jets, only the left-handed tensor couplings and the right-handed vector coupling show the forward backward asymmetry. Again, the asymmetry has the opposite sign compared to the left-handed electron dominated beams. The ability to distinguish various couplings remains intact for the polarization under consideration in this section as well. We similarly emphasize the distinguishable features of asymmetries in Tables 4.11 and 4.12 to give a clear idea by just looking in to the sign of them. A similar explanation of background suppression is expected as discussed in the case of $(-80\%, +30\%)$ beam polarization.

4.4 Discussion: Reach of the couplings

In Table 4.2, 4.3, 4.6 and 4.7 we presented the signal events along with the background events for two different beam polarization combinations, and for the two cases of muon and electron final states. The signal events here are obtained assuming unit couplings, and with the energy scale Λ set to m_t in the case of tensor couplings. Note that we have considered the electronic and muonic final states separately. It is seen that the signal-to-background ratios, in case of muonic final state is greater than the electronic case, i.e., $\frac{N_S}{N_B}|_{\mu^\pm} > \frac{N_S}{N_B}|_{e^\pm}$. The reason behind this, is due to the presence of a few non-zero backgrounds (even after cuts)

arises in case of processes having electron in the final state Ref. Tables 4.3 and 4.7 but which is not in case of muon in the final state Ref. Tables 4.2 and 4.6. For instance the process, $e^-e^+ \to W^\pm e^\mp \nu \to 2je\nu$, enhances the total background in case of electron final state. In addition, the process having muon in the final state have been reconstructed with higher efficiency than the case of electron. Thus the muonic signal can be better probe than the electronic signal for the particular process under consideration at this collider.

The cross section depends on the couplings quadratically, and thus we shall obtain reach on the couplings for the specific cases as described below.

As the first case we shall consider the best case scenario with the beam polarization of $(+80\%, -30\%)$ and muonic final state. From Table 4.6 the total background events at the projected 0.45×2 ab^{-1} integrated luminosity is 50. For signal with 95% C.L. significance we need 16 signal events, where we consider the following formula for significance calculation

$$\text{Significance} = \frac{N_S}{\sqrt{N_S + N_B}}, \tag{4.6}$$

where N_S and N_B correspond to the number of signal and background events, respectively. Setting the couplings to unity we have 83354 events with κ_γ, 30640 events with the vector coupling X_z, and 48238 events with κ_z tensor coupling. Since the cross section depends on the square of the coupling, we can scale it to get the number of events corresponding to a specific value of the coupling as per,

$$N(\kappa) = N(\kappa = 1) \times \kappa^2. \tag{4.7}$$

Thus, setting $N_S = 16$ corresponds to $\kappa_\gamma = 0.014$, $X_z = 0.023$ and $\kappa_z = 0.018$. With the electronic final state for the same beam polarization we have somewhat similar reach, with $\kappa_\gamma = 0.016$, $X_z = 0.027$ and $\kappa_z = 0.021$. We have tabulated these observations and the reach of each coupling in Table 4.10. A similar analysis in the case of beam polarizations of $(-80\%, +30\%)$ shows slightly reduced reach in this case, owing to the reduced background.

polarization	final state	Background events, N_B	Required signal, N_S	Reach of couplings for 95% CL.		
				$\kappa_{\gamma qt}^{L(R)}/m_t$	$X_{zqt}^{L(R)}$	$\kappa_{zqt}^{L(R)}/m_t$
$(+80\%, -30\%)$	muon	50	16	0.014	0.023	0.018
	electron	73	19	0.016	0.027	0.021
$(-80\%, +30\%)$	muon	361	39	0.022	0.029	0.023
	electron	515	47	0.025	0.038	0.028

TABLE 4.10: The upper limits on the couplings for 95% C.L. signal significance are quoted for two different beam polarizations considered in this study. The cases of top quark decay to final states with μ and e are presented separately. An assumed integrated luminosity of 0.45×2 ab^{-1} is used.

4.4.1 Asymmetries as discriminator

The cross section itself is insensitive to whether the coupling is right-handed or left-handed. Moreover, the dependence of the cross section on the Lorentz structure of the coupling (vector or tensor), and on whether tqz or $tq\gamma$ cannot be distinguished with single observable of number of events. The asymmetries discussed in Section 4.3.2.3 and further in Section 4.3.3 could be efficiently used to disentangle the type of coupling. Presence or absence of these asymmetries in the background can further be used to enhance the signal significance with multiple observables. In the following we shall take a closer look at the first consideration; namely the use of asymmetries in disentangling the Lorentz structure and type of FCNC coupling.

We shall first consider the asymmetries quoted in Table 4.4 and Table 4.8 for the two beam polarization cases considered. The asymmetries A_x or A_ℓ^{FB}, where ℓ corresponds to either muon or electron depending on the decay final state considered, do not have any distinguishing power and may not be useful in disentangling the type of coupling. Nevertheless they are useful in distinguishing whether a top quark or an anti-top quark is produced for both polarization samples. On the other hand, the forward backward asymmetries of the light jet, the $b-$jet and the top quark polarization asymmetry A_z can be combinely used to discriminate different Lorentz structure and further if the coupling is photon type or Z-type.

$(-80\%, +30\%)$			$(+80\%, -30\%)$		
A_z	A_j^{FB}	Coupling	A_z	A_j^{FB}	Coupling
$-$ve	$-$ve	X_{zqt}^L, $\kappa_{\gamma qt}^R$, κ_{zqt}^R	$-$ve	$+$ve	X_{zqt}^L, $\kappa_{\gamma qt}^R$, κ_{zqt}^R
absent	$+$ve	X_{zqt}^R	absent	$-$ve	X_{zqt}^R
$-$ve	$+$ve	$\kappa_{\gamma qt}^L, \kappa_{zqt}^L$	$-$ve	$-$ve	$\kappa_{\gamma qt}^L, \kappa_{zqt}^L$

TABLE 4.11: The response of the asymmetries to different type of couplings in case of top quark production, corresponding to the two different beam polarizations considered in this study, clearly indicating the power of the process in partial discrimination of the nature of the coupling.

Similarly in the case of anti top quark production, the numerical value of the asymmetries can also be used to discriminate the type of couplings as shown in the Table 4.12.

$(-80\%, +30\%)$			$(+80\%, -30\%)$		
A_z	A_j^{FB}	Coupling	A_z	A_j^{FB}	Coupling
$-$ve	$+$ve	X_{zqt}^L, $\kappa_{\gamma qt}^R$, κ_{zqt}^R	$-$ve	$-$ve	X_{zqt}^L, $\kappa_{\gamma qt}^R$, κ_{zqt}^R
absent	$-$ve	X_{zqt}^R	absent	$+$ve	X_{zqt}^R
$-$ve	$-$ve	$\kappa_{\gamma qt}^L, \kappa_{zqt}^L$	$-$ve	$+$ve	$\kappa_{\gamma qt}^L, \kappa_{zqt}^L$

TABLE 4.12: The response of the asymmetries to different type of couplings in case of anti-top quark production, corresponding to the two different beam polarizations considered in this study, clearly indicating the power of the process in partial discrimination of the nature of the coupling.

4.5 Possibilities at Higher Energy ILC

The infrastructure of the ILC will support a long future of experiments with e^+e^- collisions that would build on the success of the first 250 GeV stage. From Fig. 4.2, we see that the process we consider in this study has enhanced cross-section at higher energies for tensor couplings, whereas the cross section corresponding to the vector couplings peaks around 250 GeV. On the other hand, most

backgrounds reduced by a larger fraction at higher center-of-mass energy of the collider. In addition to the background processes present at 250 GeV, $e^+e^- \to t\bar{t}$ with the semileptonic decay (leading to final state: $2b2j\ell\nu$) contributes at center of mass energies of 350 GeV and above. However, we presume that the preliminary selection criteria demanding $N_\ell = N_j = N_b = 1$ itself will take care of this background. In Table 4.13 the cross sections of signal and background processes at $\sqrt{s} = 350$ GeV and 500 GeV are presented.

Beam	Signal cross section (fb)			Background cross sections (fb)				
polarization	$\kappa_{\gamma qt}^{L(R)}$	$X_{zqt}^{L(R)}$	$\kappa_{zqt}^{L(R)}$	$WW \to \ell\nu 2j$	$ZZ \to (2\ell + 2\nu)2j$	ffh	$t\bar{t} \to 2b2j\ell\nu$	$t\bar{t} \to 6q$
$\sqrt{s} = 350$ GeV								
unpol	417.0	92.8	254.4	2630.4	261.6	121.0	141.6	147.0
$(-80\%, +30\%)$	518.0	137.6	378.4	8155.9	564.8	256.7	316.7	328.8
$(+80\%, -30\%)$	518.0	92.8	254.4	541.8	300.1	140.2	151.5	157.3
$\sqrt{s} = 500$ GeV								
unpol	474.2	54.8	268.6	4781.6	224.2	44.9	120.1	171.7
$(-80\%, +30\%)$	588.2	81.2	398.2	11143.2	366.1	98.2	276.8	393.8
$(+80\%, -30\%)$	588.2	54.8	268.4	750.8	310.2	18.9	120.2	174.0

TABLE 4.13: The partonic cross section of the signal process $e^-e^+ \to tq$, $(t \to Wb,\ W \to \mu\nu_\mu\ (e\nu_e))$ for different anomalous $tq\gamma(Z)$ couplings and major background processes at $\sqrt{s} = 350$ and 500 GeV. Both ℓ^+ and ℓ^- arising from t and $\bar{t}$ are included. The value of the anomalous couplings are set to unity in all signal events.

We do not attempt a detailed study of these cases here. Assuming that the selection efficiency roughly hold as in the case of 250 GeV ILC, the total background remaining in the case of muonic final state is the same as around 350 events. On the other hand, the signal cross section for tensor couplings have approximately doubled, thus making the significance better by a factor of $\sqrt{2}$ compared to the 250 GeV case. At the same time, the vector couplings have a cross section reduced by a factor of almost 2, thus worsening the significance by a factor of $\sqrt{2}$.

4.6 Summary and Discussion

We present a comprehensive study of the top quark FCNC couplings through the process $e^+e^- \to tj$ with further leptonic decay of the top quark. Here t generically denote both top quark and top anti-quark, with the corresponding decay leptons of either charge. We shall consider both the $tq\gamma$ and tqZ couplings in our study. Unlike the case of HL-LHC, where the presence of these anomalous couplings are probed through the rare decays of the top quark, the process considered here in the context of a 250 GeV ILC has many promising features. Firstly, the coupling directly affects the production, the process being absent in the SM at tree level. Secondly, the associated jet carry information regarding the nature of the coupling, as also the polarization of the top quark. These reflect in the angular distributions of the jet and the top decay products, providing clear advantage to ILC over LHC. Thirdly, beam polarization can effectively used to disentangle different types of couplings. For example, while the case of γ coupling is insensitive to the beam polarization, the case of Z couplings do depend on the beam polarization.

In the study we perform a detailed study of the MC simulated signal events against the possible SM background processes leading to final state with one light jet, one $b-$jet, one isolated lepton (electron or muon of either charge) and large missing energy. Potential backgrounds are selected, and the simulated events available with the ILD repository is used. Both the signal and background events are passed through the ILD detector simulator MOKKA and the events are reconstructed using the state-of-the-art MARLINRECO, within the framework of ILCSoft. Finally, using ROOT the events are analysed, and events selection criteria are designed based on the kinematic distributions to enhance the signal sensitivity.

We considered two different beam polarization combinations of $(-80\%, +30\%)$ and $(+80\%, +30\%)$ separately, and observe that the right-handed electron case has the advantage of reduced background compared to the other case. In this combination, one could reach the couplings to the level of 0.01 in the case of $tq\gamma$, and slightly reduced reach of 0.02 in the case of tqZ coupling at 95% C.L. with the projected integrated luminosity of 0.45×2 ab^{-1}. The other polarization combination with mostly left-handed electrons can reach up to 0.02 to 0.03 with a somewhat larger irreducible background remaining. The cross section itself is insensitive to the left- or right-handed nature of the couplings, and it is not expected to distinguish the nature of the couplings from just counting the number of events. On

the other hand, we have devised different asymmetries including the top quark polarization asymmetry and the forward-backward asymmetries of the light jet, the $b-$jet and the (top quark) decay lepton. We have demonstrated that studying a combination of these observables could disentangle the couplings albeit partially.

A preliminary study of possibilities at higher centre of mass energies of $\sqrt{s} =$ 350 GeV and 500 GeV show that the reach of tensor couplings could be enhanced by a factor of $\sqrt{2}$, whereas no such improvement is possible in the case of vector type coupling due to the reduced cross section at higher energies.

To summarise, our study demonstrate the ability of the first stage of ILC with 250 GeV centre of mass energy in top quark studies involving FCNC. The single top quark production possible with the presence of large FCNC could be probed at level better than that is possible at HL-LHC. Further, multiple observables like the top polarization and forward-backward asymmetries could be employed in disentangling the effects of different couplings.

– We do not know what the rules of the game are; all we are allowed to do is to watch the playing. Of course, if we watch long enough, we may eventually catch on to a few of the rules. The rules of the game are what we mean by fundamental physics.

Richard P. Feynman

5

Tracing the anomalous tqg and $tq\gamma$ flavor changing interactions at the FCC-he

5.1 Introduction

In the previous two chapters we considered the anomalous FCNC couplings of the top quark involving photon and $Z-$boson. In this chapter we shall discuss possibilities to probe anomalous tqg couplings involving gluon. The LHC relies on the rare decays of the top quark through two light jets (one identified as a gluon jet) to probe this coupling as discussed in Section 1.2 of Chapter 1. We propose the *single-top-quark* production process along with an electron and light quark jet at Future Circular Collider for Proton and Electron (FCC-he), $e^-p \to e^-tj$, where j is a light jet, to study the effect of tqg, with the top quark further decaying leptonically. We shall work within the context of FCC-he with beam energies of 60 GeV and 50 TeV for electron and proton beams, respectively. We shall show that the process has the advantage over the HL-LHC to probe the relevant coupling and further in disentangling the effects of different possible couplings.

Working within the effective Lagrangian given in Eq. (1.5) described in Chapter 1 of the thesis, the process $e^-p \to e^-tj$ is affected by all the couplings included in there. Like the studies discussed in the previous chapters, this process is not

present in the SM at tree level. Further, with the electron in the initial state we expect the beam polarization to be of help in distinguishing the Lorentz structure. The scattered electron is going to play a crucial role in disentangling the couplings, as in the case of the $e^-p \to e^-t$ process considered in the context of LHeC presented in Chapter 3. We consider leptonic decay of the top quark, $e^-p \to e^-tj, (t \to Wb, W \to \ell\nu_\ell)$, where $\ell = e,\ \mu$ leading to final state of $e^-bj\ell\nu$. The Feynman diagrams of the process are shown in Fig. 5.1. The processes can be classified depending on the type of coupling. With non-zero $tq\gamma$ or tqZ there are two gluon initiated diagrams and two quark initiated diagram. Similarly, with non-zero tqg there are two gluon initiated diagrams and two quark initiated diagrams.

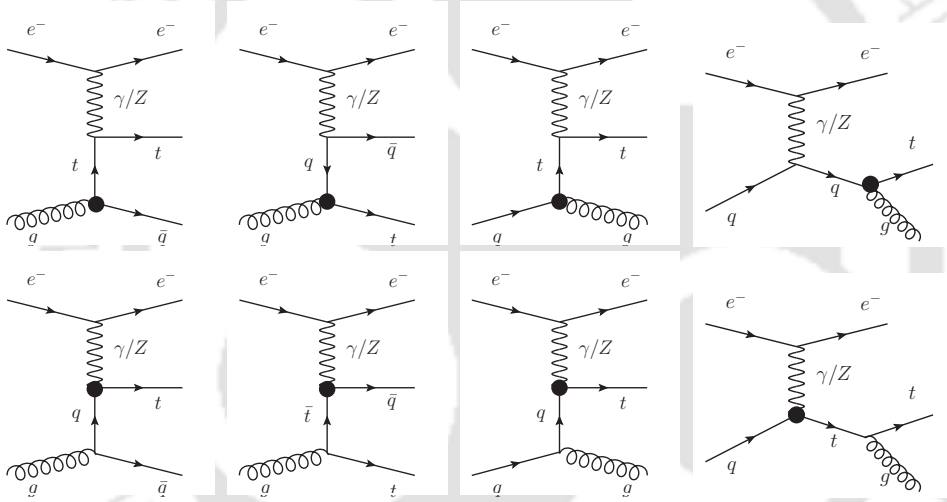

FIGURE 5.1: Signal processes $pe^- \to e^-tj$. There are 2 gluon initiated processes with either u or c quark in the final state and 2 quark (u or c quark) initiated process with gluon in the final state along with top quark and e^- having 16 diagrams each.

We shall consider the effect of these anomalous interactions assuming one type of couplings is present at a time. The light quark can be either a u-quark or a c-quark. Since photon couple democratically to the electron, irrespective of its spin orientation, the scattered electron is not of much use in discriminating the right- and left-handed $tq\gamma$ couplings. On the other hand, the tqZ and tqg with Z mediated processes will influence the scattered electron, and their angular distributions are expected to reflect this influence. As discussed in the previous chapters the top quark polarization and related asymmetries would reflect the nature of the couplings. We shall exploit this to disentangle the couplings, apart from using those in obtaining the reach of FCC-he on these couplings.

We shall organize this Chapter as follows. In Section 5.2 we discuss the signal and background process in details with cross-sections for different polarization of initial electron beam. In Section 5.3 we discuss the event generation and the cut flow analysis employed. The reach of the coupling value at 95% C.L. is discussed further. In Section 5.4 we discuss various asymmetries, used in the study of the couplings as discriminator. In Section 5.5 we conclude the chapter.

5.2 Signal and Background

At parton level the signal final state consists of $e^- b\ell\nu$, where $\ell = e,\ \mu$. This final state does not arise in the SM process at LHeC. However, the SM processes with final states (i) $e^- jj\ell\nu$, (ii) $e^- bj j\ell\nu$, (iii) $bjjj\nu$, (iv) $bjj\nu$ could potentially mimic the signal. In Table 5.1, we have listed the cross section of the signal process for the production of top and anti-top quark represented by σ_t and $\sigma_{\bar{t}}$, respectively, with their subsequent leptonic decay. We have considered the up-quark coupling with top quark taking one coupling to be present at a time, while setting all others to zero. The cross section quoted are with the relevant coupling set to unity. Noticing that the cross section scales like the square of the coupling, one can obtain this for any value of the coupling in a straight forward way. Possibility of electron beam polarization is made use of with the three cases of *unpolarized*, *left*- and *right*-polarised beams considered in all cases, with the degree of polarization assume to be 80%.

Coupling	κ^L_{gut}	κ^R_{gut}	$\kappa^L_{\gamma ut}$	$\kappa^R_{\gamma ut}$	X^L_{zut}	X^R_{zut}	κ^L_{zut}	κ^R_{zut}
unpolarized								
σ_t (fb)	526.06	556.60	1601.32	1602.06	263.35	251.40	310.44	336.57
$\sigma_{\bar{t}}$ (fb)	259.03	264.84	835.46	832.39	141.06	147.79	122.79	106.24
P_{e^-}=-0.8								
σ_t (fb)	545.90	696.07	1238.31	1968.12	332.42	273.64	319.79	441.21
$\sigma_{\bar{t}}$ (fb)	289.20	295.26	1101.71	564.12	153.81	186.75	173.16	95.58
P_{e^-}=+0.8								
σ_t (fb)	514.78	414.44	1964.81	1238.32	195.53	229.78	299.85	233.90
$\sigma_{\bar{t}}$ (fb)	230.88	235.30	565.34	1102.11	128.59	109.86	72.07	116.52

TABLE 5.1: **No Cut:** The partonic cross section of the signal process : $pe^- \to e^- tj, (t \to Wb, W \to l\nu_l)$ for different FCNC couplings. The value of the NP couplings are set to unity.

In all cases the top quark production cross section is about two times larger than that of the top antiquark production. This is mainly due to the difference in the pdf of the antiquark in proton compared to that of the u quark. The cross section in the case of gluon couplings are mostly insensitive to the electron beam polarization, with a mild dependence arising through the standard electron-Z boson coupling. This dependence is slightly more pronounced in the case of right-handed coupling. In the case of tqZ coupling too the same trend is visible. On the other hand, the anomalous $tq\gamma$ coupling, the dependence on the electron beam polarization is about 25% either way. With unpolarized beam the top quark pair production is insensitive to the chirality of the coupling. However, with left-handed beam the cross section is increased (decreased) in the case of right-(left-) handed coupling. This is reversed when right-polarized electron beam is used. When top antiquark production is considered, the whole scenario is reversed again. We shall see later, how this information can be used as a distinguishing tool in identifying the nature and type of the coupling. In Table 5.2, the corresponding cross section in the case of c-quark top-quark coupling is given. As expected, the cross section is comparable to that of $\sigma_{\bar{t}}$ in the u-quark case quoted in Table 5.1. The dependence

on the beam polarization and the nature of the coupling are similar to the case of u quark couplings discussed above.

Coupling	κ^L_{gct}	κ^R_{gct}	$\kappa^L_{\gamma ct}$	$\kappa^R_{\gamma ct}$	X^L_{zct}	X^R_{zct}	κ^L_{zct}	κ^R_{zct}
unpolarized								
σ_t (fb)	249.22	272.95	712.99	707.95	124.06	118.34	81.72	96.60
$\sigma_{\bar{t}}$ (fb)	244.54	248.96	709.93	707.11	118.58	123.67	96.71	81.79
P_{e^-}=-0.8								
σ_t (fb)	222.26	359.06	466.68	951.34	155.37	129.37	70.30	139.30
$\sigma_{\bar{t}}$ (fb)	270.92	277.01	953.73	465.11	129.70	155.03	139.47	70.27
P_{e^-}=+0.8								
σ_t (fb)	276.18	186.85	959.31	464.56	92.75	107.31	93.15	53.89
$\sigma_{\bar{t}}$ (fb)	218.17	220.91	466.12	949.10	107.45	92.30	53.96	93.31

TABLE 5.2: **No Cut:** The partonic cross section of the signal process : $pe^- \to e^- tj, (t \to Wb, W \to l\nu_l)$ for different FCNC couplings. The value of the NP couplings are set to unity.

Coming to the background, we present the cross sections of potential processes listed in Table 5.3. Purely from considerations of the cross section of the background, it is advantageous to use right-handed electron beam polarization.

Process	$\sigma(unpol)$ fb	$\sigma(-0.8)$ fb	$\sigma(+0.8)$ fb
$e^- jjl^+\nu_l$	137.97	202.62	73.32
$e^- bjjl^+\nu_l$	5.68	8.00	3.36
$bjjj\nu_l$	43.84	78.90	8.77
$bjj\nu_l$	144.32	259.77	28.86

TABLE 5.3: **No Cut:** The partonic cross section of the background process at different beam polarization at (50TeV, 60GeV) beam energy for proton and electron.

5.3 Event Generation and Analysis

We use the FeynRules implementation of the effective Lagrangian considered in the previous chapters for this study as well. For event generation of both signals and background we use the MonteCarlo event generator MADGRAPH5 is used with a customised Pythia-PSG performing the hadronisation and showering. CTEQ6L1 pdf is used setting the factorisation and remormalisation scales set to m_t. Generation level event selection of transverse momentum $p_T > 10$ GeV and pseudo rapidity $|\eta| < 5$ are imposed on all jets and leptons. The events thus generated are passed through FastJet to form the jets. We used the anti-k_T algorithm with cone size of $R = 0.4$. The detector is emulated with Delphes detector code tuned to take into account the asymmetric nature of the collider along with the very high energy proton beam resulting in highly boosted final state products. The events thus obtained after passing through Delphes are further analysed using MadAnalysis5. The pre-selection of events is performed with the basis selection criteria listed below.

- $P_T(leptons,\ jets,\ bjets) > 10$
- $|\eta_i| < 8$, where $i \equiv lepton,\ jet,\ bjet$
- $\Delta R(\ell, jet) \geq 0.4,\ \Delta R(\ell, bjet) \geq 0.4$ and $\Delta R(jet, bjet) \geq 0.4$.

For further event selection to enhance the signal over background we studied the kinematic distributions. In Figs. 5.2 and 5.3 and Fig. 5.4 some of the selected kinematic distributions are presented for the unpolarized, -80% and $+80\%$ polarized electron beam, respectively. We have considered the top quark decay into either μ^+ or e^+, and the top antiquark decaying into μ^-. With the scattered electron always present, we have not considered the case of top antiquark decaying into electron. The kinematic distributions are given for the case of top quark decaying into μ^+.

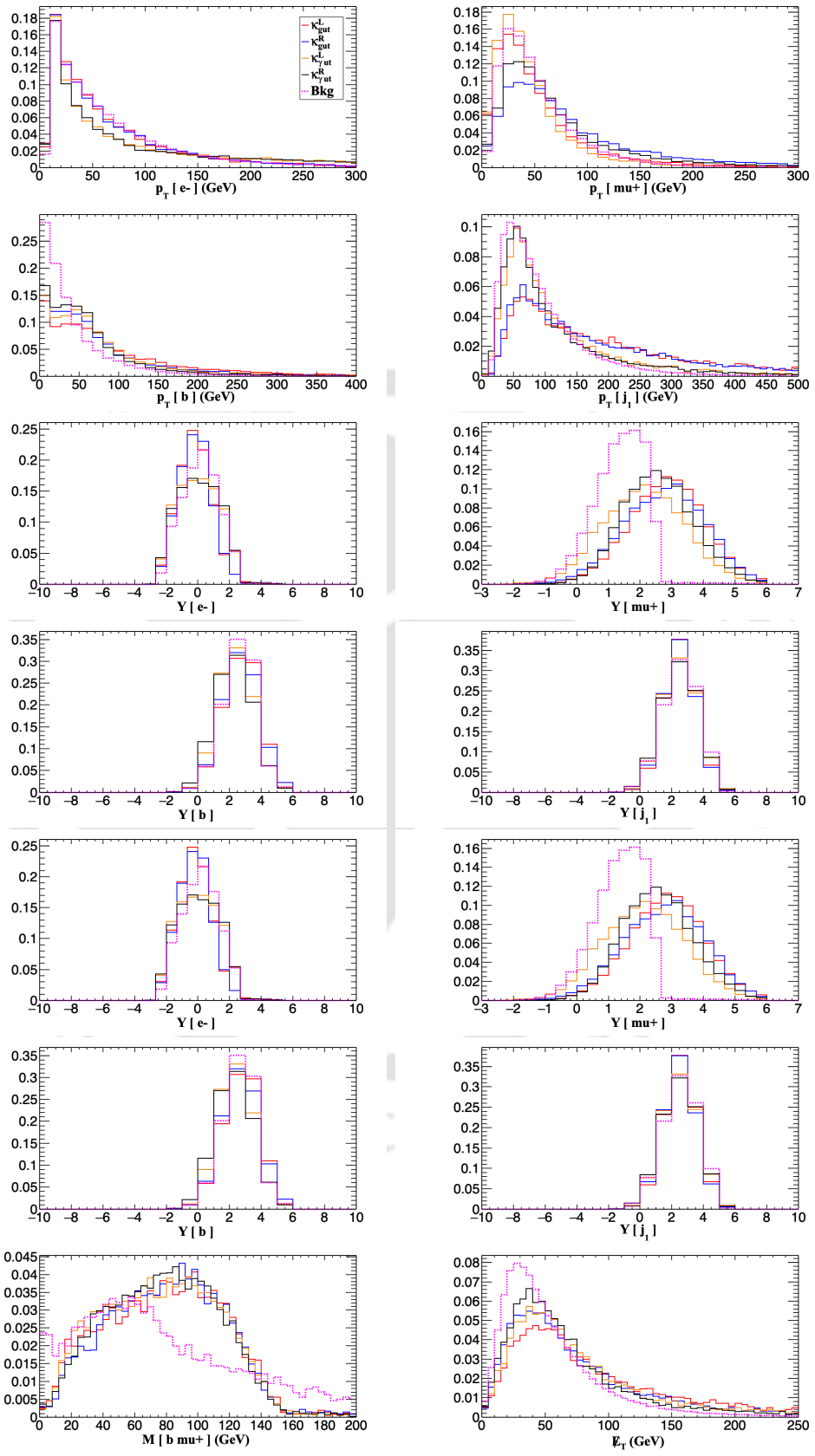

FIGURE 5.2: Unpolarized sample: Distributions of observables for signal and background. The solid (dotted) line graphs represents the signals (background) events. The legends for signal samples are indicated by the couplings parameters.

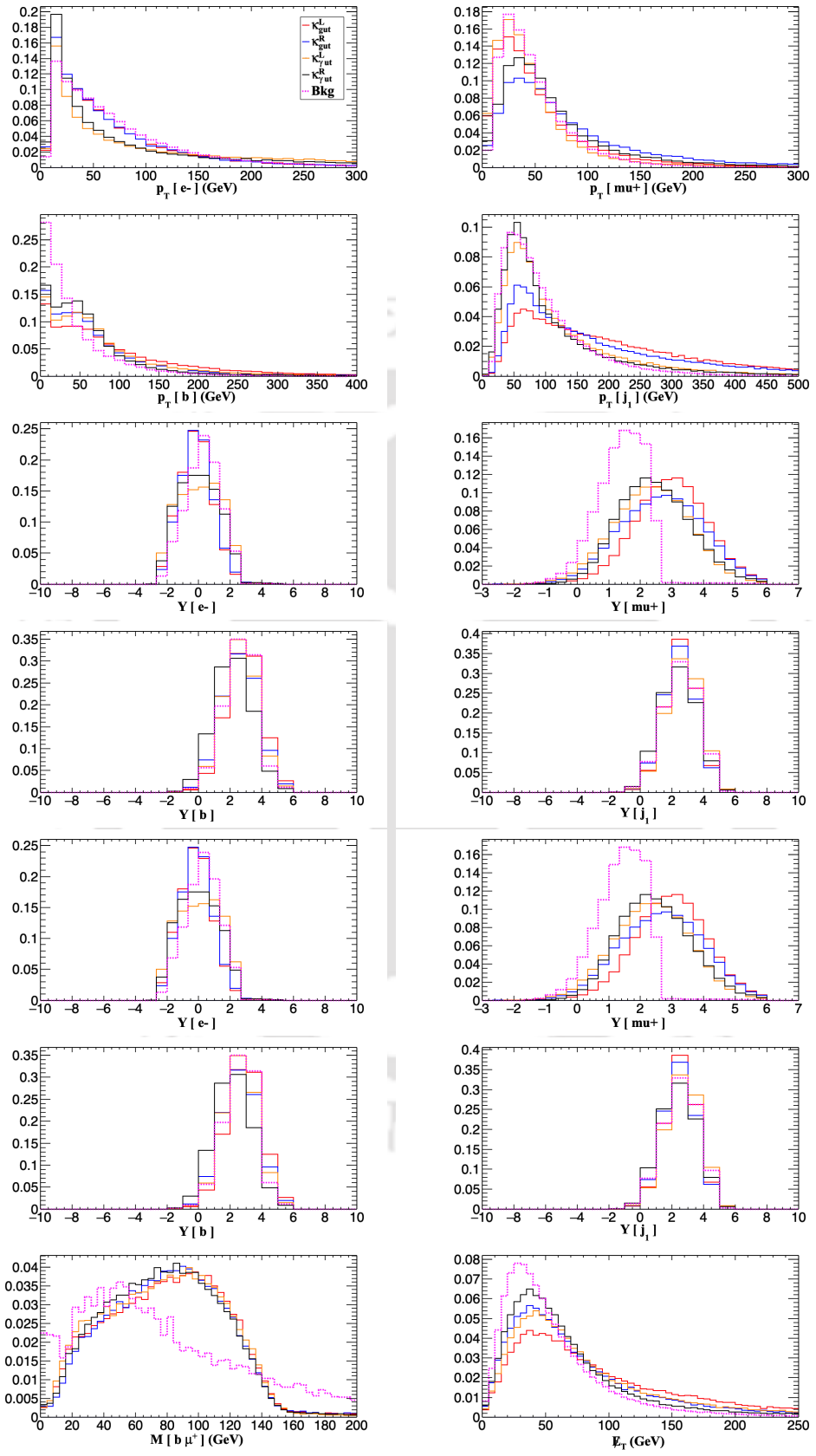

FIGURE 5.3: (-80%) sample: Distributions of observables for signal and background. The solid (dotted) line graphs represents the signals (background) events. The legends for signal samples are indicated by the couplings parameters.

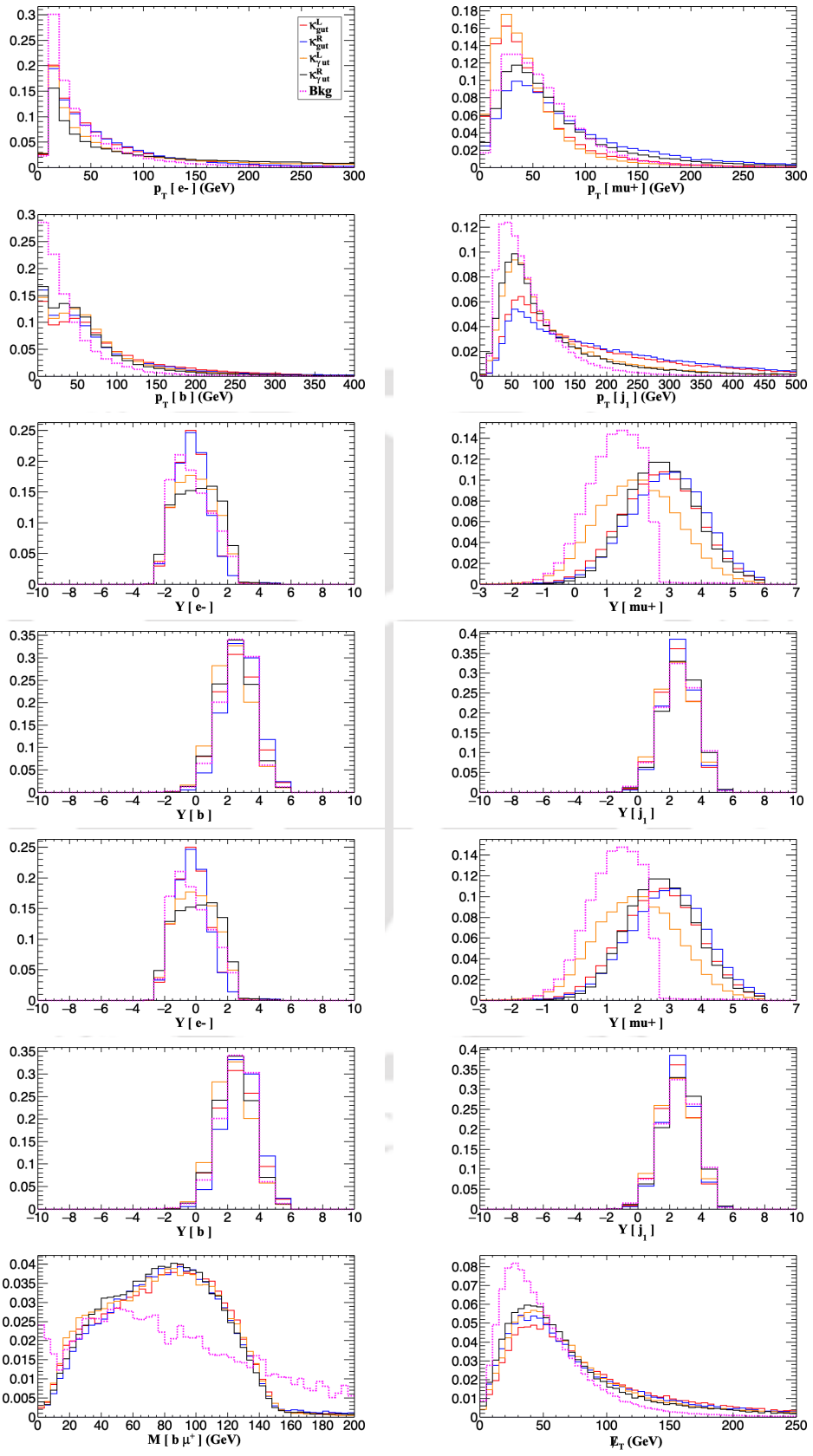

FIGURE 5.4: (-80%) sample: Distributions of observables for signal and background. The solid (dotted) line graphs represents the signals (background) events. The legends for signal samples are indicated by the couplings parameters.

The distributions for process having one e^+ also exhibit the same kinematic distributions. We have also examined the processes having one μ^+ or e^+ in the case of tgc or $t\gamma c$ anomalous couplings and found them to have the similar shape of the distributions. This is expected because the process involving u- or c-quark FCNC couplings differ by the cross sections only. Main distinguishing factor between the signal and the background is their prominent difference in the rapidity distribution of the decay lepton. We shall consider this as one of the observables and effectively made use of it to enhance the signal significance.

After demanding the events to have one electron, one muon, one $b-$jet and at least one light jet, we have the signal reduced by a factor of 2, whereas the background is reduced by a factor of 20. We have presented the cross sections after each selection in Table 5.4 for unpolarized beam, in Table 5.5 and Table 5.6 for $P_e = -0.8$ and $P_e = +0.8$ beam polarizations, respectively. We have included only the $ejj\ell\nu$ background. All the other backgrounds are almost eliminated at this stage of selection. Further we demand a rapidity region of $Y_\ell > 2.6$, which is optimized to get the best signal significance considering all cases together. This brings down the signal by another factor of 2- 4 in the case of signal events, depending on the nature of the couplings considered and the polarization of the beam used. There is a slight dependence on the final state lepton (decay production of top quark) as well. The background, on the other hand is considerably reduced.

Coupling	κ^L_{gut}	κ^R_{gut}	$\kappa^L_{\gamma ut}$	$\kappa^R_{\gamma ut}$	κ^L_{gct}	κ^R_{gct}	κ^L_{act}	κ^R_{act}	bkg
μ^+ Sample									
Basic Cuts	530.6	556.2	1601.0	1595.0	249.3	273.8	710.0	710.0	287.2
$N_{e^-,\mu^+,b} = 1, N_j \geqslant 1$	269.2	291.4	835.9	844.1	128.4	142.9	378.2	386.8	4.1
$Y_{\mu^+} > 2.6$	152.6	154.6	278.0	377.5	55.4	42.9	79.5	117.0	0.01150
μ^- Sample									
Basic Cuts	259.4	266.1	831.7	829.1	244.0	248.8	709.4	708.9	287.2
$N_{e^-,\mu^-,b} = 1, N_j \geqslant 1$	146.4	150.1	467.7	480.1	130.6	128.8	374.1	376.6	4.8
$Y_{\mu^-} > 2.6$	65.8	53.6	102.5	151.0	58.3	47.2	79.6	118.2	0.00864
e^+ Sample									
Basic Cuts	527.4	557.0	1597.0	1595.0	249.3	272.4	710.2	710.0	287.2
$N_{e^-,e^+,b} = 1, N_j \geqslant 1$	246.7	258.6	795.8	779.1	117.5	128.6	349.9	350.2	4.4
$Y_{e^+} > 2.6$	137.5	133.0	252.3	338.3	50.0	39.9	76.4	102.0	0.01150

TABLE 5.4: The table shows the value of the cross section (σ (fb)) with unpolarized electron beam after application of each cut. In the case of signal, coupling values are taken as unity.

Coupling	κ^L_{gut}	κ^R_{gut}	$\kappa^L_{\gamma ut}$	$\kappa^R_{\gamma ut}$	κ^L_{gct}	κ^R_{gct}	κ^L_{act}	κ^R_{act}	bkg
μ^+ Sample									
Basic Cuts	545.9	696.1	1238.3	1970.0	221.6	360.9	464.9	951.4	434.4
$N_{e^-,\mu^+,b} = 1, N_j \geqslant 1$	278.4	363.7	645.6	1070.1	114.6	191.4	243.5	502.9	6.0
$Y_{\mu^+} > 2.6$	168.3	180.6	261.2	430.5	55.3	58.1	67.9	134.7	0.00871
μ^- Sample									
Basic Cuts	289.2	295.3	1101.7	564.1	271.0	278.0	952.7	465.6	434.4
$N_{e^-,\mu^+,b} = 1, N_j \geqslant 1$	162.0	165.3	631.8	321.8	139.5	141.0	507.0	247.0	7.3
$Y_{\mu^+} > 2.6$	63.8	61.2	123.3	123.1	54.4	52.6	98.9	91.9	0.01307
e^+ Sample									
Basic Cuts	545.9	696.1	1238.3	1968.1	220.5	359.4	466.2	950.5	434.4
$N_{e^-,\mu^+,b} = 1, N_j \geqslant 1$	250.0	327.7	590.8	965.1	103.0	172.9	225.7	472.2	6.8
$Y_{\mu^+} > 2.6$	152.7	157.9	232.4	381.4	49.1	50.9	60.5	129.8	0.01307

TABLE 5.5: The table shows the value of the cross section (σ (fb)) with -80% electron beam polarization after application of each cut. In the case of signal, coupling values are taken as unity.

Coupling	κ^L_{gut}	κ^R_{gut}	$\kappa^L_{\gamma ut}$	$\kappa^R_{\gamma ut}$	κ^L_{gct}	κ^R_{gct}	κ^L_{act}	κ^R_{act}	bkg
μ^+ Sample									
Basic Cuts	514.8	414.4	1964.8	1238.3	275.6	188.4	947.6	466.1	139.7
$N_{e^-,\mu^+,b} = 1, N_j \geqslant 1$	272.1	210.5	1060.2	647.3	143.4	96.7	506.5	250.8	2.2
$Y_{\mu^+} > 2.6$	139.6	123.3	315.6	332.1	56.4	34.0	90.7	94.8	0.00700
μ^- Sample									
Basic Cuts	230.9	235.3	565.3	1102.1	217.4	220.8	462.4	953.4	139.7
$N_{e^-,\mu^-,b} = 1, N_j \geqslant 1$	129.5	133.4	318.7	635.2	110.7	114.0	243.0	512.7	2.3
$Y_{\mu^-} > 2.6$	65.6	46.5	85.5	177.6	56.9	37.3	67.0	132.8	0.00770
e^+ Sample									
Basic Cuts	514.8	414.4	1964.8	1238.3	276.1	187.3	953.3	465.0	139.7
$N_{e^-,e^+,b} = 1, N_j \geqslant 1$	247.6	190.1	976.3	590.3	133.3	87.5	460.2	228.4	2.2
$Y_{e^+} > 2.6$	124.2	109.7	282.1	301.4	51.0	31.0	86.2	85.3	0.00350

TABLE 5.6: The table shows the value of the cross section (σ (fb)) with +80% electron beam polarization after application of each cut. In the case of signal, coupling values are taken as unity.

In the case of u quark couplings, the fiducial cross sections of the signal events range from 100 - 300 fb, considering individual decay channels of the top quark and for unit couplings with the energy scale set to mass of the top quark ($\Lambda = m_t$). For top anti-quark this is reduced by a factor of two. For more realistic coupling values of 1 - 2 $\times 10^{-2}/m_t$, the cross section will be reduced by a factor corresponding to the square of the coupling. The best case scenario of μ^+ final state is listed in Table 5.7, taking the coupling to be $\frac{\kappa^2}{\Lambda^2} = \frac{2\times10^{-4}}{m_t^2}$, along with the signal sensitivity reachable at 2 ab^{-1} luminosity.

$\frac{\kappa^2}{\Lambda^2} = \frac{2\times10^{-4}}{m_t^2}$	κ^L_{gut}	κ^R_{gut}	$\kappa^L_{\gamma ut}$	$\kappa^R_{\gamma ut}$	κ^L_{gct}	κ^R_{gct}	κ^L_{act}	κ^R_{act}
unpolarized beam. Background events, $N_B = 23$								
Signal, N_S	61	62	111	150	22	17	32	47
Significance	6.7	6.7	9.6	11.4	3.3	2.7	4.3	5.6
$P_e = -0.8$. Background events, $N_B = 17$								
Signal, N_S	69	78	105	177	22	24	27	54
Significance	7.3	7.6	9.5	12.5	3.5	3.7	4.1	6.4
$P_e = +0.8$. Background events, $N_B = 14$								
Signal, N_S	56	50	127	133	23	14	37	38
Significance	6.7	6.2	10.7	10.9	3.7	2.6	5.1	5.3

TABLE 5.7: The table shows the signal significance with an assumed value of the coupling, $\frac{\kappa^2}{\Lambda^2} = \frac{2\times10^{-4}}{m_t^2}$ with the final state containing one μ^+.

The significance computed using

$$\text{Significance} = \frac{N_S}{\sqrt{N_S + N_B}} \tag{5.1}$$

To obtain the reach of the coupling at a given confidence level, in Fig. 5.5 we plot the significance against the number of signal events. In the graph the solid lines represents for signal samples with one μ^+ alone, whereas the dotted lines for the μ^+ and e^+ together.

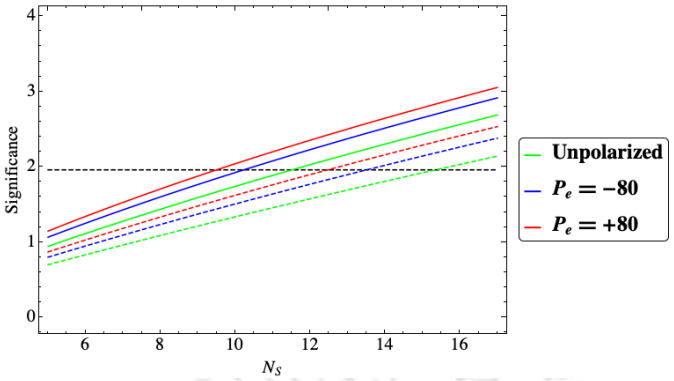

FIGURE 5.5: The graph shows the significance against the required number of signal events corresponding to the respective background events at unpolarized, −80% and +80% cases of electron beam polarizations. The solid lines are for samples with one μ^+ and dotted for combined samples of μ^+ and e^+ together.

The black dotted line parallel to $x - axis$ drawn at 95% C.L. The number of events required to have 95% C.L., for the three different cases of polarizations are given in Table 5.8.

Beam polarization	Associated quark	Background events, N_B	Required signal, $N_S(2\sigma)$	Reach of couplings for 95% CL.			
				κ^L_{gqt}/Λ	κ^R_{gqt}/Λ	$\kappa^L_{\gamma qt}/\Lambda$	$\kappa^R_{\gamma qt}/\Lambda$
Unpolarized	*up*	23	≃12	0.036	0.036	0.027	0.023
	charm			0.059	0.068	0.050	0.041
(−80%)	*up*	17	≃11	0.033	0.032	0.026	0.020
	charm			0.057	0.056	0.051	0.037
(+80%)	*up*	14	≃10	0.034	0.036	0.023	0.022
	charm			0.054	0.069	0.042	0.041

TABLE 5.8: The table shows the reach on the couplings with different beam polarizations at 2 ab^{-1} integrated luminosity. The limits are calculated for samples with one μ^+ in the final state.

The number of signal events $(N_S) \propto pdf \times |\kappa|^2$. In the case of c-quark, pdf is less than that of u-quark, so, to get the same significance over the (same) background, we need larger coupling in the case of c-quark compared to that of the u-quark. In other words, the reach of c-quark coupling is worse than that of the u-quark.

5.3.1 Combined analysis: taking μ^+ and e^+ together

We have performed the analysis considering both μ^+ and e^+ decay channels of the top quark together. In Table 5.9, we present the signal significance for combined samples. We can see that the number of signal and background both have increased by a factor of 2 from those of μ^+ or e^+ samples.

$\kappa^2 = \frac{2\times10^{-4}}{m_t^2}$	κ^L_{gut}	κ^R_{gut}	$\kappa^L_{\gamma ut}$	$\kappa^R_{\gamma ut}$	κ^L_{gct}	κ^R_{gct}	κ^L_{act}	κ^R_{act}
unpolarized beam. Background events, $N_B = 46$								
Signal, N_S	116	115	212	286	42	33	62	88
Significance	9.1	9.0	13.2	15.7	4.5	3.7	6.0	7.6
$P_e = -0.8$. Background events, $N_B = 34$								
Signal, N_S	128	135	197	324	52	70	74	157
Significance	10.1	10.4	13.0	17.1	5.6	6.9	7.1	11.3
$P_e = +0.8$. Background events, $N_B = 28$								
Signal, N_S	109	125	195	328	56	42	116	95
Significance	9.3	10.1	13.0	17.4	6.1	5.0	9.6	8.6

TABLE 5.9: The table shows the signal significance with an assumed value of the coupling, $\frac{\kappa^2}{\Lambda^2} = \frac{2\times10^{-4}}{m_t^2}$ with the final state containing one lepton (e^+, μ^+).

The reach of the couplings can be calculated as discussed in the previous section. In Table 5.10 we present the calculated reach of the couplings for 95% C.L.

Beam polarization	Associated quark	Background events, N_B	Required signal, $N_S(2\sigma)$	Reach of couplings for 95% CL.			
				κ^L_{gqt}/Λ	κ^R_{gqt}/Λ	$\kappa^L_{\gamma qt}/\Lambda$	$\kappa^R_{\gamma qt}/\Lambda$
Unpolarized	*up*	46	≃16	0.029	0.029	0.021	0.019
	charm			0.048	0.054	0.040	0.033
(−80%)	*up*	34	≃14	0.028	0.027	0.022	0.017
	charm			0.043	0.037	0.036	0.025
(+80%)	*up*	28	≃13	0.030	0.030	0.022	0.019
	charm			0.050	0.056	0.041	0.035

TABLE 5.10: The table shows the reach on the couplings with different beam polarizations at 2 ab^{-1} integrated luminosity. The limits are calculated for combined samples with μ^+ and e^+ together.

5.4 Top polarization Asymmetries

We have discussed the effect of different type of couplings on the top quark polarization, and how this is reflected in the angular asymmetries of the decay lepton, in the previous section. The asymmetries (like, A_x, A_y, A_z) are defined in the top quark rest frame whereas $A^{FB}_{e^-}$ and A^{FB}_{j} are observables constructed out of polar angle of electron and light jet (with highest P_T) in the lab frame itself. From the events obtained after passing through Delphes we reconstruct the W's and further the top-quark. The missing momentum in the case of signal arises at parton level from a single neutrino (or antinuetrino). Its four momentum can be reconstructed using the method described in Chapter 2 of the thesis. This is further used to reconstruct the top quark momentum, and the top-rest frame. The initial proton beam defines the z-axis in the Lab while the production plane of top quark defines the xz-plane (i.e., $\phi = 0$ plane). The polar angle (θ_ℓ) and azimuthal angle (ϕ_ℓ) of the top decay products are measured with respect to the top quark rest frame. The three asymmetries defined in the top quark rest frame, out of which, two defined in terms of the azimuthal angle, and one in terms of the polar angle of the decay lepton can be referred from Eq. (2.23) of Chapter 2.

The advantage of producing the top quark in association with an electron and jet can be explored in the lab frame of the experiment. In the lab frame we can construct the following asymmetries to understand the Lorentz structure of the

tqg or $tq\gamma$ couplings.

$$A_{e^-}^{FB} = \frac{\sigma(c_{\theta_{e^-}} > 0) - \sigma(c_{\theta_{e^-}} < 0)}{\sigma(c_{\theta_{e^-}} > 0) + \sigma(c_{\theta_{e^-}} < 0)}, \tag{5.2}$$

$$A_j^{FB} = \frac{\sigma(c_{\theta_j} > 0) - \sigma(c_{\theta_j} < 0)}{\sigma(c_{\theta_j} > 0) + \sigma(c_{\theta_j} < 0)}. \tag{5.3}$$

In Fig. 5.6 we plot the angular distributions of the electron (produced in association with the top quark), in the lab frame of the collider. We can see that the polar angle of the electron is sensitive to the tgq or $t\gamma q$ vertex but unable to distinguish the chirality of the couplings. On the contrary it is insensitive to the case of anti top quark production. The A_j^{FB} corresponds the forward-backward asymmetry of jet with leading P_T, doesn't seem to have feature to distinguish couplings.

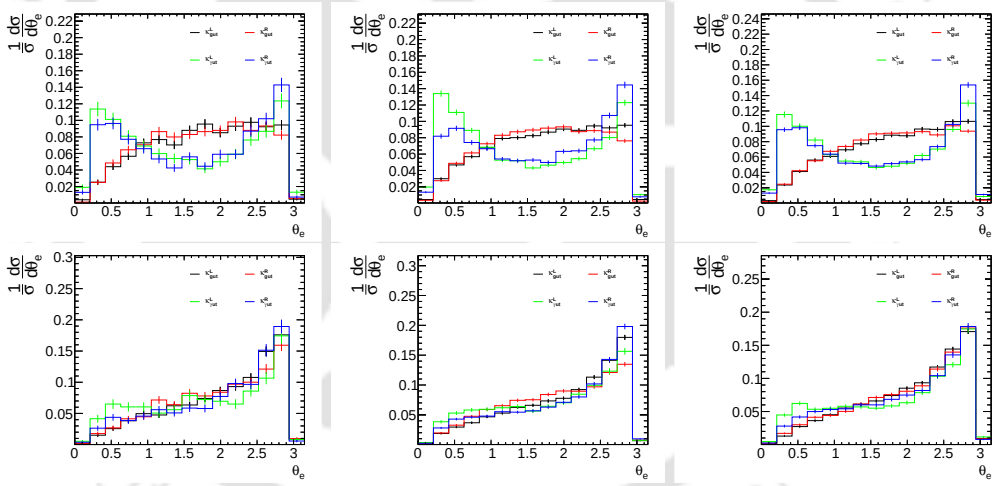

FIGURE 5.6: Figure showing the θ_{e^-} distributions at the lab frame, for unpolarized, -80% and $+80\%$ polarized initial beam samples. Fig (a), (b) and (c) in the 1st row for *top quark* events and Fig (d), (e) and (f) in the 2nd row for *anti-top quark* events are plotted.

With these distributions, the asymmetries obtained are presented in Table 5.11 in the case of top quark (with μ^+ in the final state), and in Table 5.12 in the case of top antiquark (with μ^- in the final state).

Coupling	No pol.			$P_{e^-} = -80\%$			$P_{e^-} = +80\%$		
	A_x	A_z	$A_{e^-}^{FB}$	A_x	A_z	$A_{e^-}^{FB}$	A_x	A_z	$A_{e^-}^{FB}$
κ_{gut}^{L}	-0.20	–	-0.22	-0.27	–	-0.28	-0.21	–	-0.20
κ_{gut}^{R}	0.14	0.40	-0.15	0.16	0.42	-0.23	0.11	0.41	-0.16
$\kappa_{\gamma ut}^{L}$	-0.33	-0.12	–	-0.31	-0.11	–	-0.30	-0.16	–
$\kappa_{\gamma ut}^{R}$	–	0.46	–	–	0.47	–	–	0.48	–

TABLE 5.11: For the *top quark* case, the table gives the mean value of the asymmetric observables of three possible polarization for initial electron beam. All coupling value are set to unity.

Coupling	No pol.			$P_{e^-} = -80\%$			$P_{e^-} = +80\%$		
	A_x	A_z	$A_{e^-}^{FB}$	A_x	A_z	$A_{e^-}^{FB}$	A_x	A_z	$A_{e^-}^{FB}$
κ_{gut}^{L}	-0.35	0.26	-0.48	-0.32	0.28	-0.48	-0.34	0.19	-0.46
κ_{gut}^{R}	–	0.33	-0.39	–	0.41	-0.47	–	0.32	-0.35
$\kappa_{\gamma ut}^{L}$	-0.44	–	-0.25	-0.43	–	-0.28	-0.45	–	-0.28
$\kappa_{\gamma ut}^{R}$	-0.11	0.54	-0.44	-0.14	0.56	-0.37	–	0.53	-0.39

TABLE 5.12: for the *anti-top quark* case, the table gives the mean value of the asymmetric observables of three possible polarization for initial electron beam. All coupling value are set to unity.

Notice that the value of the asymmetries for events with e^+ in the final state also follow the same trend as μ^+ does. This is expected as the anomalous coupling effect the top quark polarization and the leptonic decay follow the same trend.

5.4.1 Disentangling different types of couplings

As explained in the Introduction, one of the main advantages of $e^- p$ collider over the LHC in exploring the FCNC of top quark is its ability to disentangle the effects of different type of couplings. We shall demonstrate this in the present case

of tqg and $tq\gamma$ studied through $e^-p \to e^-tj$, with the leptonic decay of the top quark.

Let us firstly consider the top quark polarization asymmetries and the forward-backward asymmetry of the scattered electron presented in the above section. The qualitative features are captured in Table 5.13. Considering the top quark production, presence of all the three asymmetries, A_e^{FB}, A_z and A_x will indicate that the couplings is κ^R_{gqt}, whereas the absence of A_z but with the other two present will indicate that it is left-handed gluon coupling (κ^L_{gqt}). Absence of A_e^{FB} along with presence of A_z would indicate that the coupling is tqg. In this, the presence or absence of A_x could decide the chirality of the coupling. The top antiquark will have less distinguishing ability, and also somewhat more restricted statistics compared to the top quark case.

From top quark				From top antiquark			
A_x	A_z	A_e^{FB}	Coupling	A_x	A_z	A_e^{FB}	Coupling
−ve	···	−ve	κ^L_{gut}	−ve	+ve	−ve	κ^L_{gut}
+ve	+ve	−ve	κ^R_{gut}	···	+ve	−ve	κ^R_{gut}
−ve	−ve	···	$\kappa^L_{\gamma ut}$	−ve	···	−ve	$\kappa^L_{\gamma ut}$
···	+ve	···	$\kappa^R_{\gamma ut}$	−ve	+ve	−ve	$\kappa^R_{\gamma ut}$

TABLE 5.13: Qualitative properties of the top polarization asymmetries and the forward-backward asymmetry of the scattered electron, allowing one to distinguish the effects.

The above qualitative distinctions comparing the asymmetries are independent of the beam polarization. However, a comparison of event rates with different beam polarizations could add to the ability to disentangle the effects. To illustrate this, we shall consider the fiducial cross sections after the event selection, quoted in Table 5.5 and Table 5.6 for the two cases of $P_e = -0.8$ and $P_e = +0.8$, respectively. Considering the case of top quark production and further decaying to μ^+, an increase in the cross section occurs when the polarization is switched from $P_e = -0.8$ to $P_e = +0.8$ as indicated only in the case of $\kappa^L_{\gamma qt}$. On the other hand, considering the top antiquark production and decay to μ^-, an increase indicates

that it is $\kappa^R_{\gamma qt}$, whereas a decrease could be due to either κ^R_{gqt} or $\kappa^L_{\gamma qt}$. The presence of κ^L_{gqt} is practically insensitive to the beam polarization in this case. We have illustrated these features in Table 5.14.

$(P_e = -0.8) \implies (P_e = +0.8)$

	κ^L_{gqt}	κ^R_{gqt}	$\kappa^L_{\gamma qt}$	$\kappa^L_{\gamma qt}$
t production	$\Downarrow$	$\Downarrow$	$\Uparrow$	$\Downarrow$
$\bar{t}$ production	$\Leftrightarrow$	$\Downarrow$	$\Downarrow$	$\Uparrow$

TABLE 5.14: Demonstrating the power of beam polarization to disentangle the effects of different types of couplings. The arrows $\Uparrow$ and $\Downarrow$, respectively, indicate increase or decrease in the cross section when the electron beam polarization is switched from $P_e = -0.8$ to $P_e = +0.8$. The horizontal arrow ($\Leftrightarrow$) says this case is practically insensitive to the change of beam polarization.

5.5 Summary and Conclusion

The possibility of measurable FCNC connected to top quark will clearly indicate dynamics beyond that of the Standard Model (SM). While the SM predicts very tiny effects arising through higher order quantum corrections, many popular extensions of the SM indicate possibility of much larger value for these couplings, close to what could be explored at LHC and other future colliders. The LHC in its high luminosity version could probe these couplings through searches of rare decays of top quark. Being a top factory with very large statistics, the sensitivity of HL-LHC is quite competitive compared to any other planned future collider. However, when it comes to disentangling the effects of many possible couplings (like $tq\gamma$, tqZ, tqg), colliders with electronic initial states stand with clear advantages. In this work we have demonstrated the uniqueness of high energy electron-proton collider in this respect.

The process studied, namely the production of single top quark in association with a light jet and scattered electron in electron-proton collisions ($e^-p \to e^-tj$)

in the planned high energy facility of FCC-he, has the potential to fingerprint the presence of top quark FCNC involving photon and gluons. We have demonstrated the sensitivity of the collider with electron beam of 60 GeV and proton beam of 50 TeV, along with the possibility of electron beam polarization in not only detecting these FCNC, but in distinguishing the effects of different types of couplings. We have considered the leptonic decay of the top quark in our study. A way to fully reconstruct the top quark, even with a missing neutrino as presented in Appendix A is used in reconstructing the events. The process has no SM background with the same parton level final state. However all possible processes that could mimic the final state at the detector are considered in the study. Monte Carlo event generator, MadGraph5 is used to generated the signal and background events. With the help of Delphes package using a re-tuned detector card, effects of detector on the particle identification and energy and momentum measurements are incorporated. MadAnalysis is used to anlayse the events and for final selection, enhancing signal over background, with the help of appropriate kinematic regions. We could contain the background events to the level of a few tens of femtobarn at the expected luminosity of 2 ab^{-1}. With such reduced background, we have demonstrated that the presence of couplings to the level of the $\mathcal{O}(10^{-2})$ TeV^{-1} can be probed at this collider with the process considered. Further, effective use of top quark polarization asymmetries, forward-backward asymmetry of the scattered electron, along with the effect of electron beam polarization on the cross section, it is possible to fully disentangle the effects of the four relevant couplings considered in the study.

भारतीय प्रौद्योगिकी संस्थान गुवाहाटी
Indian Institute of Technology Guwahati

– It is better to perform one's own duties imperfectly than to master the duties of another.

Sri Bhagavad Gita

6

Summary and Conclusion

In the thesis, we have analyzed the flavor changing neutral current (FCNC) interactions of top quark at the proposed future colliders, (i) the *Large Hadron Electron Collider* (LHeC) with beam energies, $E_{e^-} = 60\ GeV$ and $E_p = 7\ TeV$, which provide a center-of-mass (c.m.) energy of 1.3 TeV, (ii) the *International Linear Collider* (ILC) for Run-I with c.m. energy of 250 GeV and (iii) the *Future Circular Collider for Hadron and Electron* (FCC-he) with beam energies $E_{e^-} = 60\ GeV$ and $E_p = 50\ TeV$, providing a c.m. energy of 3.5 TeV. The phenomenological study of the rare processes are carried out with the single top quark production in association with lepton or other light quark with the subsequent leptonic decay mode of the top quark. We have considered the framework of *Effective Field Theory* (EFT) for the afore said study.

The processes considered in the thesis are not possible to produce at tree level within SM. This gives a clear advantage in reducing the background from the SM processes considerably. Secondly, practically no experimental studies at LHC search for the process with FCNCs in its production vertex, rather these studies choose the decay vertex of top quark for this purpose. In addition, our study considered the simultaneous presence of more than one parameter for setting bounds on the couplings, by using the observables of top quark polarization along with the cross section of the single top quark production. We considered the production vertex to be anomalous in three of the processes described in the thesis. Moreover the colliders considered have additional advantages. First they will be much more free of pile-up due to the absence of QCD processes. This lies on

the fact that the colliders are proposed to have at least one electron beam out of the two beams. Secondly, electron beam can be polarized to large degree (up to 80%). This can be exploited in enhancing the cross section, as well as provide a distinguishing feature to disentangle the type of couplings.

The study also shows that the careful use of angular distributions of associated fermions (electron/light quark) produced along with the top quark, are sensitive to the type of coupling, along with the polarization of the top quark. We have made use of these facts in our study to probe the nature of the coupling.

The Chapter 1 and Chapter 2 of the thesis describes the theoretical background and computational tools used in the thesis work. In the Chapter 3, 4 and 5, we have mentioned our three different projects, which are the heart of the thesis. In the following I summaries conclusion of each chapters of my thesis.

In **Chapter 2**, we have discussed various tools including necessary theoretical framework, analysis techniques and software used in detail. The model file used for the study of FCNC processes involves the top quark, event generator, detector simulator and the analysis softwares for the study are introduced in brief. This chapter also helps the reader to set the tempo for the further reading of the chapters with a better understanding.

In **Chapter 3**, we present the study of top quark *Flavor Changing Neutral Current* interactions with the Z-boson in the proposed LHeC, of beam energies, $E_{e(p)} = 60$ (7000) GeV. Contrary to LHC searches where the decay of the top quark processes are via FCNC interactions, we consider the production of the top quark itself via the FCNC vertex. For the analysis, we consider an effective theory where the anomalous FCNC couplings are of vector and tensor in nature. The effect of these couplings is probed in the single top production along with the scattered electron via the only possible t-channel process ($e^- p \to e^- t$). The polar angle of the electron in association with the top quark polarization asymmetries constructed from the angular distribution of the secondary lepton arising from the top decay, allows to distinguish the Lorentz structure of the coupling. We conclude the chapter with the multi-parameter statistical analysis at the end. Our study shows that a reach of $\mathcal{O}(10^{-2})$ in the case of Ztu and Ztc couplings at an integrated luminosity of 2 ab^{-1} at 95% C.L can be obtained assuming presence of all NP couplings simultaneously.

In **Chapter 4**, we study the possibility of single top quark production at Run I of the ILC for $\sqrt{s}$=250 GeV. The ILC study mostly focus on Higgs couplings because of the insufficient c.m. energy to produce top quark pairs. Therefore, the top quark physics has not drawn much interest in the community. We propose the production of single top quark possible through top quark FCNC interactions at tree level. The single top production process $e^-e^+ \to tj$, with light quark jet (j) is studied against a complete set of background processes provided by the ILD group at KEK, Japan. The significance of signal over background samples for different *Lorentz structures* (tensor structure for the $tq\gamma$ and vector and tensor structure tqZ couplings), has been studied. We quote the reach of the couplings at 95% C.L. and shown that the observables used are sufficient to distinguish various different couplings for two different sets of initial beam polarizations, i.e. $(P_{e^-}, P_{e^+}) = (-80\%, +30\%)$ and $(+80\%, -30\%)$. The latter arrangement seems to have less irreducible background than the earlier does. Our study shows that the reach of the coupling value 0.01 in the case of $tq\gamma$, and 0.02 in the case of tqZ coupling at 95% C.L. The study also provide sensitivity of different couplings to various kinematic asymmetries constructed, which provides a way to distinguish them. In addition we also indicate the FCNC study at higher c.m. energy, such as 350 and 500 GeV at ILC, can have better significance.

In **Chapter 5**, we complete our study with the strong FCNC interactions in the top quark sector through $tqg-$anomalous couplings along with the FCNC through $tq\gamma$ couplings. The process under study is considered at the FCC-he with beam energy $E_{e(p)} = 60\ (50,000)$ GeV through the process of $e^-p \to e^-tj$, with j being a light quark jet. We have shown that this is the best process for the study of tqg vertex and can probe the couplings with better signal significance. We have demonstrated that the presence of couplings to the level of a few times 10^{-2} TeV^{-1} can be probed at this collider with the process considered.

We believe that our study shows a new way forward in discriminating the signal from the SM background at future colliders. In addition, it gives a way for collider physics community to understand the spin/polarization of the intermediate top quark, if we are able to get better signal-significance in the real time. More over the study of top quark itself gives the handle to understand the nature of bare quark phenomenon precisely. At the end we conclude that the top quark can be better studied at proposed future colliders, which are equipped with better

configurations to understand its nature and interactions, than the current run of LHC and somewhat comparable to the HL-LHC.

A

Reconstruction of Neutrino and Top quark Momenta for Semi-leptonic decay of top quark

In the following I have discussed the reconstruction technique implemented for the Neutrino momentum and consequently the top quark momentum for the generic process : $A+B \to tX \to bWX \to Xb\ell\nu$, with X being any fermion except neutrino.

The four momentum of a particle can be represented as, $P_i = \{E_i, p_i^x, p_i^y, p_i^z\} = \{E_i, p_i\}$, where for $i = X,\ t,\ b,\ \ell,\ \nu$, represents the particle index. At colliders like LHeC or ILC or FCC-he, the transverse component of the final state particles is zero; i.e., $\sum_i P_i^T = 0$, due to the four-momentum conservation. The we can write the neutrino transverse momentum as,

$$P_\nu^T = -\sum_k P_k^T \tag{A.1}$$
$$\implies p_\nu^x = -\sum_k p_k^x, \quad p_\nu^y = -\sum_k p_k^y$$

for $k = X,\ \ell,\ b$.

For the full reconstruction of the top quark, we need to reconstruct the $Z-$component of the missing momentum. As the neutrino is massless, i.e. $P_\nu^2 =$

$m_\nu^2 = 0$, which implied that energy of the neutrino can be expressed as $E_\nu = \sqrt{(p_\nu^x)^2 + (p_\nu^y)^2 + (p_\nu^z)^2}$. Similarly for light leptons ℓ (massless as compared to top quark mass), we have $E_\ell = \sqrt{(p_\ell^x)^2 + (p_\ell^y)^2 + (p_\ell^z)^2}$.

Considering the W-boson to be on-shell, we can write,

$$\begin{aligned}
& P_W^2 = m_W^2 \\
\implies & (P_\ell + P_\nu)^2 = m_W^2 \\
\implies & 2P_\ell.P_\nu = m_W^2 \\
\implies & E_\ell E_\nu - p_\ell^x p_\nu^x - p_\ell^y p_\nu^y - p_\ell^z p_\nu^z = \frac{m_W^2}{2} \\
\implies & E_\ell \sqrt{(P_\nu^T)^2 + (p_\nu^z)^2} - p_\ell^x p_\nu^x - p_\ell^y p_\nu^y - p_\ell^z p_\nu^z = \frac{m_W^2}{2} \\
\implies & E_\ell \sqrt{(P_\nu^T)^2 + (p_\nu^z)^2} = \{\frac{m_W^2}{2} + p_\ell^x p_\nu^x + p_\ell^y p_\nu^y\} + p_\ell^z p_\nu^z \\
\implies & E_\ell^2((P_\nu^T)^2 + (p_\nu^z)^2) = (\Delta + p_\ell^z p_\nu^z)^2 \\
\implies & E_\ell^2 (P_\nu^T)^2 + E_\ell^2 (p_\nu^z)^2 = \Delta^2 + (p_\ell^z)^2 (p_\nu^z)^2 + 2\Delta p_\ell^z p_\nu^z \\
\implies & (p_\nu^z)^2[(p_\ell^z)^2 - E_\ell^2] + p_\nu^z (2\Delta p_\ell^z) + \Delta^2 - E_\ell^2 (P_\nu^T)^2 = 0
\end{aligned} \tag{A.2}$$

where, $\Delta = \frac{m_W^2}{2} + p_\ell^x p_\nu^x + p_\ell^y p_\nu^y$.

Solution for (p_ν^z) -: We have to solve the quadratic Eq. (A.2), to find the roots of (p_ν^z). Let us consider the quadratic equation as $ax^2 + bx + c = 0$. The value of a, b and c are the known parameters and $x = p_\nu^z$ is the only unknown to be calculated.

$$\begin{aligned}
a &= (p_\ell^z)^2 - E_\ell^2 \\
&= (p_\ell^z)^2 - \{(p_\ell^x)^2 + (p_\ell^y)^2 + (p_\ell^z)^2\} \\
&= -(p_\ell^x)^2 - (p_\ell^y)^2 = -(P_\ell^T)^2, \\
b &= 2\Delta p_\ell^z, \\
c &= \Delta^2 - E_\ell^2 (P_\nu^T)^2
\end{aligned} \tag{A.3}$$

Thus the discriminant will be,

$$\begin{aligned} D &= b^2 - 4ac \\ &= 4\Delta^2 E_\ell^2 - 4E_\ell^2 (P_\ell^T)^2 (P_\nu^T)^2 \\ &= 4E_\ell^2 [\Delta^2 - (P_\nu^T)^2 (P_\ell^T)^2] \\ &= 4E_\ell^2 D' \end{aligned} \tag{A.4}$$

Condition for real solutions $D' \geq 0$ or $\Delta^2 \geq (P_\nu^T)^2 (P_\ell^T)^2$. The two real solution gives the following.

$$\begin{aligned} x_\pm =& \frac{-b \pm \sqrt{D}}{2a} \\ \implies (p_\nu^z)_\pm =& \frac{-1}{2(P_\ell^T)^2} \big[-2\Delta p_\ell^z \pm 2E_\ell \sqrt{D\prime} \big] \\ \implies (p_\nu^z)_\pm =& \big[\frac{\Delta p_\ell^z \mp E_\ell \sqrt{\Delta^2 - (P_\nu^T)^2 (P_\ell^T)^2}}{(P_\ell^T)^2} \big] \end{aligned} \tag{A.5}$$

Therefore the two possible neutrino four momenta can be $P_\pm(\nu) = \{E_\pm(\nu), p_\nu^x, p_\nu^y, (p_\nu^z)_\pm\}$ where, $E_\pm(\nu) = \sqrt{(P_\nu^T)^2 + (p_\nu^z)_\pm^2}$. Out of the two solutions, only that momentum which is closer to the TRUE value will be consider and other will be discarded. Now to get the right solution, we need to take the top mass constraints into consideration.

Condition : Onshell top quark,

$$\begin{aligned} (P_b + P_W)^2 &= M_t^2 \\ \implies (P_b + P_\ell + (P_\nu)_\pm)^2 &= (M_t^2)_\pm \end{aligned} \tag{A.6}$$

But, the top mass can't be degenerate and hence the above condition will be satisfied only for the TRUE value of top mass i.e., $M_t \simeq 173$ GeV. As we are dealing with high energy collider and by far the neutrino is not exactly determinable; therefore it is always a common practice to take the nearest possible true value of $M_t \simeq 173$ GeV.

भारतीय प्रौद्योगिकी संस्थान गुवाहाटी
Indian Institute of Technology Guwahati

B

EFT Lagrangian implementation as UFO model file

The UFO model file used in the projects for the Thesis is built and tested at home. In Chapter 1, we have discussed the NP Lagrangian for the study of FCNCs in top quark. To generate events and do the analysis we have implemented the EFT Lagrangian using the Mathematica based package called FeynRules-v2.0 [75]. We obtained the UFO model file, which is used to generate events in MadGraph5. Below I mention the $\mathcal{L}_{fcnc}$ coded in Mathematica to generate the UFO file along with the SM Lagrangian($\mathcal{L}_{SM}$)part of the Mathematica file used for the model implementation. The detail of the nomenclature can be found from [53].

```
(* *** Interaction orders as used by mg5*** *)

M$InteractionOrderHierarchy = {
{QCD, 1},
{QED, 2},
{NP, 1}
};

  (* NP Parameters *)

kg == {
ParameterType -> External,
BlockName -> NPINPUTS,
```

```
    TeX -> Subscript[k, g],
15  InteractionOrder -> {NP, 1},
    Value -> 0.,
17  Description -> "FCNC gluon coefficient"},


19
    ka == {
21  ParameterType -> External,
    BlockName -> NPINPUTS,
23  TeX -> Subscript[k, a],
    InteractionOrder -> {NP, 1},
25  Value -> 0.,
    Description -> "FCNC photon coefficient"},
27
    kzt == {
29  ParameterType -> External,
    BlockName -> NPINPUTS,
31  TeX -> Subscript[k, zt],
    InteractionOrder -> {NP, 1},
33  Value -> 0.,
    Description -> "FCNC Z-tensor coefficient"},
35
    kzv == {
37  ParameterType -> External,
    BlockName -> NPINPUTS,
39  TeX -> Subscript[k, zv],
    InteractionOrder -> {NP, 1},
41  Value -> 0.,
    Description -> "FCNC Z-vector coefficient"},
43


45  guR == {
    ParameterType -> External,
47  BlockName -> NPChiralINPUTS,
    TeX -> Subscript[g, uR],
49  Value -> 0.,
    Description -> "FCNC gluon uR coefficient"},
51
    guL == {
53  ParameterType -> External,
    BlockName -> NPChiralINPUTS,
55  TeX -> Subscript[g, uL],
    Value -> 0.,
57  Description -> "FCNC gluon uL coefficient"},
```

```
59
gcR == {
61 ParameterType -> External,
BlockName -> NPChiralINPUTS,
63 TeX -> Subscript[g, cR],
Value -> 0.,
65 Description -> "FCNC gluon cR coefficient"},

67 gcL == {
ParameterType -> External,
69 BlockName -> NPChiralINPUTS,
TeX -> Subscript[g, cL],
71 Value -> 0.,
Description -> "FCNC gluon cL coefficient"},
73
auR == {
75 ParameterType -> External,
BlockName -> NPChiralINPUTS,
77 TeX -> Subscript[a, uR],
Value -> 0.,
79 Description -> "FCNC photon uR coefficient"},

81 auL == {
ParameterType -> External,
83 BlockName -> NPChiralINPUTS,
TeX -> Subscript[a, uL],
85 Value -> 0.,
Description -> "FCNC photon uL coefficient"},
87
acR == {
89 ParameterType -> External,
BlockName -> NPChiralINPUTS,
91 TeX -> Subscript[a, cR],
Value -> 0.,
93 Description -> "FCNC photon cR coefficient"},

95 acL == {
ParameterType -> External,
97 BlockName -> NPChiralINPUTS,
TeX -> Subscript[a, cL],
99 Value -> 0.,
Description -> "FCNC photon cL coefficient"},
101
```

```
zutR == {
ParameterType -> External,
BlockName -> NPChiralINPUTS,
TeX -> Subscript[z, utR],
Value -> 0.,
Description -> "FCNC tensor ZuR coefficient"},

zutL == {
ParameterType -> External,
BlockName -> NPChiralINPUTS,
TeX -> Subscript[z, utL],
Value -> 0.,
Description -> "FCNC tensor ZuL coefficient"},

zctR == {
ParameterType -> External,
BlockName -> NPChiralINPUTS,
TeX -> Subscript[z, ctR],
Value -> 0.,
Description -> "FCNC tensor ZcR coefficient"},

zctL == {
ParameterType -> External,
BlockName -> NPChiralINPUTS,
TeX -> Subscript[z, ctL],
Value -> 0.,
Description -> "FCNC tensor ZcL coefficient"},

zuvR == {
ParameterType -> External,
BlockName -> NPChiralINPUTS,
TeX -> Subscript[z, uvR],
Value -> 0.,
Description -> "FCNC vector ZuR coefficient"},

zuvL == {
ParameterType -> External,
BlockName -> NPChiralINPUTS,
TeX -> Subscript[z, uvL],
Value -> 0.,
Description -> "FCNC vector ZuL coefficient"},

zcvR == {
ParameterType -> External,
```

```
BlockName -> NPChiralINPUTS,
TeX -> Subscript[z, cvR],
Value -> 0.,
Description -> "FCNC vector ZcR coefficient"},

zcvL == {
ParameterType -> External,
BlockName -> NPChiralINPUTS,
TeX -> Subscript[z, cvL],
Value -> 0.,
Description -> "FCNC vector ZcL coefficient"},

La == {
ParameterType -> External,
BlockName -> SCALE_EFT,
TeX -> \[Lambda],
Value -> 173.0,
Description -> "Scale of the theory"},

(* FCNC Lagrangian *)

ONPg := Block[{Sga},
I/2 gs kg/2/La ( guR ubar.Ga[mu].Ga[nu].T[aa].ProjP.t.
FS[G,mu,nu,aa] + guL ubar.Ga[mu].Ga[nu].T[aa].ProjM.t.
FS[G,mu,nu,aa] + gcR cbar.Ga[mu].Ga[nu].T[aa].ProjP.t.
FS[G,mu,nu,aa] + gcL cbar.Ga[mu].Ga[nu].T[aa].ProjM.t.
FS[G,mu,nu,aa]) - I/2 gs kg/2/La (guR ubar.Ga[nu].
Ga[mu].T[aa].ProjP.t.FS[G,mu,nu,aa] + guL
ubar.Ga[nu].Ga[mu].T[aa].ProjM.t.FS[G,mu,nu,aa]+ gcR
cbar.Ga[nu].Ga[mu].T[aa].ProjP.t.FS[G,mu,nu,aa] + gcL
cbar.Ga[nu].Ga[mu].T[aa].ProjM.t.FS[G,mu,nu,aa])
];
Ltqg:= ONPg + HC[ONPg];

ONPa := Block[{Sga},
I/2 ee ka/2/La ( auR ubar.Ga[mu].Ga[nu].ProjP.t.
FS[A,mu,nu] + auL ubar.Ga[mu].Ga[nu].ProjM.t.
FS[A,mu,nu] + acR cbar.Ga[mu].Ga[nu].ProjP.t.
FS[A,mu,nu] + acL cbar.Ga[mu].Ga[nu].ProjM.t.
FS[A,mu,nu]) - I/2 ee ka/2/La ( auR ubar.Ga[nu].
Ga[mu].ProjP.t. FS[A,mu,nu] + auL ubar.Ga[nu].
Ga[mu].ProjM.t.FS[A,mu,nu]  + acR
cbar.Ga[nu].Ga[mu].ProjP.t.FS[A,mu,nu] + acL
cbar.Ga[nu].Ga[mu].ProjM.t.FS[A,mu,nu])
```

```
];
Ltqa:= ONPa + HC[ONPa];

ONPzt := Block[{Sga},
I/2 gw/2/cw kzt/2/La ( zutR ubar.Ga[mu].Ga[nu].ProjP.t.
FS[Z,mu,nu] + zutL ubar.Ga[mu].Ga[nu].ProjM.t.FS[Z,mu,nu]
+ zctR cbar.Ga[mu].Ga[nu].ProjP.t.FS[Z,mu,nu] + zctL
cbar.Ga[mu].Ga[nu].ProjM.t.FS[Z,mu,nu])
- I/2 gw/2/cw kzt/2/La ( zutR ubar.Ga[nu].Ga[mu].ProjP.t.
FS[Z,mu,nu] + zutL ubar.Ga[nu].Ga[mu].ProjM.t.
FS[Z,mu,nu] + zctR cbar.Ga[nu].Ga[mu].ProjP.t.
FS[Z,mu,nu] + zctL cbar.Ga[nu].Ga[mu].ProjM.t.FS[Z,mu,nu])
];
Ltqzt:= ONPzt + HC[ONPzt];

ONPzv := Block[{Sga},
-gw/2/cw kzv ( zuvR ubar.Ga[mu].ProjP.t.Z[mu] + zuvL
ubar.Ga[mu].ProjM.t.Z[mu] + zcvR cbar.Ga[mu].ProjP.t.Z[mu] +
zcvL cbar.Ga[mu].ProjM.t.Z[mu])
];
Ltqzv:= ONPzv + HC[ONPzv];

(* Total Lagrangian *)

LTotal:= LSM + Ltqg + Ltqa + Ltqzt + Ltqzv;
```

C

Analytical expression of Invariant Amplitude and Cross Section for $pe^- \to e^- t, (t \to b\ell^+\nu_\ell)$

This appendix dedicated to a complete calculations of invariant amplitude of the process considered in the helicity basic of the top quark. The calculation can be extended to any process at tree level with even more than one light fermions production in association with the top quark. The calculation is also independent of the initial state and also valid for s-channel processes. The later requires the assignment of momentum different from the discussed one. The calculation assumes the Narrow Width Approximation (NWA) to be true for the process of top quark production due to the fact that the $\frac{\Gamma_t}{m_t} \to 0$.

With the assumption in hand, lets us consider the process $pe^- \to e^- t, (t \to b\ell^+\nu_\ell)$ for calculation. The initial proton momentum is considered to be in the $+$ve direction of $z-$axis.

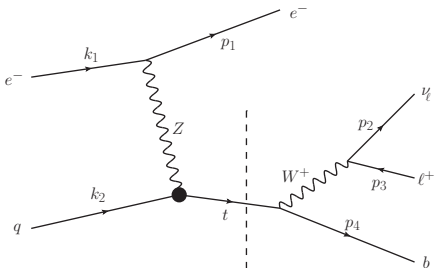

FIGURE C.1: Flavour Changing Neutral Current (FCNC) process in e^-p collider. The dashed line separates the top quark production and decay amplitude.

The momentum assignment of the involving particles are :

- Initial state electron : $k_1 = E(1, 0, 0, -1)$
- Initial state parton : $k_2 = E(1, 0, 0, 1)$
- final state electron : $p_1 = (E_1, \mathbf{p_1})$
- top quark : $p_t = (E_t, \mathbf{p_t})$
- final state $b-$quark : $p_4 = p_b = (E_b, \mathbf{p_b})$
- secondary lepton : $p_3 = p_\ell = (E_\ell, \mathbf{p}_\ell)$

The phase space of the diagram of Fig. C.1 is given by

$$d\Pi = \frac{d^3p_1}{(2\pi)^3 2E_1}\frac{d^3p_b}{(2\pi)^3 2E_b}\frac{d^3p_\ell}{(2\pi)^3 2E_\ell}\frac{d^3p_\nu}{(2\pi)^3 2E_\nu}(2\pi)^4\delta^4(k_1 + k_2 - p_1 - p_b - p_\ell - p_\nu). \tag{C.1}$$

Where k_1 and k_2 are the momentum of initial parton and electron. We are going to use the following two identities, which are true for the on-shell top quark consideration.

$$\begin{aligned} 1 &= \frac{d^4p_{b\ell\nu}}{(2\pi)^4}\ \theta(E_{b\ell\nu})(2\pi)^4\delta^4(p_{b\ell\nu} - p_b - p_\ell - p_\nu) \\ 1 &= \frac{ds_{b\ell\nu}}{2\pi}2\pi\delta(s_{b\ell\nu} - p^2_{b\ell\nu}) \end{aligned} \tag{C.2}$$

where $p_{b\ell\nu} = p_b + p_\ell + p_\nu$. $E_{b\ell\nu}$ and $s_{b\ell\nu}$ are the corresponding energy and the invariant mass respectively. $\theta(E) = 1$ for $E \geq 0$ and zero otherwise. The θ-function implies that the energy is positive everywhere. Since it is a trivial assumption

in any calculation, we will drop θ-function whenever it is not necessary. Now combining the above two identities we arrive at

$$\begin{aligned} 1 =& \frac{d^4p_{b\ell\nu}}{(2\pi)^4}\frac{ds_{b\ell\nu}}{2\pi}\ \theta(E_{b\ell\nu})(2\pi)^4\delta^4(p_{b\ell\nu}-p_b-p_\ell-p_\nu)2\pi\delta(s_{b\ell\nu}-p^2_{b\ell\nu}) \\ =& \frac{ds_{b\ell\nu}}{2\pi}\frac{d^3p_{b\ell\nu}}{(2\pi)^3 2E_{b\ell\nu}}\ (2\pi)^4\delta^4(p_{b\ell\nu}-p_b-p_\ell-p_\nu). \end{aligned} \tag{C.3}$$

Using the above identity, we can separate the 4-body phase space of Eq. (C.1) into the top quark production and decay part as follows

$$\begin{aligned} d\Pi = \frac{ds_{b\ell\nu}}{2\pi}\frac{d^3p_1}{(2\pi)^3 2E_1}\frac{d^3p_{b\ell\nu}}{(2\pi)^3 2E_{b\ell\nu}}(2\pi)^4\delta^4(k_1+k_2-p_1-p_{b\ell\nu})\frac{d^3p_b}{(2\pi)^3 2E_b}\frac{d^3p_\ell}{(2\pi)^3 2E_\ell}\frac{d^3p_\nu}{(2\pi)^3 2E_\nu} \\ (2\pi)^4\delta^4(p_{b\ell\nu}-p_b-p_\ell-p_\nu) \\ \implies d\Pi = \frac{ds_{b\ell\nu}}{2\pi}\times d\Pi_P \times d\Pi_D \end{aligned} \tag{C.4}$$

where $d\Pi_P$ is the phase space of the top quark production cross section and $d\Pi_D$ is for the top quark decay, given by,

$$d\Pi_P = \frac{d^3p_1}{(2\pi)^3 2E_1}\frac{d^3p_{b\ell\nu}}{(2\pi)^3 2E_{b\ell\nu}}(2\pi)^4\delta^4(k_1+k_2-p_1-p_{b\ell\nu}) \tag{C.5}$$

$$d\Pi_D = \frac{d^3p_b}{(2\pi)^3 2E_b}\frac{d^3p_\ell}{(2\pi)^3 2E_\ell}\frac{d^3p_\nu}{(2\pi)^3 2E_\nu}(2\pi)^4\delta^4(p_{b\ell\nu}-p_b-p_\ell-p_\nu) \tag{C.6}$$

C.1 Production Cross Section

The phase space of Eq. (C.5) for the top quark production cross section from Eq. (2.8) of Chapter 2, can be written as

$$\begin{aligned} d\Pi_P =& \frac{d^3p_1}{(2\pi)^3 2E_1}\frac{d^3p_{b\ell\nu}}{(2\pi)^3 2E_{b\ell\nu}}(2\pi)^4\delta^4(k_1+k_2-p_1-p_{b\ell\nu}) \\ =& \frac{d^3p_1}{(2\pi)^3 2E_1}\frac{d^3p_t}{(2\pi)^3 2E_t}(2\pi)^4\delta^4(k_1+k_2-p_1-p_t) \\ =& \frac{d^3p_1}{(2\pi)^3 2E_1}d^4p_t\theta(E_t)\delta(p_t^2)(2\pi)\delta^4(k_1+k_2-p_1-p_{b\ell\nu}) \\ =& \frac{d^3p_1}{(2\pi)^2 2E_1}\delta[(k_1+k_2-p_1)^2] \end{aligned} \tag{C.7}$$

The above expression is in the c.m. frame, where the four momenta of the initial e^- and quark (from proton) are $k_1 = E(1,0,0,-1)$ and $k_2 = E(1,0,0,1)$. The c.m. energy is given by, $\sqrt{\hat{s}} = 2E$. The vertex factor for e^+e^-Z and $t\bar{q}Z$ vertices are given by,

$$\mathrm{i}\,\Gamma^{\mu}_{e^+e^-Z} = \frac{-\mathrm{i}g}{2\mathrm{c}_W}\gamma^{\mu}(g_L P_L + g_R P_R), \tag{C.8}$$

$$\mathrm{i}\,\Gamma^{\mu}_{t\bar{q}Z} = \frac{-\mathrm{i}g}{2\mathrm{c}_W}\Big[\gamma^{\mu}(X^L P_L + X^R P_R) + \frac{\mathrm{i}\sigma^{\mu\alpha}(p_t - k_2)_{\alpha}}{\Lambda}(\kappa^L P_L + \kappa^R P_R)\Big] \tag{C.9}$$

where g_L and g_R represents the left- and right-chiral couplings for the e^+e^-Z vertex, respectively. P_L and P_R represent the left and right handed projection operators respectively. $X^{L(R)}$ and $\kappa^{L(R)}$ are equivalent to $X^{L(R)}_{zqt}$ and $\kappa^{L(R)}_{zqt}$ defined in Eq. (1.5) of Chapter 1 of the thesis, represents the vector and tensor coupling of the NP. α represents the Lorentz index and Λ is the cut-off scale of the theory. The invariant amplitude is given by,

$$\mathcal{M}_P(\lambda) = \frac{g^2}{4\mathrm{c}_W^2}\Delta_Z(p_Z^2)\Big[\bar{u}(p_1)\Gamma^{\mu}_{e^+e^-Z}u(k_1)\Big]\Big[\bar{u}(p_t,\lambda)\Gamma^{t\bar{q}Z}_{\mu}u(k_2)\Big] \tag{C.10}$$

where $\Delta_Z(p_Z^2) = \frac{-\mathrm{i}\left[g_{\mu\nu} - \frac{(k_1-p_1)_{\mu}(k_1-p_1)_{\nu}}{m_Z^2}\right]}{p_Z^2 - m_Z^2 + \mathrm{i}m_Z\Gamma_Z}$ represents the $Z-$boson propagator. Finally we calculate the production density matrix as follows.

$$\rho(\lambda,\lambda') = \mathcal{M}_P^*(\lambda)\mathcal{M}_P(\lambda') = \frac{g^4}{16\mathrm{c}_W^4}|\Delta_Z(p_Z^2)|^2\mathrm{tr}\Big[\not{p}_1\Gamma^{\mu}_{e^+e^-Z}\not{k}_1\gamma^0\Gamma^{\nu}_{e^+e^-Z}\gamma^0\Big]$$
$$\times\mathrm{tr}\Big[\frac{1}{2}(\delta_{\lambda\lambda'} + \gamma_5\not{S}^a\tau^a_{\lambda\lambda'})(\not{p}_t + m_t)\Gamma^{tqZ}_{\mu}\not{k}_2\Gamma^{tqZ}_{\nu}\Big] \tag{C.11}$$

Here we have used the following identity for helicity projection,

$$u(p_t,\lambda)\bar{u}(p_t,\lambda') = \frac{1}{2}(\delta_{\lambda'\lambda} + \gamma_5\not{S}^a \otimes \tau^a_{\lambda'\lambda})(\not{p}_t + m_t), \qquad a = 1,2,3. \tag{C.12}$$

The above identity gives us the relations,

$$u(p_t,+)\bar{u}(p_t,+) = \frac{1}{2}(1+\gamma_5 \not{S}^3)(\not{p}_t + m_t), \tag{C.13}$$

$$u(p_t,+)\bar{u}(p_t,-) = \frac{1}{2}\gamma_5(\not{S}^1 + i\not{S}^2)(\not{p}_t + m_t), \tag{C.14}$$

$$u(p_t,-)\bar{u}(p_t,+) = \frac{1}{2}\gamma_5(\not{S}^1 - i\not{S}^2)(\not{p}_t + m_t), \tag{C.15}$$

$$u(p_t,-)\bar{u}(p_t,-) = \frac{1}{2}(1-\gamma_5 \not{S}^3)(\not{p}_t + m_t). \tag{C.16}$$

where, $S^{\mu a}$ are the spin vectors. Using the trace algebra we calculate calculate the right hand side of Eq. (C.11), which is shown below.

The production density matrix element from Eq. (C.11) is computed in the rest frame of the top quark, with z-axis along the boost direction of top. We used FORM to perform the trace calculation and simplification of the expression in the section below.

C.1.1 Analytical calculation of the production density matrix

To simplify the expression and make use of the production density matrix to calculate the polarization asymmetries as discussed in Chapter 2 of the thesis, we choose a frame such that the top quark is always produced in the xz-plane with a boost vector $\beta_t = \sqrt{1-\frac{m_t^2}{E^2}}$ along the z-axis. The four momenta of the top quark and scattered electron is given by,

$$\begin{aligned} p_t &= E_t(1, \beta_t \sin\theta_t, 0, \beta_t \cos\theta_t), \\ p_1 &= k_1 + k_2 - p_t. \end{aligned} \tag{C.17}$$

where θ_t represents the polar angle of the top quark in the xz-plane. To get the spin vector of the top quark in xz-plane, we perform the following operation on the spin vector :

1. The spin vectors of the top quark in the rest frame of it are,

$$S^1 = (0,1,0,0), \qquad S^2 = (0,0,1,0), \qquad S^3 = (0,0,0,1), \tag{C.18}$$

2. Boost the vector with β_t along the z-axis

3. Rotate along the y-axis through an angle θ_t

Finally the top quark spin vector in the xz-plane is given by,

$$S^1 = (0, \mathrm{c}_{\theta_t}, 0, -s_{\theta_t}), \qquad S^2 = (0, 0, 1, 0), \qquad S^3 = \frac{E_t}{m_t}(\beta_t, s_{\theta_t}, 0, \mathrm{c}_{\theta_t}), \tag{C.19}$$

Note that all the four momenta are written in the contravariant form.

In the following we have given the final expression of the production density matrix for all possible combination of helicity. The density matrix for similar helicity is given by,

$$\begin{aligned}
\rho(\pm,\pm) =& 8\Big[(X^L)^2 g_L^2 + (X^R)^2 g_R^2\Big] E^2 \Big[\beta_t^2 E_t^2 \mathrm{c}_{\theta_t}^2 + 2EE_t(1-\beta_t \mathrm{c}_{\theta_t}) \\
&+ 4EE_t(1+\beta_t \mathrm{c}_{\theta_t}) - E_t^2 - 2m_t^2\Big] - 8\Big[X^L\kappa^L + X^R\kappa^R\Big]\Big[g_L^2 + g_R^2\Big] \\
&\times \frac{m_t}{\Lambda} E^2 \Big[-\beta_t^2 E_t^2 \mathrm{c}_{\theta_t}^2 - 4EE_t(1-\beta_t \mathrm{c}_{\theta_t}) - 2E(\beta_t E_t \mathrm{c}_{\theta_t} \\
&- 2E + E_t) + E_t^2 + m_t^2\Big] - 4\Big[(\kappa^L)^2 g_R^2 + (\kappa^R)^2 g_L^2\Big]\frac{E^2}{\Lambda^2} \\
&\times \Big[E_t(\beta_t \mathrm{c}_{\theta_t} - 1)\Big\{E\left(2E_t^2(1-\beta_t^2\mathrm{c}_{\theta_t}^2) + 6m_t^2\right) + 4E^2E_t(\beta_t \mathrm{c}_{\theta_t} - 1) \\
&- 3E_t m_t^2(\beta_t \mathrm{c}_{\theta_t} + 1)\Big\} + 2E\Big(4E\left(E_t^2\left(\beta_t^2\mathrm{c}_{\theta_t}^2 - 1\right) + 2m_t^2\right) \\
&+ 4E^2E_t(\beta_t \mathrm{c}_{\theta_t} - 1) + E_t^3(\beta_t \mathrm{c}_{\theta_t} - 1)(\beta_t \mathrm{c}_{\theta_t} + 1)^2\Big)\Big] \\
&\pm \Big[-8X^L X^R\Big[g_R^2 - g_L^2\Big] E^2 E_t(\beta_t - \mathrm{c}_{\theta_t})(\beta_t \mathrm{c}_{\theta_t} E_t - 2E + E_t) \\
&- 8\Big[X^R\kappa^L g_R^2 - X^L\kappa^R g_L^2\Big]\frac{E^2E_t}{\Lambda m_t}\Big[-2E\beta_t^3\mathrm{c}_{\theta_t}^2 E_t^2 + \beta_t^2 \mathrm{c}_{\theta_t} E_t \\
&\left(-2E\mathrm{c}_{\theta_t}^2 E_t - 4E^2 + 4E^2 + m_t^2\right) \\
&+ \beta_t\Big(4\left(\mathrm{c}_{\theta_t}^2 + 1\right)E^2E_t + 2EE_t\left(E_t - 6\left(\mathrm{c}_{\theta_t}^2 - 1\right)E\right) \\
&+ \left(\mathrm{c}_{\theta_t}^2 - 1\right)E_t m_t^2 - 4Em_t^2\Big)
\end{aligned}$$

$$
\begin{aligned}
&- \mathrm{c}_{\theta_t}\left(4E^2E_t + 2EE_t(2E - E_t) - 4Em_t^2 + E_tm_t^2\right)\Big] \\
&+ 4\Big[\kappa^R\kappa^L g_R^2 - \kappa^L\kappa^R g_L^2\Big]\frac{E^2E_t}{\Lambda^2}(\beta_t - \mathrm{c}_{\theta_t})(\beta_t\mathrm{c}_{\theta_t}E_t - 2E + E_t) \\
&\times \Big[3\left(2EE_t(\beta_t\mathrm{c}_{\theta_t} - 1) + m_t^2\right) - 2E(\beta_t\mathrm{c}_{\theta_t}E_t - 2E + E_t)\Big]\Big]. \qquad \text{(C.20)}
\end{aligned}
$$

The production density for the dissimilar helicity is given by,

$$
\begin{aligned}
\rho(\pm,\mp) =& 8X^LX^R\Big[g_R^2 - g_L^2\Big]E\mathrm{c}_{\theta_t}Em_t(\beta_t\mathrm{c}_{\theta_t}E_t - 2E + E_t) \\
&+ 8\Big[X^R\kappa^L g_R^2 - X^L\kappa^R g_L^2\Big]\frac{E^2\mathrm{c}_{\theta_t}}{\Lambda} \\
&\times \Big[2EE_t\left(E_t\left(\beta_t^2\mathrm{c}_{\theta_t}^2 - 1\right) + E(6\beta_t\mathrm{c}_{\theta_t} + 2)\right) - 4E^2E_t(\beta_t\mathrm{c}_{\theta_t} - 1) \\
&+ E_tm_t^2(1 - \beta_t\mathrm{c}_{\theta_t}) - 4Em_t^2\Big] \\
&+ 4\Big[\kappa^R\kappa^L g_R^2 - \kappa^L\kappa^R g_L^2\Big]\frac{E^2m_t}{\Lambda^2}\mathrm{c}_{\theta_t}(\beta_t\mathrm{c}_{\theta_t}E_t - 2E + E_t) \\
&\left(2E(\beta_t\mathrm{c}_{\theta_t}E_t - 2E + E_t) - 3\left(2EE_t(\beta_t\mathrm{c}_{\theta_t} - 1) + m_t^2\right)\right) \qquad \text{(C.21)}
\end{aligned}
$$

In the above equations, we define $\sin\theta_t$ and $\cos\theta_t$ as s_{θ_t} and c_{θ_t} respectively. The cross section in terms of the production density matrix can be now calculated from Eq. (2.9) of Chapter 2.

C.2 Decay width

The top quark decay phase space can be simplified as

$$
\begin{aligned}
d\Pi_D =& \frac{d^3p_b}{(2\pi)^3 2E_b}\frac{d^3p_\ell}{(2\pi)^3 2E_\ell}\frac{d^4p_\nu}{(2\pi)^3}\theta(E_\nu)\delta(p_\nu^2)(2\pi)^4\delta^4(p_{b\ell\nu} - p_b - p_\ell - p_\nu) \\
=& \frac{d^3p_b}{(2\pi)^3 2E_b}\frac{d^3p_\ell}{(2\pi)^3 2E_\ell}(2\pi)\theta(E_\nu)\delta[(p_{b\ell\nu} - p_b - p_\ell)^2] \qquad \text{(C.22)}
\end{aligned}
$$

The arguments of the δ-function above can be expanded into

$$
\begin{aligned}
\delta[(p_{b\ell\nu} - p_b - p_\ell)^2] =& \delta(p_t^2 + p_b^2 + p_\ell^2 - 2p_t\cdot p_b - 2p_t\cdot p_\ell + 2p_b\cdot p_\ell) \\
=& \delta(p_t^2 + p_b^2 + p_\ell^2 - 2p_t\cdot p_b - 2p_t\cdot p_\ell + 2E_b\cdot E_\ell + 2|\mathbf{p}_b||\mathbf{p}_\ell|\cos\theta_{b\ell}) \\
=& \frac{\delta(\cos\theta_{b\ell} - \cos\theta_{b\ell}^0)}{2|\mathbf{p}_b||\mathbf{p}_\ell|} \qquad \text{(C.23)}
\end{aligned}
$$

Now we assume that the p_t and p_ℓ lie on the $x-z$ plane, where p_ℓ is along the positive z-axis. Then we can change the angular variables $[\cos\theta_{b\ell}, \phi_{b\ell}]$ to $[\cos\theta_b, \phi_b]$. Hence on integrating over the $\cos\theta_b$ from Eq. (C.22) we get

$$d\Pi_D = \frac{|\mathbf{p}_b| E_b dE_b d\phi_b}{(2\pi)^3 2E_b} \frac{d^3p_\ell}{(2\pi)^3 2E_\ell}(2\pi)\frac{1}{2|\mathbf{p}_b||\mathbf{p}_\ell|} = \frac{1}{(2\pi)^5}\frac{dE_b d\phi_b}{4E_\ell}\frac{d^3p_\ell}{2E_\ell}. \tag{C.24}$$

Now in the rest frame of the top quark

$$p_W^2 = (p_t - p_b)^2 = m_t^2 + m_b^2 - 2m_t E_b \qquad \Rightarrow \qquad dp_W^2 = 2m_t dE_b. \tag{C.25}$$

Using the above result in Eq. (C.24) we get

$$d\Pi_D = \frac{1}{(2\pi)^5}\frac{dE_b d\phi_b}{4E_\ell}\frac{d^3p_\ell}{2E_\ell} = \frac{1}{(2\pi)^5}\frac{dp_W^2 d\phi_b}{16 m_t E_\ell} E_\ell dE_\ell d\Omega_\ell \tag{C.26}$$

$$\begin{aligned}\overline{|\mathcal{M}|^2} =& \frac{\overline{|\mathcal{M}(ep\to et)|^2} \times \overline{|\mathcal{M}(t\to b\ell^+\nu_\ell)|^2}}{(s_{b\ell\nu} - m_t^2)^2 + m_t^2\Gamma_t^2} \\ =& \frac{\pi}{m_t\Gamma_t}\,\delta(s_{b\ell\nu} - m_t^2)\,\overline{|\mathcal{M}(ep\to et)|^2} \times \overline{|\mathcal{M}(t\to b\ell^+\nu_\ell)|^2}\end{aligned} \tag{C.27}$$

$$\Gamma^\mu_{tbW} = -\frac{ig}{\sqrt{2}}\Big[\gamma^\mu(f_{1L}P_L + f_{1R}P_R) - \frac{i\sigma^{\mu\nu}q_\nu}{m_W}(f_{2L}P_L + f_{2R}P_R)\Big] \tag{C.28}$$

From Eq. (2.5) of Chapter 2, the invariant amplitude for decay of the top quark can be written as,

$$\begin{aligned}\mathcal{M}_D(\lambda) \;=\; & \frac{g^2}{2}\Delta_W(p_W^2)\Big[\bar{u}(p_\nu)\gamma^\mu P_L v(p_\ell)\Big] \times \Big[\bar{u}(p_b)\Big[\gamma_\mu(f_{1L}P_L + f_{1R}P_R) \\ & - \frac{i\sigma_{\mu\alpha}(p_t-p_b)^\alpha}{m_W}(f_{2L}P_L + f_{2R}P_R)\Big]u(p_t,\lambda)\Big]\end{aligned}$$

where $\Delta_W(p_W^2) = \frac{i\left[-g_{\mu\nu} + \frac{(p_\ell+p_\nu)_\mu (p_t-p_b)_\nu}{m_W^2}\right]}{p_W^2 - m_W^2 + im_W\Gamma_W}$ is the $W-$boson propagator.

Therefore we can write the decay width of top quark as,

$$\Gamma_D(\lambda,\lambda') = \mathcal{M}_D^*(\lambda)\mathcal{M}_D(\lambda') = \frac{g^4}{4}|\Delta_W(p_W^2)|^2 \mathrm{tr}\Big[\not{p}_\nu\gamma^\mu P_L \not{p}_\ell \gamma^\nu P_L\Big]$$
$$\mathrm{tr}\Big[(\not{p}_b + m_b)\Big[\gamma_\mu(f_{1L}P_L + f_{1R}P_R) - \frac{\mathrm{i}\sigma_{\mu\alpha}(p_t-p_b)^\alpha}{m_W}(f_{2L}P_L + f_{2R}P_R)\Big]$$
$$\frac{1}{2}(\delta_{\lambda\lambda'} + \gamma_5 \not{S}^a \tau^a_{\lambda\lambda'})(\not{p}_t + m_t)\Big[\gamma_\nu(f_{1L}P_L + f_{1R}P_R) - \frac{\mathrm{i}\sigma_{\nu\beta}(p_t-p_b)^\beta}{m_W}(f_{2L}P_L + f_{2R}P_R)\Big]\Big] \tag{C.29}$$

In the SM the values of f_{1R}, f_{2L}, and f_{2R} can be set to zero and the value of $f_{1L} \simeq g_L$, which corresponds to the fact that the weak couplings prefer $\gamma^\mu P_L$ vertex structure only. In the top quark rest frame, let us choose the four momenta of the decay particles as,

$$\begin{aligned} p_t &= m_t(1,0,0,0), \\ p_b &= E_b(1, \sin\theta_b\cos\phi_b, \sin\theta_b\sin\phi_b, \cos\theta_b), \\ p_\ell &= E_\ell(1, \sin\theta_\ell\cos\phi_\ell, \sin\theta_\ell\sin\phi_\ell, \cos\theta_\ell), \\ p_\nu &= p_t - p_b - p_\ell. \end{aligned} \tag{C.30}$$

where θ_ℓ and ϕ_ℓ represent the polar and azimuthal angles of the lepton, in the top quark rest frame. The spin vectors of the top quark in its rest frame are,

$$S^1 = (0,1,0,0), \qquad S^2 = (0,0,1,0), \qquad S^3 = (0,0,0,1), \tag{C.31}$$

Note that all the four momenta are written in the contravariant form.

Thus the expression for decay density matrix is given by,

$$\begin{aligned} \Gamma_D(\pm,\pm) &= 4g_L^2\Big(m_t^2 - m_b^2 - 2m_t.E_\ell\Big) \times m_t.E_\ell(1 \pm \mathrm{c}_{\theta_\ell}) \\ \Gamma_D(\pm,\mp) &= 4g_L^2\Big(m_t^2 - m_b^2 - 2m_t.E_\ell\Big) \times m_t.E_\ell \mathrm{s}\theta_\ell.e^{\pm \mathrm{i}\phi_\ell} \end{aligned} \tag{C.32}$$

Note that, Eqs. (C.20), (C.21) and (C.32) are used to calculate polarization asymmetries as described in Eq. (2.23) of Chapter 2 of the thesis.

भारतीय प्रौद्योगिकी संस्थान गुवाहाटी
Indian Institute of Technology Guwahati

Bibliography

[1] Aad G, et al. Observation of a new particle in the search for the Standard Model Higgs boson with the ATLAS detector at the LHC. Phys Lett. 2012;B716:1–29.

[2] Chatrchyan S, et al. Observation of a new boson at a mass of 125 GeV with the CMS experiment at the LHC. Phys Lett. 2012;B716:30–61.

[3] Schmaltz M. Physics beyond the standard model (theory): Introducing the little Higgs. Nucl Phys Proc Suppl. 2003;117:40–49. [,40(2002)].

[4] Bernreuther W. Top quark physics at the LHC. J Phys. 2008;G35:083001.

[5] Kane GL, Ladinsky GA, Yuan CP. Using the Top Quark for Testing Standard Model Polarization and CP Predictions. Phys Rev. 1992;D45:124–141.

[6] First combination of Tevatron and LHC measurements of the top-quark mass. Geneva: CERN; 2014. ATLAS-CONF-2014-008. ATLAS-CONF-2014-008. CDF-NOTE-11071. CMS-PAS-TOP-13-014. D0-NOTE-6416. Work within the Tevatron Electroweak (TEV-EW-WG) and the Top Physics LHC (TOP-LHC-WG) working groups. Available from: http://cds.cern.ch/record/1669819.

[7] Aaboud M, et al. Measurement of the top quark mass in the $t\bar{t} \to$ lepton+jets channel from $\sqrt{s} = 8$ TeV ATLAS data and combination with previous results. Eur Phys J. 2019;C79(4):290.

[8] Incandela JR, Quadt A, Wagner W, Wicke D. Status and Prospects of Top-Quark Physics. Prog Part Nucl Phys. 2009;63:239–292.

[9] Abazov VM, et al. An Improved determination of the width of the top quark. Phys Rev. 2012;D85:091104.

[10] Godbole RM, Rindani SD, Singh RK. Lepton distribution as a probe of new physics in production and decay of the t quark and its polarization. JHEP. 2006;12:021.

[11] Quadt A. Top quark physics at hadron colliders. Eur Phys J. 2006;C48:835–1000.

[12] Aaboud M, et al. Combinations of single-top-quark production cross-section measurements and $|f_{\rm LV}V_{tb}|$ determinations at $\sqrt{s} = 7$ and 8 TeV with the ATLAS and CMS experimentsCombinations of single-top-quark production cross-section measurements and $|f_{LV}V_{tb}|$ determinations at $\sqrt{s} = 7$ and 8 TeV with the ATLAS and CMS experiments. JHEP. 2019;05:088.

[13] Aaboud M, et al. Measurement of the cross-section for producing a W boson in association with a single top quark in pp collisions at $\sqrt{s} = 13$ TeV with ATLAS. JHEP. 2018;01:063.

[14] Tait TMP, Yuan CP. Single top quark production as a window to physics beyond the standard model. Phys Rev. 2000;D63:014018.

[15] Aaboud M, et al. Measurement of the W boson polarisation in $t\bar{t}$ events from pp collisions at $\sqrt{s} = 8$ TeV in the lepton + jets channel with ATLAS. Eur Phys J. 2017;C77(4):264. [Erratum: Eur. Phys. J.C79,no.1,19(2019)].

[16] Czarnecki A, Korner JG, Piclum JH. Helicity fractions of W bosons from top quark decays at NNLO in QCD. Phys Rev. 2010;D81:111503.

[17] Godbole RM, Rao K, Rindani SD, Singh RK. On measurement of top polarization as a probe of $t\bar{t}$ production mechanisms at the LHC. JHEP. 2010;11:144.

[18] Rindani SD, Sharma P. Probing anomalous tbW couplings in single-top production using top polarization at the Large Hadron Collider. JHEP. 2011;11:082.

[19] Cabibbo N. Unitary Symmetry and Leptonic Decays. Phys Rev Lett. 1963;10:531–533. [,648(1963)].

[20] Kobayashi M, Maskawa T. CP Violation in the Renormalizable Theory of Weak Interaction. Prog Theor Phys. 1973;49:652–657.

[21] Bargiotti M, et al. Present knowledge of the Cabibbo-Kobayashi-Maskawa matrix. Riv Nuovo Cim. 2000;23N3:1.

[22] Glashow SL, Iliopoulos J, Maiani L. Weak Interactions with Lepton-Hadron Symmetry. Phys Rev. 1970;D2:1285–1292.

[23] Agashe K, et al. Working Group Report: Top Quark. In: Proceedings, 2013 Community Summer Study on the Future of U.S. Particle Physics: Snowmass on the Mississippi (CSS2013): Minneapolis, MN, USA, July 29-August 6, 2013; 2013. Available from: https://inspirehep.net/record/1263763/files/arXiv:1311.2028.pdf.

[24] Aguilar-Saavedra JA, Nobre BM. Rare top decays t $\rightarrow$ c γ, t $\rightarrow$ cg and CKM unitarity. Phys Lett. 2003;B553:251–260.

[25] Atwood D, Reina L, Soni A. Phenomenology of two Higgs doublet models with flavor changing neutral currents. Phys Rev. 1997;D55:3156–3176.

[26] Martin SP. A Supersymmetry primer. 1997;p. 98. [Adv. Ser. Direct. High Energy Phys.18,1(1998)].

[27] Drees M. An Introduction to supersymmetry. In: Current topics in physics. Proceedings, Inauguration Conference of the Asia-Pacific Center for Theoretical Physics (APCTP), Seoul, Korea, June 4-10, 1996. Vol. 1, 2; 1996. .

[28] Cao JJ, Eilam G, Frank M, Hikasa K, Liu GL, Turan I, et al. SUSY-induced FCNC top-quark processes at the large hadron collider. Phys Rev. 2007;D75:075021.

[29] Couture G, Hamzaoui C, Konig H. Flavor changing top quark decay within the minimal supersymmetric standard model. Phys Rev. 1995;D52:1713–1716.

[30] Antoniadis I. From extra-dimensions: Multiple brane scenarios and their contenders. Int J Mod Phys. 2010;A25:5817–5845.

[31] Rizzo TG. Extended gauge sectors. In: Beyond the standard model 4. Proceedings, 4th International Conference on High-Energy Physics, Tahoe City, USA, December 13-18, 1994; 1994. p. 24–31. Available from: http://www-public.slac.stanford.edu/sciDoc/docMeta.aspx?slacPubNumber=SLAC-PUB-6741.

[32] Murayama H. Dynamical (super)symmetry breaking. In: 11th Rencontres de Blois on Frontiers of Matter Chateau de Blois, France, June 28-July 3, 1999; 1999. .

[33] Kidonakis N, Belyaev A. FCNC top quark production via anomalous tqV couplings beyond leading order. JHEP. 2003;12:004.

[34] Khanpour H, Khatibi S, Khatiri Yanehsari M, Mohammadi Najafabadi M. Single top quark production as a probe of anomalous $tq\gamma$ and tqZ couplings at the FCC-ee. 2014;.

[35] Aad G, et al. Search for single top-quark production via flavour-changing neutral currents at 8 TeV with the ATLAS detector. Eur Phys J. 2016;C76(2):55.

[36] CMS Collaboration. Prospects for the search for gluon-mediated FCNC in top quark production with the CMS Phase-2 detector at the HL-LHC. 2018;.

[37] Aaboud M, et al. Search for flavour-changing neutral current top-quark decays $t \to qZ$ in proton-proton collisions at $\sqrt{s} = 13$ TeV with the ATLAS detector. JHEP. 2018;07:176.

[38] ATLAS Collaboration. Expected sensitivity of ATLAS to FCNC top quark decays $t \to Zu$ and $t \to Hq$ at the High Luminosity LHC. Geneva: CERN; 2016. ATL-PHYS-PUB-2016-019. Available from: https://cds.cern.ch/record/2209126.

[39] Khachatryan V, et al. Search for Anomalous Single Top Quark Production in Association with a Photon in pp Collisions at $\sqrt{s} = 8$ TeV. JHEP. 2016;04:035.

[40] Collaboration C. The Phase-2 Upgrade of the CMS Endcap Calorimeter. Geneva: CERN; 2017. CERN-LHCC-2017-023. CMS-TDR-019. Technical Design Report of the endcap calorimeter for the Phase-2 upgrade of the CMS experiment, in view of the HL-LHC run. Available from: https://cds.cern.ch/record/2293646.

[41] Manohar AV. Effective field theories. Lect Notes Phys. 1997;479:311–362.

[42] Manohar AV. Introduction to Effective Field Theories. In: Les Houches summer school: EFT in Particle Physics and Cosmology Les Houches, Chamonix Valley, France, July 3-28, 2017; 2018. .

[43] Gavela B, Jenkins EE, Manohar AV, Merlo L. Analysis of general power counting rules in effective field theory. The European Physical Journal C. 2016 Sep;76(9):485. Available from: https://doi.org/10.1140/epjc/s10052-016-4332-1.

[44] Aguilar-Saavedra JA. A Minimal set of top anomalous couplings. Nucl Phys. 2009;B812:181–204.

[45] Aguilar-Saavedra JA. Top flavor-changing neutral interactions: Theoretical expectations and experimental detection. Acta Phys Polon. 2004;B35:2695–2710.

[46] Abelleira Fernandez JL, et al. A Large Hadron Electron Collider at CERN: Report on the Physics and Design Concepts for Machine and Detector. J Phys. 2012;G39:075001.

[47] Kumar M, Ruan X, Islam R, Cornell AS, Klein M, Klein U, et al. Probing anomalous couplings using di-Higgs production in electron–proton collisions. Phys Lett. 2017;B764:247–253.

[48] Aihara H, et al. The International Linear Collider. A Global Project. 2019;.

[49] Alwall J, Frederix R, Frixione S, Hirschi V, Maltoni F, Mattelaer O, et al. The automated computation of tree-level and next-to-leading order differential cross sections, and their matching to parton shower simulations. JHEP. 2014;07:079.

[50] Murayama H, Watanabe I, Hagiwara K. HELAS: HELicity amplitude subroutines for Feynman diagram evaluations. 1992;.

[51] de Aquino P, Link W, Maltoni F, Mattelaer O, Stelzer T. ALOHA: Automatic Libraries Of Helicity Amplitudes for Feynman Diagram Computations. Comput Phys Commun. 2012;183:2254–2263.

[52] Maltoni F, Stelzer T. MadEvent: Automatic event generation with MadGraph. JHEP. 2003;02:027.

[53] Degrande C, Duhr C, Fuks B, Grellscheid D, Mattelaer O, Reiter T. UFO - The Universal FeynRules Output. Comput Phys Commun. 2012;183:1201–1214.

[54] Artoisenet P, Frederix R, Mattelaer O, Rietkerk R. Automatic spin-entangled decays of heavy resonances in Monte Carlo simulations. JHEP. 2013;03:015.

[55] Backovic M, Kong K, McCaskey M. MadDM v.1.0: Computation of Dark Matter Relic Abundance Using MadGraph5. Physics of the Dark Universe. 2014;5-6:18–28.

[56] Artoisenet P, Lemaitre V, Maltoni F, Mattelaer O. Automation of the matrix element reweighting method. JHEP. 2010;12:068.

[57] Hirschi V, Frederix R, Frixione S, Garzelli MV, Maltoni F, Pittau R. Automation of one-loop QCD corrections. JHEP. 2011;05:044.

[58] Alwall, Johan and Duhr, Claude and Fuks, Benjamin and Mattelaer, Olivier and Öztürk, Deniz Gizem and Shen, Chia-Hsien. Computing decay rates for new physics theories with FeynRules and MadGraph 5_aMC@NLO. Comput Phys Commun. 2015;197:312–323.

[59] Sjostrand T, Mrenna S, Skands PZ. PYTHIA 6.4 Physics and Manual. JHEP. 2006;05:026.

[60] Cacciari M, Salam GP, Soyez G. FastJet User Manual. Eur Phys J. 2012;C72:1896.

[61] de Favereau J, Delaere C, Demin P, Giammanco A, Lemaître V, Mertens A, et al. DELPHES 3, A modular framework for fast simulation of a generic collider experiment. JHEP. 2014;02:057.

[62] Sjöstrand T, Ask S, Christiansen JR, Corke R, Desai N, Ilten P, et al. An Introduction to PYTHIA 8.2. Comput Phys Commun. 2015;191:159–177.

[63] Mora de Freitas P. Mokka, main guidelines and future. In: Linear colliders. Proceedings, International Conference, LCWS 2004, Paris, France, April 19-23, 2004; 2004. p. 441–444.

[64] Musat G. Geant4 simulation for the FLC detector models with Mokka. In: Linear colliders. Proceedings, International Conference, LCWS 2004, Paris, France, April 19-23, 2004; 2004. p. 437–439.

[65] Mora de Freitas P, Videau H. Detector simulation with MOKKA / GEANT4: Present and future. In: Linear colliders. Proceedings, International Workshop on physics and experiments with future electron-positron linear colliders,

LCWS 2002, Seogwipo, Jeju Island, Korea, August 26-30, 2002; 2002. p. 623–627. Available from: http://www-library.desy.de/cgi-bin/showprep.pl?lc-tool03-010.

[66] Aarons G, et al. ILC Reference Design Report Volume 4 - Detectors. 2007;.

[67] Bambade P, et al. The International Linear Collider: A Global Project. 2019;.

[68] Gaede F. Marlin and LCCD: Software tools for the ILC. Nucl Instrum Meth. 2006;A559:177–180.

[69] Behnke T, Gaede F. Software for the International Linear Collider: Simulation and reconstruction frameworks. Pramana. 2007;69:1089–1092.

[70] Wendt O, Gaede F, Kramer T. Event Reconstruction with MarlinReco at the ILC. Pramana. 2007;69:1109–1114.

[71] Abernathy J, et al. MarlinTPC: A Marlin based common TPC software framework for the LC-TPC collaboration. eConf. 2007;C0705302:TRK01. [,457(2007)].

[72] Abernathy J, et al. MarlinTPC: A common software framework for TPC development. In: Proceedings, 2008 IEEE Nuclear Science Symposium, Medical Imaging Conference and 16th International Workshop on Room-Temperature Semiconductor X-Ray and Gamma-Ray Detectors (NSS/MIC 2008 / RTSD 2008): Dresden, Germany, October 19-25, 2008; 2008. p. 1704–1708.

[73] Antcheva I, et al. ROOT: A C++ framework for petabyte data storage, statistical analysis and visualization. Comput Phys Commun. 2009;180:2499–2512.

[74] Conte E, Fuks B, Serret G. MadAnalysis 5, A User-Friendly Framework for Collider Phenomenology. Comput Phys Commun. 2013;184:222–256.

[75] Alloul A, Christensen ND, Degrande C, Duhr C, Fuks B. FeynRules 2.0 - A complete toolbox for tree-level phenomenology. Comput Phys Communication. 2014;185:2250–2300.

[76] Boudjema F, Singh RK. A Model independent spin analysis of fundamental particles using azimuthal asymmetries. JHEP. 2009;07:028.

[77] Tevatron Electroweak Working Group. Combination of CDF and D0 Results on the Mass of the Top Quark Using Up to 5.6 fb^{-1} of Data. 2010;.

[78] First combination of Tevatron and LHC measurements of the top-quark mass. 2014;.

[79] Dutta S, Goyal A, Kumar M. Top quark physics in the vector color-octet model. Phys Rev. 2013;D87(9):094016.

[80] Boos E, Brandt O, Denisov D, Denisov S, Grannis P. The top quark (20 years after its discovery). Phys Usp. 2015;58(12):1133–1158. [Usp. Fiz. Nauk185,no.12,1241(2015)].

[81] Kroninger, Kevin and Meyer, Andreas B and Uwer, Peter. Top-Quark Physics at the LHC. In: Schörner-Sadenius T, editor. The Large Hadron Collider: Harvest of Run 1; 2015. p. 41.

[82] Coleppa B, Kumar M, Kumar S, Mellado B. Measuring CP nature of top-Higgs couplings at the future Large Hadron electron collider. Phys Lett. 2017;B770:335–341.

[83] Dutta S, Goyal A, Kumar M, Mellado B. Measuring anomalous Wtb couplings at $e^{-}p$ collider. Eur Phys J. 2015;C75(12):577.

[84] Kumar M. Single Top and Higgs Production in $e^{-}p$ collisions. J Phys Conf Ser. 2015;645(1):012005.

[85] Lewis A. Efficient sampling of fast and slow cosmological parameters. Phys Rev. 2013;D87(10):103529.

[86] He XG, Valencia G. The $Z \to b\bar{b}$ decay asymmetry and left-right models. Phys Rev. 2002;D66:013004. [Erratum: Phys. Rev.D66,079901(2002)].

[87] Langacker P, Plumacher M. Flavor changing effects in theories with a heavy Z' boson with family nonuniversal couplings. Phys Rev. 2000;D62:013006.

[88] Fox PJ, Liu J, Tucker-Smith D, Weiner N. An Effective Z'. Phys Rev. 2011;D84:115006.

[89] Abramowicz H, et al. The International Linear Collider Technical Design Report - Volume 4: Detectors. 2013;.

[90] Fujii K, et al. Physics Case for the 250 GeV Stage of the International Linear Collider. 2017;.

[91] Evans L, Michizono S. The International Linear Collider Machine Staging Report 2017. 2017;.

भारतीय प्रौद्योगिकी संस्थान गुवाहाटी
Indian Institute of Technology Guwahati

Publications and Presentations

Publications

1. Sher Alam, **Subhasish Behera**, Satendra Kumar, Shibananda Sahoo "Constraining Capability of Zγh Production at ILC", *Int.J.Mod.Phys. A* **32** *(2017) no.02n03, 1750017.* arxiv: 1701.08250.

2. **Subhasish Behera**, Rashidul Islam (Indian Inst. Tech., Guwahati), Mukesh Kumar (Witwatersrand U.), Poulose Poulose (Indian Inst. Tech., Guwahati), Rafiqul Rahaman (IISER, Kolkata). "Fingerprinting the Top quark FCNC via anomalous Ztq couplings at the LHeC", *Published : Phys. Rev. D 100, 015006 (2019).*

3. **Subhasish Behera**, ILD Collaboration. "The ILD detector at the ILC", [physics.ins-det], arXiv 1912.04601.

4. **Subhasish Behera**, Daniel Jeans (KEK Tsukuba, Japan), Poulose Poulose (Indian Inst. Tech., Guwahati). "Investigating FCNC anomalous top quark coupling through $e^+e^- \to tj$ at the ILC", *Preparation for ILD note is under progress.*

5. **Subhasish Behera**, Poulose Poulose (Indian Inst. Tech., Guwahati). "Tracing the anomalous tqg and $tq\gamma$ flavor changing interactions at the FCC-he", *Manuscript is under preparation.*

Student Visit Program

- I was selected for the prestigious **KEK Student Program 2018, KEK, Japan** for one month visit to KEK, Japan between November 06 - December 04, 2019.

Schools/Workshops/Conferences attended

1. **Discussion Meeting on EWSB and Flavours in the light of LHC** held at IIT Guwahati, Assam during February 20-22, 2014.

2. **Workshop on High Energy Physics Phenomenology** held at IIT Kanpur, Kanpur, Uttap Pradesh during December 04-13, 2015.

3. **Sangam@ 2016:Instructional Workshop in Particle Physics** held at HRI, Allahabad, during February 12-15, 2016.

4. **Linear Collider School 2016** organized by DESY Hamburg, Germany, held at Frauenchiemsee, Germany during July 20-27, 2016.

5. **SERC Preparatory School in THEP** held at IIT Gandhinagar, Gandhinagar, Gujrat during September 05 - October 01, 2016.

6. **XXI DAE-BRNS High Energy Physics Symposium** held at IIT Guwahati, Assam during December 8-12, 2016.

7. **Collider Physics Workshop: Events, Analysis, QCD** held at IIT Guwahati, Assam during 27th-31st March in 2017.

8. **25th INTERNATIONAL CONFERENCE ON SUPERSYMMETRY AND THE UNIFICATION OF FUNDAMENTAL INTERACTIONS (SUSY17)** held at TIFR, Mumbai during December 11-15, 2017.
   (Presented a talk entitled as **"Flavor Changing Neutral Current interaction in single top quark production at ep-collider."**)

9. **GIAN Course on Electroweak Symmetry Breaking, Flavour Physics and BSM** held at IIT Guwahati, Assam during December 18-22, 2017.

10. **Workshop on Top Quark Physics at Present and Future Colliders** held at IISER Kolkata, Kolkata, West Bangel during January 27-30, 2018.

11. **Workshop on Machine Learning** held at SINP Kolkata, Kolkata, West Bangel during January 31 - February 03, 2018.

12. **International Meeting on High Energy Physics(IMHEP)** held at IOP Bhubaneswar, Odisha during January 17-22, 2019.

Vitae

Mr. Subhasish Behera, born in Odisha, India, received his Bachelor of Science degree with Honours in Physics in 2009 from Govt. Autonomous College, Bhawanipatna, Kalahandi, Odisha, and Master of Science degree in Physics in 2012 from School of Physics, Sambalpur University, Sambalpur, Odisha. He joined IIT Guwahati for Ph.D. in 2013. He was awarded Junior Research Fellowship in 2013 and Senior Research Fellowship in 2015 by MHRD, India.